Doctoral Thesis

Studies on the mechanisms of assembly and activation of the MotA/B proton channel complex of the proton-driven bacterial flagellar motor

Yusuke V. Morimoto

Graduate School of Frontier Biosciences
Osaka University

March 2011

Abstract

The bacterial flagellum, which is responsible for motility, is a reversible rotary motor powered by the electrochemical potential difference of protons or sodium ions across the cytoplasmic membrane. Five proteins, MotA, MotB, FliG, FliM, and FliN, are responsible for torque generation in the proton-driven flagellar motor. MotA and MotB form the stator complex of the motor in the cytoplasmic membrane, which also functions as a proton channel to couple proton flow with torque generation. FliG, FliM and FliN forms the C ring on the cytoplasmic side of the MS ring, which is composed of FliF, and acts as the rotor. Torque is generated by an electrostatic interaction between MotA and FliG. The proton-conductivity of the MotA/B complex is thought to be suppressed by a plug segment of MotB when the MotA/B complex is not assembled into a motor. However, it remains unknown how the stator complex is installed into the motor, how its proton-conductivity is activated, and how the proton flow through the proton channel is coupled with torque generation.

To clarify the regulatory mechanism of the proton-conductivity of the MotA/B complex, I measured the proton-conductivity of the plugged and unplugged MotA/B complex of *Salmonella* using a pH-sensitive green fluorescent protein, pHluorin, and showed that the proton-conductivity of the MotA/B complex not incorporated into the motor was two orders of magnitude lower than that of the complex that was incorporated and activated one. This proton leakage was, however, large enough to change the cytoplasmic pH to a level at which the chemotactic signal transduction system responds.

To investigate the stator assembly mechanism, I constructed *Salmonella*

strains expressing GFP-MotB and MotA-mCherry and studied their subcellular localization by fluorescence microscopy. I showed that the process of proton translocation through the channel is not required for stator assembly. I also showed that over-expression of MotA significantly reduced the number of stators in a rotating motor and hence considerably inhibited wild-type motility. These results suggest that MotA alone can be installed into the flagellar motor. And I showed that the electrostatic interaction of the cytoplasmic loop of MotA with FliG is required for the efficient assembly of the stators around the rotor.

The proton influx coupled with flagellar motor rotation must be measured with high spatial and temporal resolution to understand the energy coupling mechanism. I introduced the M153R mutation to pH sensitive fluorescent protein pHluorin to improve the stability and brightness. And I constructed *Salmonella* cells with its flagellar motor components (MotB or FliG) fused to pHluorin(M153R) for measuring pH around the motor. Next I have developed an intracellular pH imaging system that can measure local pH using the pHluorin probe. This system can measure the intracellular pH distribution with a pH resolution of 0.02 and a time resolution of 3 msec. Future experiments will use this technique to investigate the energy conversion mechanism of the flagellar motor by simultaneously measuring proton influx and motor rotation at the single-motor level.

Contents

Abbreviations

ATP: Adenosine 5-triphosphate

CCCP: carbonyl cyanide m-chlorophenylhydrazone:

CCD: charge coupled device

CCW: counterclockwise

CW: clockwise

EDTA: ethylenediaminetetraacetic acid

EMCCD: electron multiplying charge coupled device

GFP: Green fluorescent protein

IPTG: isopropyl-β-D-1-thiogalactopyranoside

OD_{600}: optical density (at 600 nm wavelength)

PAGE: polyacrylamide gel electrophoresis

PBS: phosphate buffered saline

PCR: polymerase chain reaction

PG: peptidoglycan

IMF: ion motive force

PMF: proton motive force

SMF: sodium motive force

rpm: revolutions per minute

SDS: sodium dodecyl sulfate

TBS-T: Tris-buffered saline Tween-20

TEMED: N,N,N',N'-tetramethylethylenediamine

TMRM: tetramethyl rhodamine methyl ester

Tris: tris (hydroxymethyl) aminomethane

Introduction

Bacterial flagellum

Many bacteria can swim towards favorable conditions in liquid environments by rotating long helical filaments called flagella (Fig. 1A) [Berg, 2003; Blair, 2003]. At the base of each flagellum, there is a rotary motor powered by an electrochemical potential gradient of specific ions across the cytoplasmic membrane (Fig. 1B) [Berg and Anderson, 1973; Silverman and Simon, 1974; Larsen *et al*., 1974; Manson *et al*., 1977; Matsuura *et al*., 1977; Ravid *et al*., 1984].

When bacteria swim straight, the motors rotate CCW and the filaments form a bundle that produces thrust. By quick reversal rotation of the motor to CW, the bundle is disrupted so that bacteria tumble and change their swimming direction to move toward more favorable environments from less favorable ones (Fig. 1C) [Macnab and Ornston, 1974; Turner *et al*., 2000]. *Escherichia coli* and *Salmonella enterica* response to their chemical environments via receptors such as Tar and Tsr. These receptors have a remarkable ability to sense chemoattractants, chemorepellents, temperature and pH. Tar and Tsr are transmembrane proteins having periplasmic aspartate or serine binding domains, respectively. The cytoplasmic domains of receptors bind a histidine kinase CheA, and an adaptor protein CheW. The autophosphorylation activity of CheA is regulated by binding of chemoeffector to receptors. Then this phospho group is transferred to the response regulator CheY. Phosphorylated CheY (CheY-P) binds to the cytoplasmic face of flagellar motor, resulting in changing the direction of flagellar motor to CW rotation [Perkinson *et al*., 1993; Armitage, 1999; Sourjik, 2004].

Energy source of the flagellar motor

The source of energy for rotation of the bacterial flagellar motor is not ATP hydrolysis but proton motive force, the electrochemical gradient that allows inward-directed flow of protons across the cytoplasmic membrane [Larsen *et al*., 1974; Manson *et al*., 1977; Matsuura *et al*., 1977; Ravid *et al*., 1984]. It was shown that motility of *Bacillus subtilis*, a gram-positive bacterium, was inhibited by a combination of valinomycin and a high concentration of potassium ions in the medium at neutral pH [Matsuura *et al*., 1977]. The inhibition of motility was due to a decrease in the electric potential difference of the proton motive force because valinomycin is a passive carrier for potassium across the cytoplasmic membrane. This confirmed earlier indications that the motor was ion-driven [Larsen *et al*., 1974]. The existence of Na^+-driven motors in alkalophilic *Bacillus* and *Vibrio* species was first demonstrated by the dependence of flagellar motility upon sodium concentration and its insensitivity to proton ionophores that collapse the PMF [Chernyak *et al.,* 1983; Hirota and Imae, 1983; Hirota *et al*., 1981]. There is significant similarity between the mechanisms of proton and sodium motors.

Structure of the bacterial flagellum

The flagellum is a large macromolecular complex composed of about 30 different proteins with copy numbers ranging from a few to a few tens of thousands (Fig. 2A) [DeRosier, 1998; Berg, 2003; Macnab, 2003]. The flagellum consists of at least three parts: the basal body, the hook and the filament (Fig. 1B) [DePamphilis and Adler, 1971a, b]. The basal body is embedded within the cell membranes and acts as a reversible rotary motor [Macnab and Ornston, 1974; Nakamura *et al*., 2010]. The hook and filament extend outwards in the cell exterior. The filament acts as a helical

propeller. The hook exists between the basal body and filament and functions as a universal joint to smoothly transmit torque produced by the motor to the helical filament [Wagenknecht *et al*., 1981; Smatey *et al*., 2004].

The basal body includes the C-ring, the MS-ring, the protein export apparatus, the rod and the LP-ring. The C-ring and MS-ring form the rotor, which is surrounded by the stator units. The flagellar protein export apparatus is postulated to be located in a putative central pore of the MS-ring to unfold and translocate flagellar protein subunits into the central channel of the growing flagellum to construct the flagellum beyond the cell membranes [Minamino and Macnab, 1999, 2000]. The rod is the drive shaft that connects the MS-ring with the hook [Okino *et al.*, 1989; Minamino *et al.*, 2000]. The LP-ring is embedded in the peptidoglycan layer and the outer membrane and acts as a molecular bushing (Fig. 2) [Jones *et al.*, 1989]. In *E. coli* and *Salmonella*, five flagellar proteins, MotA, MotB, FliG, FliM and FliN, are responsible for torque generation [Ueno *et al.*, 1992; Khan *et al.*, 1992; Francis *et al.*, 1994; Kojima and Blair, 2004]. MotA and MotB are transmembrane proteins that form the stator as well as the proton channel (Fig. 3) [Block and Berg, 1984; Blair and Berg, 1988, 1990; Wilson and Macnab, 1990; Stolz and Berg, 1991, Tang *et al.*, 1997; Morimoto *et al.*, 2010a]. FliG, FliM and FliN form the C-ring on the cytoplasmic face of the MS-ring [Francis *et al*., 1994] and are responsible not only for torque generation but also for switching the direction of motor rotation [Yamaguchi *et al*., 1986]. Torque is generated by the electrostatic interactions of the cytoplasmic loop of MotA with FliG [Zhou and Blair, 1997; Zhou *et al.*, 1998a].

Function of MotA and MotB

The MotA/B complex consists of four copies of MotA and two copies of MotB (Fig. 2-4).

A highly conserved aspartic acid residue of *Salmonella* MotB, Asp-33, plays an important role in the proton-relay mechanism [Sharp *et al.*, 1995; Togashi *et al.*, 1997; Zhou *et al.*, 1998b; Che *et al.*, 2008; Morimoto *et al.*, 2010a]. MotA consists of four transmembrane spans (TM1-TM4), two short periplasmic loops and two extensive cytoplasmic regions (Fig. 3) [Kojima and Blair, 2001, 2004]. Two conserved charged residues, Arg-90 and Glu-98, in the cytoplasmic loop between TM2 and TM3 interact electrostatically with charged residues in the C-terminal domain of FliG to produce torque [Zhou and Blair, 1997; Zhou *et al.*, 1998a]. A high-resolution observation of flagellar motor rotation has revealed a fine stepping motion with 26 steps per revolution, and the number corresponds to that of FliG subunits in the C ring [Suzuki *et al.*, 2004; Sowa *et al*., 2005]. Two highly conserved proline residues of MotA, Pro-173 and Pro-222, are postulated to be involved in cyclic conformational changes of the cytoplasmic loop of MotA complex that is coupled with proton translocation [Braun *et al.*, 1999; Kojima and Blair, 2001; Nakamura *et al.*, 2009b] The TM3 and TM4 helices form a proton pathway along with MotB-TM [Braun *et al.*, 2004]. Stator complexes function with surrounding the basal body (Fig. 5). About 11 copies of MotA/B are installed into a motor to act as stators [Reid *et al*., 2006]. Stator resurrection experiments have shown that abrupt drops in the rotation rate occur frequently [Block and Berg, 1984; Blair and Berg, 1988; Sowa *et al*., 2005]. Consistently, total reflection fluorescence microscopy has revealed a turnover of GFP-fused MotB between the membrane pool and the basal body [Leake *et al*., 2006]. These results suggest that the association between MotA/B and its target site on the basal body are highly dynamic although MotB has a highly conserved peptidoglycan (PG)-binding motif in its C-terminal periplasmic domain ($MotB_C$) [De Mot and Vanderleyden, 1994; Kojima *et al*., 2009].

Interestingly, it has been shown that polar localization of the PomA/B complex of *Vibrio alginolyticus*, which are homologs of the MotA/B complex and acts as the stator of the motor fueled by the sodium motive force across the cytoplasmic membrane (SMF), is greatly affected by changes in the external concentration of sodium ions [Fukuoka *et al*., 2009]. This suggests that sodium ions are required not only for torque generation but also for the efficient assembly process of PomA/B [Fukuoka *et al*., 2009]. Furthermore, *Shewanella oneidensis* MR-1 has two distinct MotA/B and PomA/B stators within a single flagellar motor and selects for which stators to use at the level of protein localization in response to sodium concentration [Paulick *et al*., 2009] (Fig. 6).

It has been proposed that the plug segment of MotB, which consists of residues 53-66, just after its single transmembrane segment, inserts into a proton channel within the cytoplasmic membrane to prevent from premature proton translocation through the channel before association with a motor and that upon stator assembly in the motor, the plug leaves the channel, allowing the stator to conduct protons [Hosking *et al*., 2006; Morimoto *et al*., 2010a]. Dimerization of $MotB_C$ is proposed to be responsible for the proper targeting and stable anchoring of the MotA/B complex to the putative stator binding sites of the basal body [Kojima *et al*., 2008, 2009]. A deletion variant of *Salmonella* MotB, MotB(Δ51-100), missing residues 51-100, can form a functional stator along with MotA [Muramoto and Macnab, 1998; Kojima *et al*., 2009]. Since the crystal structure of *Salmonella* $MotB_C$ indicates that $MotB_C$ is so small that MotB(Δ51-100) cannot reach the PG layer, it is proposed that an interaction between MotA and FliG may trigger conformational changes in $MotB_C$ that open the proton channel and allow the stator to be anchored to the PG layer when the stator encounters a rotor of the motor [Kojima *et al*., 2009]. Although a

low-resolution structure of the entire basal body containing the stator complexes has been visualized by electron cryotomography (Fig. 6B) [Murphy *et al*., 2006, Liu *et al*., 2009, Kudryashev *et al*., 2010], the stators are missing in highly purified flagellar basal bodies [Thomas *et al*., 2001, 2006]. Therefore, it is still unclear how the MotA/B complex is localized to the basal body.

The first chimera reported was made by replacing PomA in the Na^+-driven *Vibrio alginolyticus* motor with the highly homologous MotA from the H^+-driven *Rhodobacter sphaeroides* motor [Asai *et al.*, 1999]. The resulting chimera was driven by Na^+, which ruled out the possibility that ion selectivity was determined by the A stator protein. Following functional chimeras have been replaced both A and B stator proteins, the C-terminal domain of FliG and the C- and N-terminal domains of MotB or PomB, into species with a motor that works by a different type of ion [Asai *et al.*, 2000, 2003; Gosink and Hase, 2000; Yorimitsu *et al.,* 2003]. These results have demonstrated that there is no single determining component for ion selectivity. *Vibrio* specific motor protein, MotX and MotY are not required to specify ion selectivity, but they are required for anchoring sodium stators [McCarter, 1994a, b]. MotX and MotY form the T ring in the periplasmic space, which is not found in *E. coli* and *Salmonella* [Terashima *et al.,* 2006; Thomas *et al.,* 2006]. Furthermore, in *Bacillus subtilis*, two separate stator systems, designated MotA/B and MotP/S, are functionally linked to a single peritrichous flagella system. Interestingly, MotA/B is proton-driven and MotP/S is driven by sodium [Ito *et al.*, 2004]. And in *Bacillus clausii* MotA/B, single stator-rotor uses both protons and sodium ions for ion coupling, depending upon the external pH [Terahara *et al.*, 2008].

Proton motive force

A molecular motor is a machine that converts chemical or electrical energy to mechanical work. It works close to the level of thermal energy. In the bacterial flagellar motor of such as *E. coli* and *Salmonella*, proton through the cytoplasmic membrane is defined as PMF. The PMF consists of an electrical voltage and a chemical component of concentration difference across the membrane and is defined as

$$PMF = \Delta\Psi - \frac{kT}{e}\ln\frac{[H^+]_{out}}{[H^+]_{in}}$$

where $\Delta\Psi$ is the membrane potential (inside minus outside) and *k*, *T* and e are Boltzmann's constant, absolute temperature and the charge, respectively.

In the study of flagellar motor, the only measurement of ion flux was based on shifts in the rate of pH change of a weakly buffered dense suspension of swimming *Streptococcus,* when motors were stopped by cross-linking their filaments with anti-filament antibody [Meister *et al.*, 1987]. The estimated flux was around 1200 H^+ per revolution per motor. Kami-ike *et al.* directly controlled the membrane voltage at the flagellar motor by voltage clamp using custom-made micropipettes, and monitored motor rotation simultaneously [Kami-ike *et al.,* 1991]. With this method, it was shown that speed was proportional to the applied voltage up to -150 mV [Fung and Berg, 1995], consistent with earlier measurements of the speed of tethered gram-positive bacteria, *Streptococcus* and *Bacillus*, energized by a K^+ diffusion potential [Manson *et al.,* 1980; Khan *et al.,* 1985; Meister and Berg, 1987].

Torque versus speed

In order to understand the mechanism of flagellar motor rotation, it is essential to

know in detail the relationship between input energy and output work. The input energy for flagellar motor rotation is derived from proton flux through the MotA/B complex by the proton-motive force across the cytoplasmic membrane, and the work of the motor is characterized by its torque and rotation rate.

The most common method for investigating flagellar rotation has been the tethered cell method (Fig. 7A) [Silverman and Simon, 1974]. In this method, a bacterial cell tethered by its flugellum on the glass slide rotates its cell body at around 10 Hz. This method does not require any specialized equipment to measure the rotation rate. Conventional microscopic video recording of rotating cells is sufficient. However, the motors rotate at around 10 Hz due to high loads of own cell body rotation imposed on the motor. The flagella rotate at approximately 300 Hz with near zero load [Yuan and Berg, 2008]. In an extension of the tethered cell method, the method of electro-rotation has been introduced to measure the motor rotation at high speed. This method controls the rotation rate of cells by applying external torque and clarifies the torque-speed relationship of the motor [Berg and Turner, 1993; Washizu *et al.*, 1993]. However, this method is not sufficient due to artifacts arising from angular variation in the torque generated by the electro-rotation apparatus.

Recently, the bead assay method has been developed to measure the motor rotation rate by tracking beads attached to the filament (Fig. 7B). This technique has several advantages to the previous methods such as less damage on cells and an easy set-up protocol [Chen and Berg, 2000b; Ryu *et al.*, 2000]. In this method, the motor rotation rate can be measured within different ranges of speeds by changing the size of bead.

In bead assay method, the torque-speed relationship of the flagellar motor was determined [Chen and Berg, 2000a, b], and novel information about the motor

properties was obtained. Motor torque remained approximately constant from zero speed (stall) to the knee point and sharply decreased to zero beyond the knee point. In the low-speed regime, up to the knee point, torque was independent of temperature [Chen and Berg, 2000b], and solvent isotope effects by D_2O were relatively small [Chen and Berg, 2000a]. Therefore, at low speeds, the motor operates in thermodynamic equilibrium where proton translocation rates are not limiting. However, in the high-speed regime, motor torque dropped linearly with increased speed. In this high-speed regime, torque was strongly temperature dependent [Chen and Berg, 2000b], and solvent isotope effects were large [Chen and Berg, 2000a]. Thus, at high speed, the motor operates far from thermodynamic equilibrium and the proton translocation rate became a rate-limiting factor for the torque generation cycle.

The torque-speed relationship is consistent with a simulation result predicted by the power stroke model [Iwazawa *et al.*, 1993; Berry and Berg 1999; Xing *et al.*, 2006], in which chemical energy is used directly to drive rotation, and not consistent with the thermal ratchet model in which chemical energy is used to rectify thermally driven movements of motor components. Therefore, the mechanical motion of the motor component during torque generation cycle is driven by the dissipation of proton free energy.

Intracellular pH measurement

To understand the energy coupling mechanism exactly, pH changes near the proton-driven motor should be measured. The measurement of cytoplasmic pH has been done using ^{31}P nuclear magnetic resonance (NMR) [Slonczewksi *et al.*, 1982; Minamino *et al.*, 2003] or the transmembrane equilibration of radiolabeled permeant acids [Zilberatein *et al.*, 1984]. However, these methods have limitations. ^{31}P NMR, for

example, requires a high density of cell suspensions with OD_{600} of 20 to 200 while radiolabeled permeant acids measure only the transmembrane pH difference. Furthermore, both methods measure cell suspensions, not single cells. To overcome these obstacles, it is used the pH-sensitive fluorescent probe such as fluoescent proteins or dye. pH-sensitive fluorescent proteins have shown to be capable of measuring intracellular pH [Kneen *et al.*, 1998; Llopis *et al.*, 1998; Miesenböck *et al.*, 1998; Olsen *et al.*, 2002; Wilks and Slonczewski, 2007]. In general, fluorescent proteins offer highly sensitivity and have no toxicity to living cells [Chalfie *et al.*, 1994; Olsen *et al.*, 2002] while GFP derivatives are ideal pH indicators during specific kinetic studies [Chattoraj *et al.*, 1996; Hess *et al.*, 2004]. This is especially true for ratiometric pHluorin, which has two excitation peaks that are changeable with pH in less than 0.5 ms allowing for rapid pH change detection (Fig. 8) [Miesenböck *et al.*, 1998; Hess *et al.*, 2004]. Another advantage is that the ratiometric probe is independent of other variables like fluorescent protein concentration. In previous reports, pH-dependent changes in fluorescent proteins have been observed using a spectrofluorophotometer [Wilks and Slonczewski, 2007]. Spectrophotometers, however, only measure the average of cell cultures in liquid medium, not single cells. And this method suffers from poor temporal resolution. On the other hand, fluorescence microscopy gets around these problems [Kneen *et al.*, 1998; Llopis *et al.*, 1998; Orij *et al.*, 2009]. A general-purpose fluorescence microscopy detect fluorescence signal at low resolution under the requirement for calculation of subcellular local pH in a bacteria, hence we need an original high-resolution fluorescence microscopy for pH imaging.

Focuses of my Ph. D. work

In proton-driven flagellar motor, MotA and MotB form the stator complex and functions

as a proton channel to couple proton flow to torque generation. Torque is generated by an electrostatic interaction between MotA and FliG. However, it remains unknown how the stator complex is installed into the motor, how its proton-conductivity is activated, and how the proton flow through the proton channel is coupled to torque generation.

First, to clarify the regulatory mechanism of the proton-conductivity of the MotA/B complex, I measured the proton-conductivity of the plugged and unplugged MotA/B complex of *Salmonella* using a pH-sensitive green fluorescent protein, pHluorin. Next, to investigate the stator assembly mechanism, I constructed *Salmonella* strains expressing GFP-MotB and MotA-mCherry and studied their subcellular localization by fluorescence microscopy. Finally, I have developed a bright and stable pH sensitive fluorescent protein pHluorin(M153R) and an intracellular pH imaging system with high spatial and temporal resolution to measure the local pH aroud the flagellar motor.

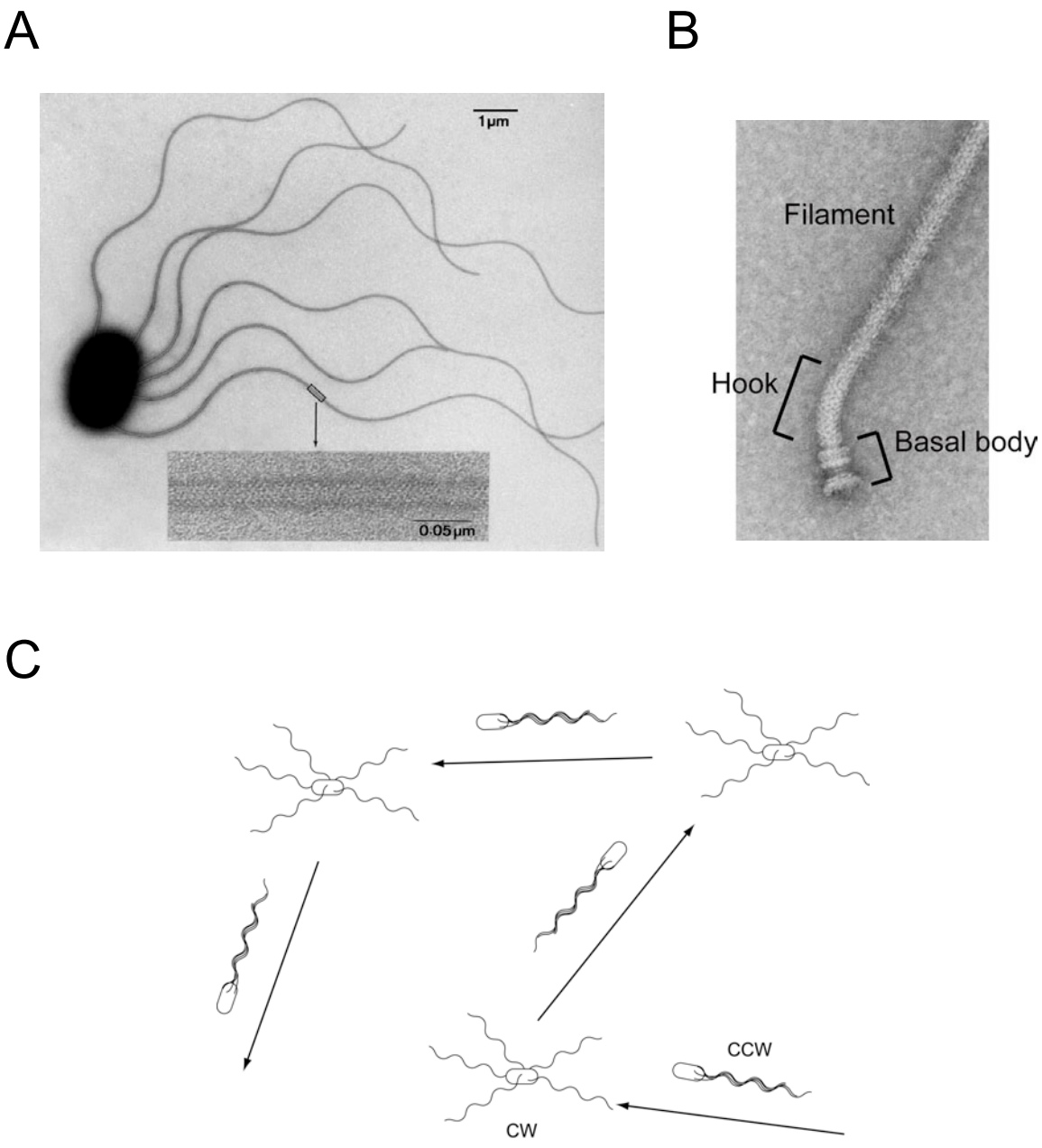

Fig. 1. Bacterial flagella and bacterial behavior

(A) Electron micrograph of *Salmonella.* Bacteria swim by rotating flagella. The flagellum consists of a rotary motor and a helical filamentous propeller. The motor is at the base of the each filament. (B) Electron micrograph of the flagellum isolated from *Salmonella* wild-type strain (SJW1103). (C) A typical swimming pattern of *Salmonella* cells.

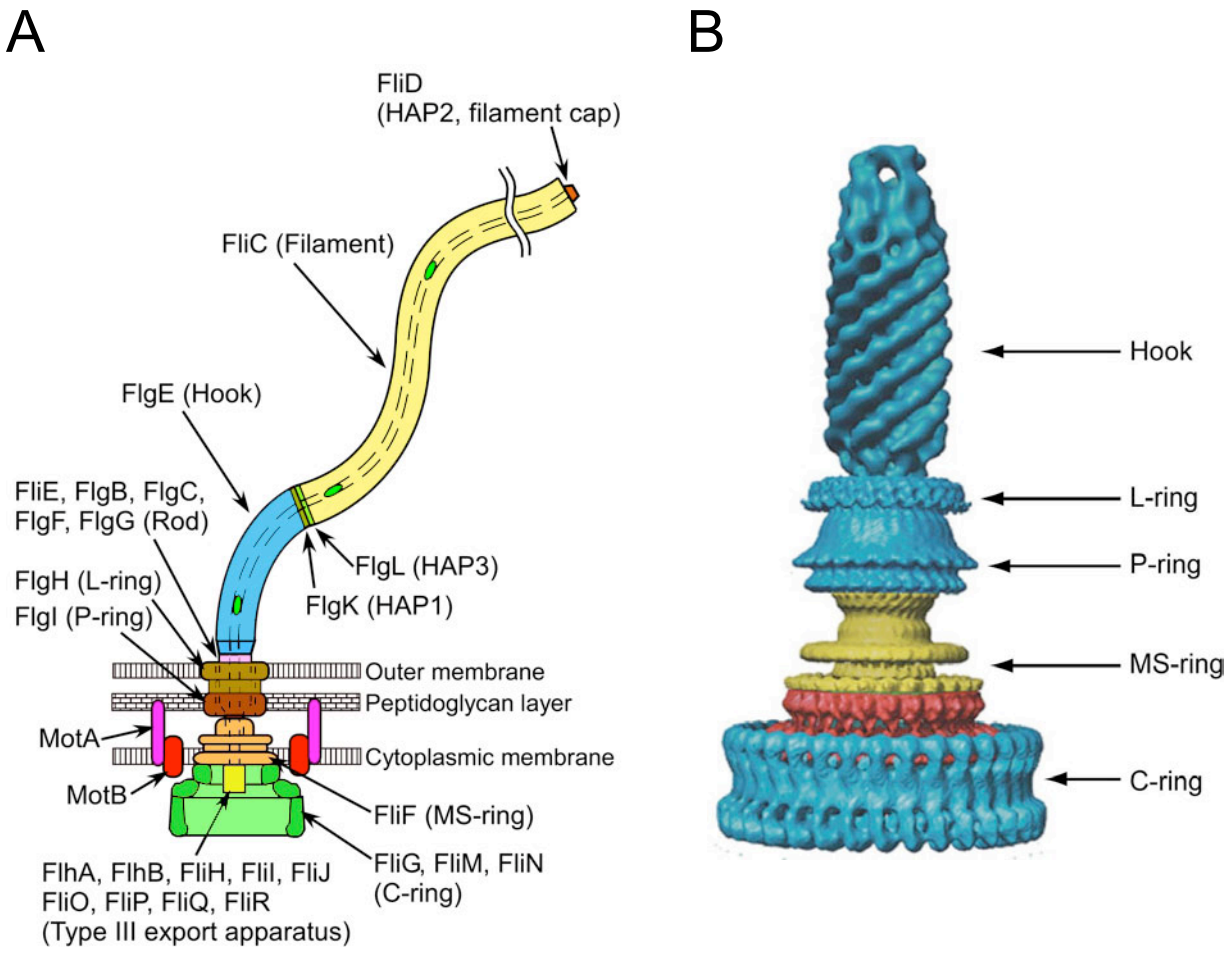

Fig. 2. Structure of bacterial flagellum

(A) Schematic diagram of the bacterial flagellum. (B) The structure of the flagellar basal body from *Salmonella typhimurium* obtained by electron cryomicroscopy (Modified from Thomas *et al*., 2006).

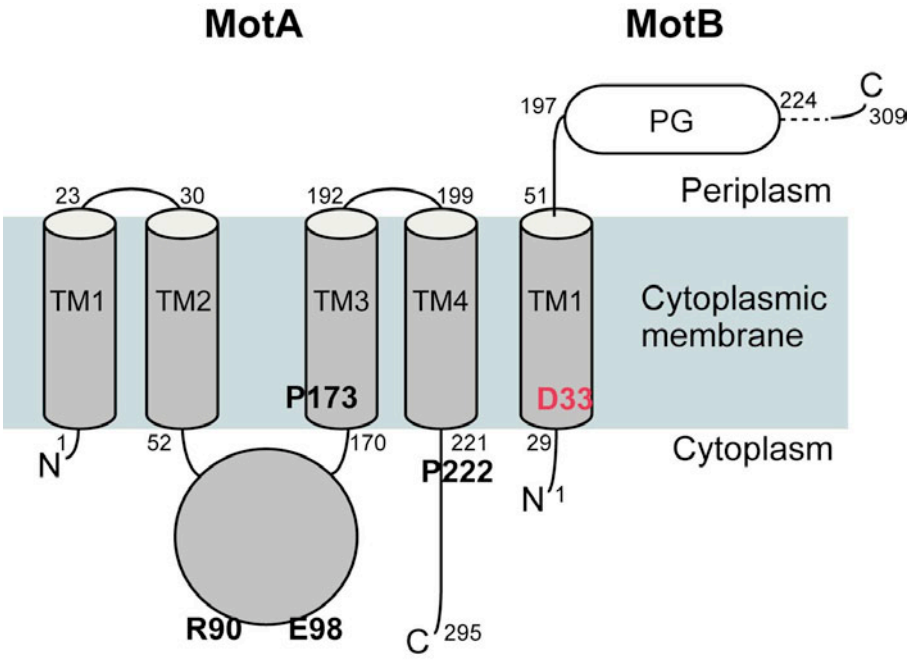

Fig. 3. Membrane topology of MotA and MotB

Salmonella MotA and MotB consist of 295 and 309 amino acid residues, respectively. MotA has four transmembrane segments (TM1-TM4), two short periplasmic loops and two large cytoplasmic regions, while MotB has an N-terminal cytoplasmic region, one transmembrane segment (TM) and a large periplasmic domain containing a putative peptidoglycan-binding motif (PG). Charged residues, Arg-90, and Glu-98, which exist in the cytoplasmic loop of MotA, are responsible for the electrostatic interactions with charged residues of FliG to generate torque. Asp-33 of *Salmonella* MotB, which corresponds to Asp-32 of *E. coli* MotB, is located near the cytoplasmic end of its transmembrane segment and is postulated to be responsible for proton translocation through the proton conducting pathway formed by the MotA/B complex. N and C indicate the N and C termini of the proteins [Braun *et al*., 1999, 2004; Kojima *et al*., 2004; Che *et al*., 2008; Nakamura *et al*., 2009b]

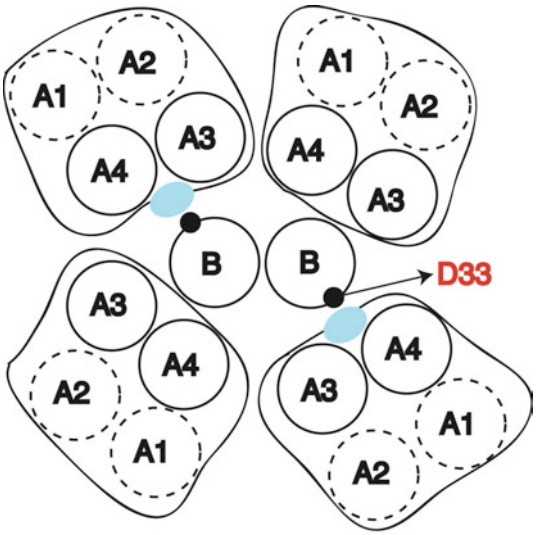

Fig. 4. Arrangement of MotA and MotB transmembrane segments within the MotA/B complex

The complex consists of 4 copies of MotA and 2 copies of MotB. The view is from the periplasmic side of the membrane. The complex is postulated to have two proton conducting pathway shown by blue ellipsoids. Cross-linking experiments have shown that four MotA subunits are positioned with their TM3 (A3) and TM4 (A4) segments adjacent to the MotB dimer, and their TM1 (A1) and TM2 (A2) segments on the outside, although exact positions of TM1 and TM2 remains unknown (indicated by dashed lines) [Braun *et al*., 2004; Che *et al*., 2008].

A

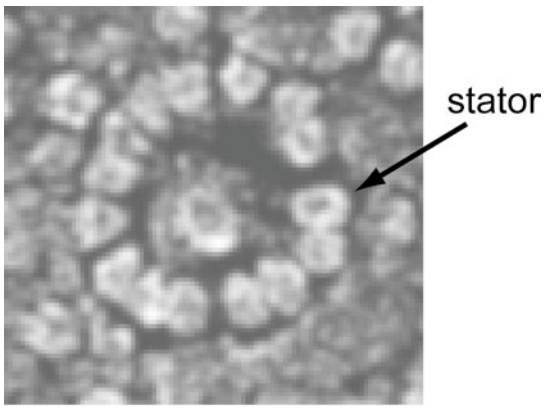

B

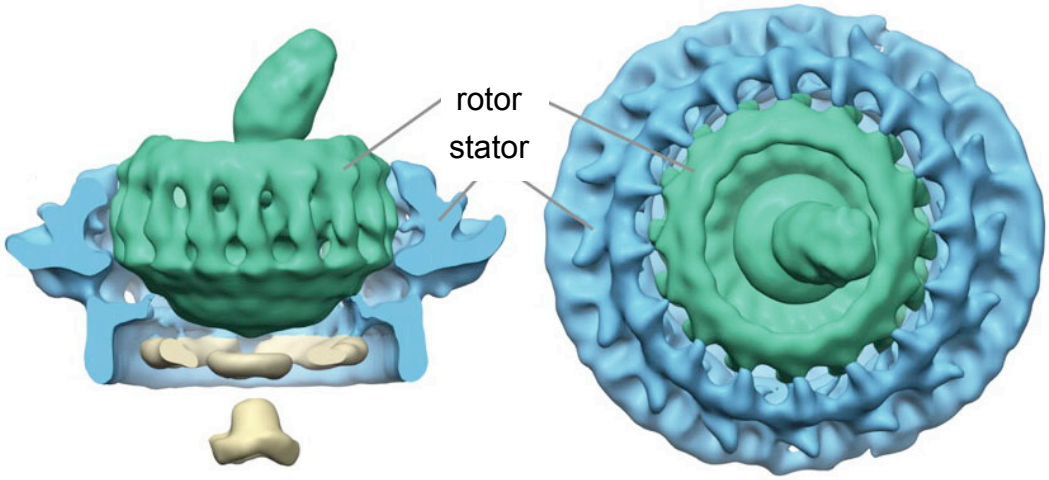

Fig. 5. Stator complexes around the motor.

(A) Freeze fraction EM image of a ring of stators surrounding a hole left by the MS-ring in a *Streptococcus* motor. Fifteen stators can be counted in this motor. Depending on species, the number of stators found by this method. [Khan *et al*., 1988]. (B) The 3-D structure of the flagellar motor, obtained by electron cryotomography of *Borrelia burgdorferi*. The segmented structure was color coded as follows: rotor, green; C-ring and stator, blue; export apparatus, gray [Liu *et al*., 2009].

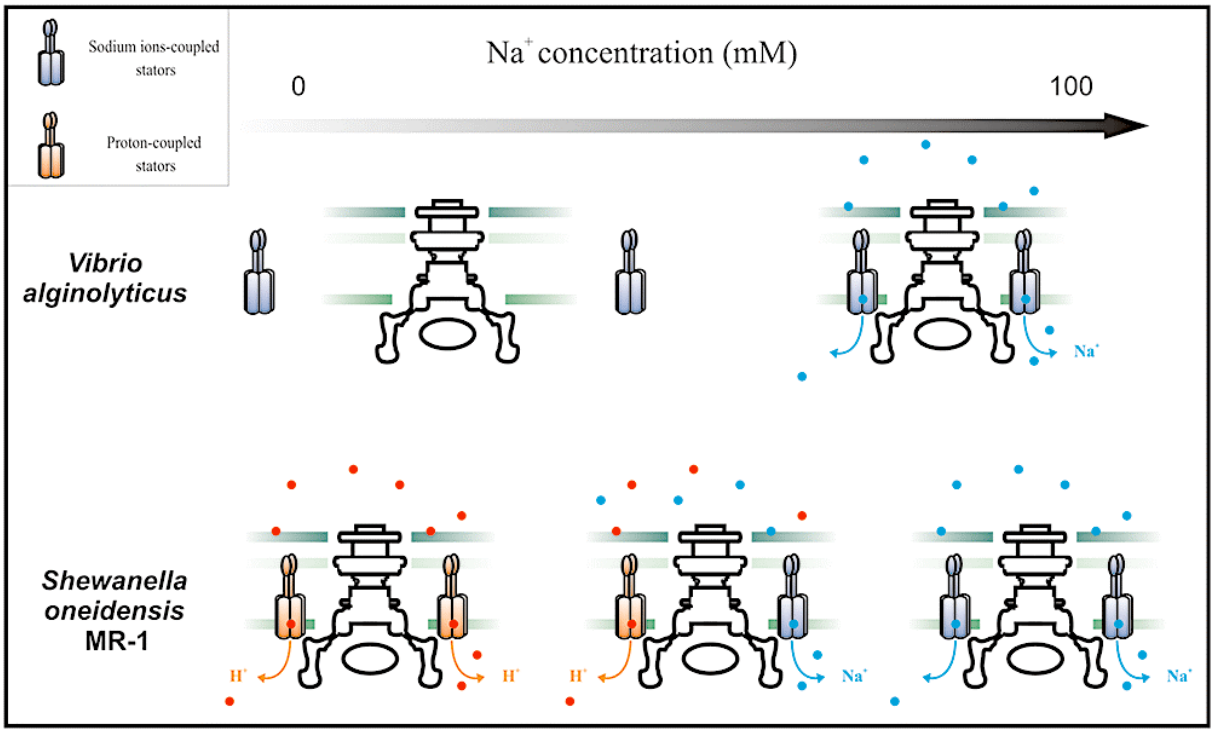

Fig. 6. Dependence on sodium concentration of the localization and type of stator units

Localization of the *Vibrio alginolyticus* PomA/B stator units is lost in the absence of Na^+ but restored with increasing Na^+ concentrations. In *Shewanella oneidensis* MR-1, both types of stator units are expressed at all Na^+ concentrations but motor function mainly depends on PomA/B stator units. However, when Na^+ concentration is decreasing, localization of the MotA/B stator units increases while the localization of the PomA/B stator units decreases. [Fukuoka *et al*., 2009; Paulick *et al*., 2009; Delalez and Armitage, 2009]

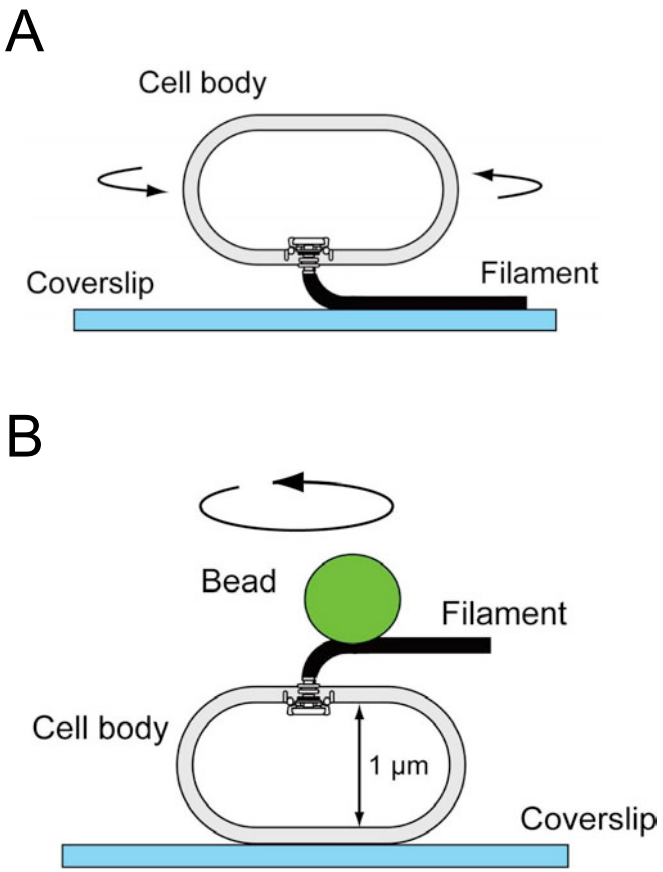

Fig. 7. Measurement systems of flagellar motor rotation

(A) Schematic diagram of the tethered cell method. A cell is tethered to a microscope coverslip through a single flagellum and the cell body rotation is observed. (B) Schematic diagram of beads assay. A cell is fixed on a coverslip and a bead is attached to its flagellar filament. The position of the bead is detected.

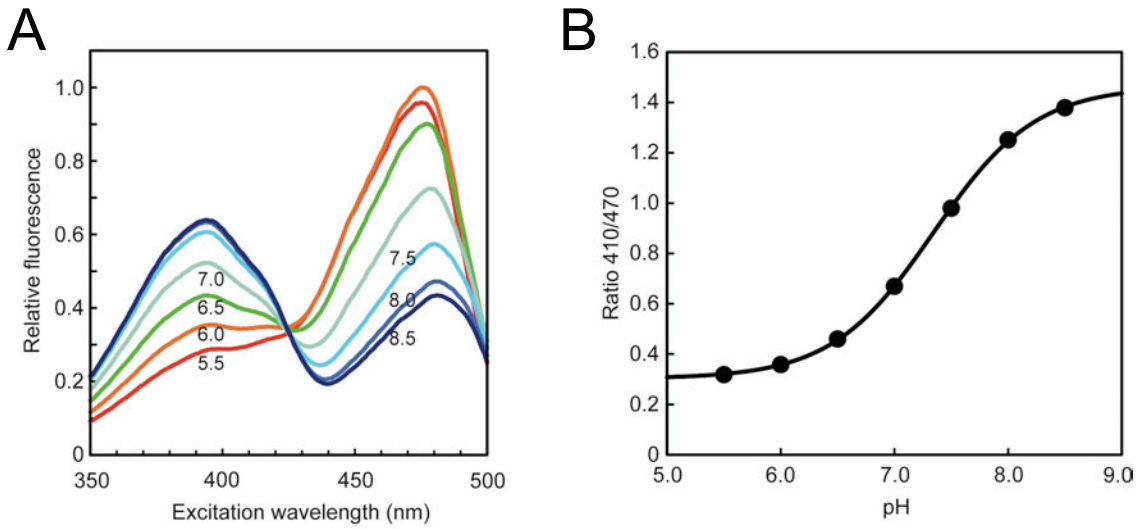

Fig. 8. pH measurement using ratiometric pHluorin

(A) Fluorescence-excitation spectra of ratiometric pHluorin. (B) Standard curve. The fluorescence-excitation spectra of purified pHluorin were recorded on a fluorescence spectrophotometer. Emission intensities of the pHluorin probe were monitored at 508 nm. The 410/470-nm excitation ratios were calculated and converted to pH values. [Miesenböck *et al*., 1998; Morimoto *et al*., 2010a]

Chapter 1. Proton-conductivity assay of plugged and unplugged MotA/B proton channel by cytoplasmic pHluorin expressed in *Salmonella*

Introduction

Cell growth is not impaired by over-expression of either *E. coli* MotA/B or MotA alone [Stolz and Macnab, 1991; Wilson and Macnab, 1988]. In contrast, an in-frame deletion of residues 51-70 within the periplasmic domain of *E. coli* MotB, a region which is highly conserved among the MotB family, causes considerable proton leakage, thereby arresting cell growth [Hosking *et al.*, 2006]. This result suggests that the deleted region acts as a plug that interferes with proton channel formation, resulting in suppression of undesirable proton flow through the channel when the MotA/B complex is not assembled into the motor. Interestingly, however, neither motility nor cell growth is significantly impired by in-frame deletion of residues 51-100 in *Salmonella* MotB, which contains the putative plug segment [Muramoto and Macnab, 1998; Kojima *et al.*, 2009]. Therefore, it is not clear how the proton-conductivity of the *Salmonella* MotA/B complex is regulated.

In this study, I expressed pHluorin in *Salmonella* cells to study the effect of varying copy numbers of MotA/B and its unplugged variant on intracellular pH change to assay the proton-conductivity of the plugged and unplugged MotA/B complex. I show that the plug segment of *Salmonella* MotB suppresses proton leakage. However, the suppression is not very tight. Therefore, over-expression of the intact MotA/B complex results in a small decrease in the cytoplasmic pH that is sufficient to bias the motor towards CW rotation.

Materials and Methods

Chemicals

Unless mentioned otherwise, chemicals used in this study were produced by Wako Pure Chemical Industries, Ltd.

Media

Composition of Luria-Bertani broth medium (LB) : H_2O 1 l, Bacto™ Tryptone (Becton, Dickinson and Company) 10 g, Bacto™ Yeast Extract (Becton, Dickinson and Company) 5 g, NaCl 5 g; LA : LB 1 l, Bacto™ Agar (Becton, Dickinson and Company) 15 g; T-broth (TB) : H_2O 1 l, Bacto™ Tryptone 10 g, NaCl 5 g; Soft tryptone motility plates : TB 1 l, Bacto™Agar 3.5 g; Tetracycline sensitive plates : H_2O 1 l, Bacto™ Tryptone 5 g, Bacto™ Yeast Extract 5 g, Bacto™ Agar 15 g, 12.5 mg/ml chlortetracycline hydrochloride 4 ml, NaCl 10 g, $NaH_2PO_4 \cdot 2H_2O$ 11.31 g, Fusaric acid 12 mg, 2 mg/ml Fuzaric acid 6 ml, 20 mM $ZnCl_2$ 5 ml; motility medium : 10 mM potassium phosphate pH 7.0, 0.1 mM EDTA ,10 mM sodium lactate.

Ampicillin and tetracycline were added as needed to the medium at a final concentration of 50 μg/ml, 15 μg/ml, respectively.

Bacterial strains and plasmids

All strains and plasmids used in this study chapter are listed in Table 1-1 and 1-2, respectively. NovaBlue (Novagen) was used as the recipient for cloning experiments. JR501 (r^- m^+) was used for conversion of *E. coli* based plasmids to *Salmonella* compatibility. *E. coli* BL21(DE3)pLysS (Novagen) was used for overproduction of protein. All the *Salmonella* mutant strains were derived from SJW1103 (wild type for motility and chemotaxis). MMPH001 (Δ*araBAD::pHluorin*) and YVM021

(Δ*fliC::pHluorin*) were constructed using the λ-Red-mediated recombination [Datsenko and Wanner, 2000]. In YVM021 strain, TcR-element (*tetRA*) from transposon Tn10 were inserted at the 5' or 3' end of the *fliC* gene by PCR amplification of *pHluorin* gene with primers that had 5'- and 3'-flanking sequences with homology to either the 5'-40 bases of the upstream of amino acid codon or the 3'-40 bases of those downstream of amino acid codon followed by to replace the *tetRA* cassette with *pHluorin* gene to create the fusions expressed from the chromosomal *fliC* promoter. MMPH001, which is wild-type for motility and chemotaxis, expresses the *pHluorin* gene from the *araBAD* promoter on the chromosome. PCR primers used in construction of mutant strain were listed in Table 1-3.

DNA sequencing

DNA sequencing was performed with an Applied Biosystems 3130 Genetic Analyzer (Applied Biosystems). Sources of DNA sequences were from Entrez Gene at NCBI.

Immunoblotting

Salmonella cells were grown overnight at 30ºC in LB with shaking. Cell pellets were suspended in a SDS-loading buffer and normalized by cell density to give a constant amount of cells. After the proteins in each fraction had been separated by SDS-polyacrylamide gel (12.5% acrylamide) electrophoresis (PAGE), they were transferred onto a nitrocellulose membrane (Bio-Rad Laboratories) with a transblotting apparatus (GE Healthcare). The membrane was then blocked for 1 hour with TBS-T (20 mM Tris-HCl, pH 7.5, 500 mM NaCl, 0.1% Tween 20) containing 5% skim milk. After washing with TBS-T, the membrane was probed with polyclonal anti-MotA, anti-MotB antibody (MBL Co., Ltd) for 1 hour, respectively. After washing

three times with TBS-T, the membrane was incubated with Immun-Star Goat Anti-Rabbit (GAR)-HRP Conjugate (Bio-Rad Laboratories) for 1 hour and then washed three times with TBS-T. Detection was performed with the enhanced chemiluminescence immunoblotting detection kit (GE Healthcare) and Luminescent Image Analyzer LAS-3000 (FujiFilm).

Swarming motility assay in semi-solid agars

Fresh colonies were inoculated onto soft tryptone agar plates and incubated at 30°C.

Swimming speed measurement

Salmonella cells were grown at 30°C in LB until the cell density reached an OD_{600} of ca. 1.0. Motility of the cells was observed at ca. 23ºC under a phase contrast microscope (CH40, Olympus) and recorded on videotape or hard disk drive. The positions of individual cells were identified using Move-tr/2D software (Library Co., Ltd.) and swimming speed was determined.

Beads assay

Salmonella cells having sticky flagellar filaments were grown exponentially in LB at 30ºC with shaking. The cells were passed through a 25G needle to partially shear their flagellar filaments. Bead assays with polystyrene beads with diameters of 1.5 and 0.8 μm (Invitrogen) were carried out. The rotation speed was measured by projecting the phase contrast image of each bead onto a quadrant photodiode through a 60×oil immersion objective lens as described previously. [Sowa *et al.*, 2003, Che *et al.*, 2008]. The data were recorded at 1.0 msec intervals by a 16-bit A-D board (Microscience) using the LaBDAQ software (Matsuyama Advance). The data

analyzed by a program developed based on the Igor Pro 6 software. All the experiments were done at ca. 23ºC.

Spectroscopy of pHluorin for intracellular pH measurement.

Intracellular pH measurements were carried out at an external pH value of 5.5 using ratiometric pHluorin, a pH-sensitive green fluorescent protein [Miesenböck *et al.*, 1998]. Glutathione S-transferase (GST)-pHluorin was purified from the soluble fractions of BL21(DE3)pLysS carrying pGST-pHluorin, by affinity chromatography with a GSTrap™HP column (GE Healthcare). After removal of the GST tag by thrombin, pHuorin was purified by affinity chromatography with the GST column to remove the GST tag and noncleaved GST-pHluorin, followed by gel-filtration chromatography. Excitation spectra were recorded using the spectrofluorophotometer (RF-5300PC, Shimadzu) over a range of wavelength from 350 to 500 nm (slit width, 5 nm) and by using an emission wavelength of 508 nm (slit width, 5 nm). Spectra were recorded twice under each condition. To generate the calibration curve, the 410/470-nm excitation ratios of purified pHluorin were determined at different pH values. The calibration curve was determined for each fluorophore and purified protein. A standard curve was fitted to the sigmoid curve and used to convert the 410/470 intensity ratio ($R_{410/470}$) to pH units.

Results

Effect of the plug segment of MotB on the proton-conductivity of the MotA/B complex

In-frame deletion of residues 51-100 in *Salmonella* MotB does not affect cell growth although the conserved plug segment is missing [Muramoto and Macnab, 1998; Kojima *et al.*, 2009]. To confirm this, I measured the growth rate of *Salmonella* cells over-expressing the MotA/B(Δ51-100) complex and observed no growth impairment (Fig. 1-1A), indicating that a proton channel is not formed. Then, to test whether the plug segment suppresses proton leakage through *Salmonella* MotA/B complex in the similar way to that observed in *E. coli* MotB, an in-frame deletion variant of MotB, MotB(Δ52-71) missing residues 52-71, was co-expressed with MotA from the pBAD24-based plasmid. Cell growth was totally inhibited by induction of MotA/B(Δ52-71) but not by MotA/B (Fig. 1-1B), even though the expression level of MotA/B(Δ52-71) was about 5-fold lower than MotA/B expressed from the same vector and almost the same as that of MotA/B expressed from the chromosome (Fig. 1-1C).

To test whether the growth arrest is a consequence of proton leakage, I measured intracellular pH at an external pH value of 5.5 (Fig. 1-1D). While the intracellular pH of the cells expressing MotA/B from the plasmid did not change significantly after induction with arabinose, the intracellular pH decreased by approximately 0.35 units in 15 min, and 0.6 units in 60 min, after induction of MotA/B(Δ52-71). This finding is consistent with previous data [Hosking *et al.*, 2006]. Thus, residues 52-71 of *Salmonella* MotB are critical for preventing proton leakage before association of the MotA/B complex with a motor.

Effect of the L119P and L119E mutations of MotB on the proton-conductivity of

the MotA/B(Δ51-100) complex

It has been shown that cell growth is severely impaired when MotB(Δ51-100) with the L119P or L119E mutation is co-expressed with MotA [Kojima *et al.*, 2009]. To test whether the growth impairment results from proton leakage, I measured the intracellular pH. In agreement with a previous report [Kojima *et al.*, 2009], over-expression of MotA/B(Δ51-100/L119P) and MotA/B(Δ51-100/L119E) resulted in significant growth impairment (Fig. 1-2A), although the expression levels of the double-mutant proteins were slightly lower than that of MotB(Δ51-100) (Fig. 1-2B). The intracellular pH of the cells over-expressing MotA/B(Δ51-100) with either of these point mutations dropped by ca. 0.32 units in 15 min after their induction, whereas no significant change in the intracellular pH of the MotA/B(Δ51-100)-expressing cells was observed (Fig. 1-2C). Interestingly, the drop in intracellular pH caused by MotA/B(Δ51-100) with the L119P or L119E mutation was smaller than that by MotA/B(Δ52-71). These results suggest that the L119P and L119E mutations alter a conformation of the MotA/B(Δ51-100), allowing protons to flow through the proton channel of the MotA/B(Δ51-100) to a considerable degree, as suggested before [Kojima *et al.*, 2009].

Multicopy effect of the MotA/B complex on proton leakage

Accumulation of MotA/B in the cytoplasmic membrane up to a level of 5-fold greater than normal did not cause any proton leakage (Fig. 1-1). Therefore, I investigated the effect of further increases in the copy number of MotA/B on intracellular pH change. Quantitative immunoblotting revealed that the expression level of MotA/B from a plasmid, pKSS13, was about 50-fold higher than the chromosomal level (Fig. 1-3). At this level of expression, no significant growth impairment was observed (Fig. 1-7). The

intracellular pH was then measured in the MMPH001 cells transformed with pKSS13. Since it has been shown that the D33N mutation in MotB abolishes proton translocation through the MotA/B complex [Zhou *et al.*, 1998], I used a plasmid, pKSS13(D33N), which encodes MotA/B(D33N), as a negative control. The amounts of MotA and MotB(D33N) expressed from pKSS13(D33N) were essentially the same as those from pKSS13 (Fig. 1-3A). There was a drop in the intracellular pH of 0.16 units for the MotA/B-expressing cells, but no change was observed with the MotA/B(D33N)-expressing cells (Fig. 1-3B), indicating that the small decrease in the intracellular pH by overproduced MotA/B is a consequence of the remaining proton conductivity of the plugged channel.

Multicopy effect of the MotA/B complex on the motility of wild-type cells

It has been shown that proton leakage caused by deletion of the plug segment in MotB results in a strong CW bias in motor rotation [Hosking *et al.*, 2006]. Therefore, I investigated whether overproduction of MotA/B influences motility of wild-type cells in semi-solid agar plates. When MotA/B was overproduced, the colony size decreased significantly compared to the vector control (Fig. 1-4A). Since cell growth was not impaired by over-expression of the MotA/B (data not shown), I conclude that the reduced colony size is not a consequence of the growth impairment.

MotA interacts with the switch protein FliG, which is not only responsible for torque generation and switching of rotational direction of the motor, but is also needed for export of flagellar proteins [Yamaguchi *et al.*, 1986]. Excess MotA/B might titrate FliG away from the motor, resulting in inhibition of the protein export process. To test this possibility, I analyzed flagellar protein export by immunoblotting and found that the levels of secreted flagellar proteins were not affected by overproduction of MotA/B

(data not shown). This result indicates that the poor swarming is not due to reduction in the export of flagellar proteins. Furthermore, high-intensity dark-field light microscopy revealed that flagellation and the swimming speed were normal in cells over-expressing MotA/B (data not shown).

I next investigated whether the decrease in chemotactic ring expansion results from either a reduced torque or a CW bias in motor rotation. I carried out beads assays for quantitative characterization of motor rotation. The rotation speeds were 80 to 90 Hz with 0.8 μm beads and 20 to 25 Hz with 1.5 μm beads, with or without overproduction of MotA/B (data not shown), indicating that torque generation is not affected. The motors of the cells carrying the vector rotated exclusively CCW under my experimental condition (Fig. 1-4B left panel). In contrast, the cells overproducing MotA/B switched the direction of motor rotation frequently and stayed in CW rotation for much longer periods of time (Fig. 1-4B right panel). Tumbling cells were consistently more often observed in liquid media when MotA/B was over-expressed.

Chemotaxis occurs through changes in the CCW-CW bias of the motor rotation [Berg, 2003]. I therefore introduced a Δ*cheA-cheZ* deletion, which causes motors to rotate only in the CCW direction, and found that the motor rotation of the cells overproducing MotA/B remained exclusively CCW (data not shown). These results suggest that the decrease in colony expansion seen in semi-solid agar results from an increased probability of tumbling.

Effect of small intracellular pH changes on *Salmonella* motility

To further investigate whether *Salmonella* cells actually respond to decreases in the intracellular pH as small as 0.16 units, I analyzed motility and intracellular pH at an

external pH value of 7.0 in the presence of varying concentrations of potassium benzoate. Benzoate is able to cross the cytoplasmic membrane in the neutral form and then release a hydrogen ion, thereby lowering the intracellular pH [Kihara and Macnab, 1981]. The colony size in soft tryptone agar decreased as the concentration of benzoate was increased (Fig. 1-5A). In agreement with a previous report [Kihara and Macnab, 1981], such impaired motility results from an increase in the probability of tumbling (data not shown). Intracellular pH also decreased as the benzoate concentration increased (Fig. 1-5B). Benzoate did not affect the fluorescence excitation spectra of pHluorin (data not shown). These results indicate that a small change in intracellular pH affects chemotaxis.

Discussion

The MotA/B complex acts as a proton channel of the proton-driven flagellar motor. Since in-frame deletion of residues 51-70 in *E. coli* MotB, a region just after the MotB-TM, causes significant proton leakage and arrests cell growth, the deleted region has been proposed to act as a plug that prevents the MotA/B complex from leaking protons before it assembles into the motor [Hosking *et al.*, 2006]. However, in-frame deletion of residues 51-100 in *Salmonella* MotB, which contain the putative plug segment, does not affect cell growth, although MotA/B(Δ51-100) is still functional as the stator [Muramoto and Macnab, 1998; Kojima *et al.*, 2009]. Therefore, I analyzed the role of the plug segment in *Salmonella* MotB and found that in-frame deletion of residues 52-71 causes a considerable decrease in the intracellular pH and arrests cell growth (Fig. 1-1). This suggests that the deleted segment acts as the plug in a similar way to the corresponding region of *E. coli* MotB. Since the expression level of MotA/B(Δ52-71) from the plasmid pYC109 was the same as that of chromosomal expression of MotA/B, the proton-conductivity of unplugged MotA/B seems to show its full channel activity, thereby stopping growth.

Growth was not impaired by over-expression of MotA/B(Δ51-100) (Fig. 1-1A), in agreement with a previous report [Kojima *et al.*, 2009], indicating that a proton-channel of the MotA/B(Δ51-100) complex is not formed although the plug is missing. It has been shown that the introduction of the L119P or L119E substitution into MotB(Δ51-100) causes growth impairment [Yamaguchi *et al.*, 1984]. Consistently, these mutations at Leu-119 allowed MotA/B(Δ51-100) to leak protons to a significant degree (Fig. 1-2). Therefore, it is possible that some other region within the periplasmic domain of MotB regulates proper proton-channel formation at least in the MotB(Δ51-100) protein, as suggested before [Kojima *et al.*, 2009].

To compare the proton conductivities between plugged and unplugged MotA/B, I analyzed the effect of varying copy numbers of MotA/B on motility, motor function and intracellular pH. An increase of 50-fold in the expression level of MotA/B impaired chemotaxis in soft agar, and decreased the intracellular pH by 0.16 units. These cells also a strong CW-bias in motor rotation (Fig. 1-2 and 1-3). CW-biased rotation was not observed in a Δ*cheA-cheZ* non-chemotactic and smooth-swimming mutant (data not shown), providing additional evidence that over-expression affects motility by changing chemotaxis behavior. From the expression level of MotA/B and the decrease in the intracellular pH, the proton conductivity of MotA/B not incorporated into the motor is estimated to be two orders of magnitude lower than that of the unplugged, activated channel, but it is significant enough to change the cytoplasmic pH sufficiently to evoke a repellent response.

50-fold over-expression of the MotA/B resulted in a small proton leakage (Fig. 1-3), indicating that the conserved plug segment in MotB does not tightly suppress proton leakage. There are two possible reasons: 1) the plug may breathe in and out of the cytoplasmic membrane, as suggested previously [Hosking *et al.*, 2006], or 2) even with the plug place in there is some leakage.

Finally, I show here that a change in the intracellular pH as small as ca. 0.2 units can be detected either by pHluorin expressed in the cell or by the chemotaxis signal transduction system of *Salmonella*. This observation suggests that the proton conductivity of potential, but unproven, transmembrane proton channels and conductors may be done easily and quickly by expressing the proteins to be characterized in *Salmonella* cells expressing cytoplasmic pHluorin. Therefore, the *Salmonella* MMPH001 strain can be used as a potentially powerful tool for determining of the proton-conductivity of membrane proteins.

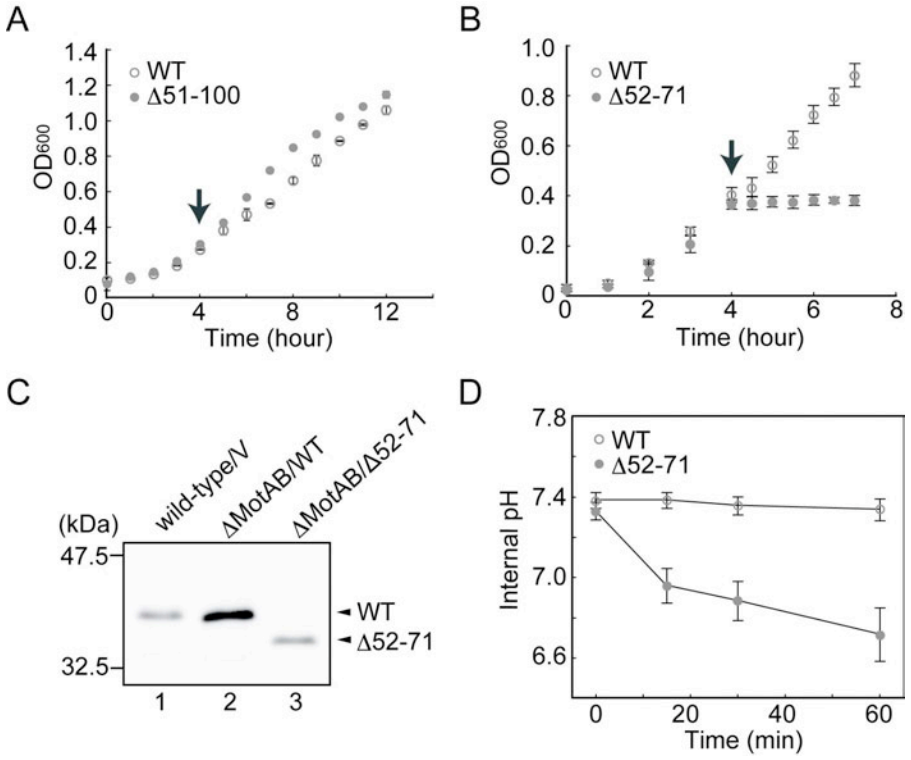

Fig. 1-1. Effects of deletion of the plug segment of *Salmonella* MotB on cell growth and proton leakage. (A) Growth curve of SJW2241 (Δ*motAB*) harboring pNSK9 (wild-type MotA/B, indicated as WT) (open circles) or pTSK30 (MotA/B(Δ51-100), indicated as Δ51-100) (closed circles). The arrow indicates the time when 1 mM IPTG was added. The optical density at 600 nm (OD_{600}) was measured. (B) Growth curve of SJW2241 expressing wild-type MotA/B (open circles) or MotA/B(Δ52-71) (indicated as Δ52-71) (closed circles). The arrow indicates the time when 1 mM arabinose was added. (C) Immunoblotting, using polyclonal anti-MotB antibody, of total proteins from *Salmonella* cells transformed with the pBAD24-based plasmids: lane 1, SJW1103 (wild-type) carrying pBAD24 (V); lane2, SJW2241 transformed with pYC20 (WT); lane 3, SJW2241 harboring pYC109 (Δ52-71). (D) Measurement of the intracellular pH of YVM021 cells (Δ*fliC*::*pHluorin*) using the pHluorin probe after induction of MotA/B or MotB(Δ52-71) expression at an external pH of 5.5.

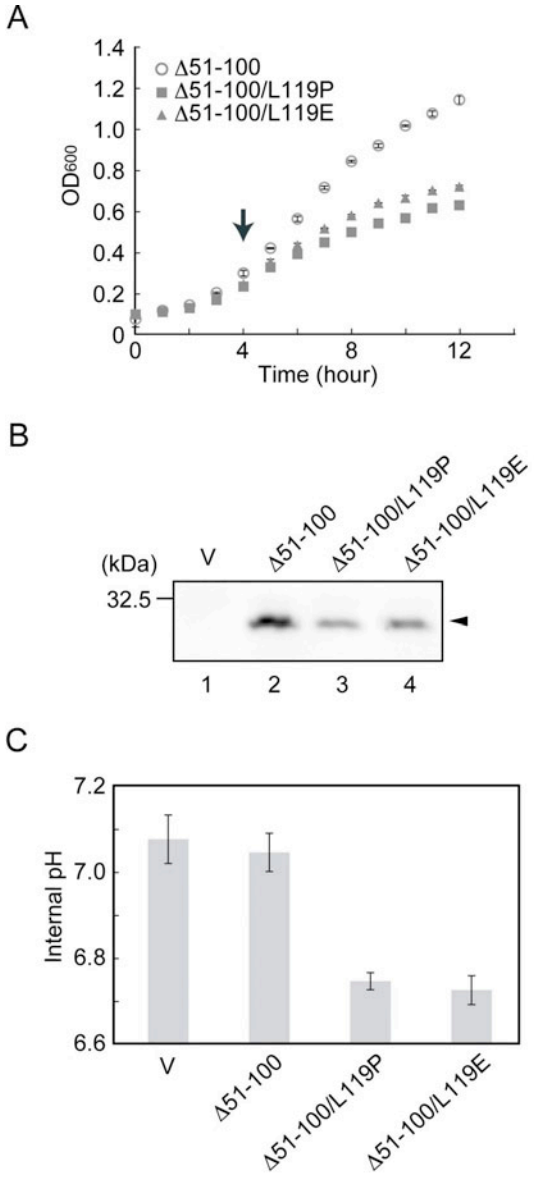

Fig. 1-2. Effects of the L119P and L119E mutations on cell growth and proton leakage. (A) Growth curve of SJW2241 transformed with pTSK30 (MotA/B(Δ51-100)) (open circles), pTSK30(L119P) (MotA/B(Δ51-100/L119P), indicated as Δ51-100/L119P) (closed squares) or pTSK30(L119E) (MotA/B(Δ51-100/L119E), indicated as Δ51-100/L119E) (closed triangles). The arrow indicates the time when 1 mM IPTG was added. (B) Immunoblotting, using polyclonal anti-MotB antibody, of total proteins from the same transformants. (C) Measurements of intracellular pH of YVM021 cells carrying pTrc99A (V), pTSK30 (Δ51-100), pTSK30(L119P) or pTSK30(L119E) at an external pH of 5.5.

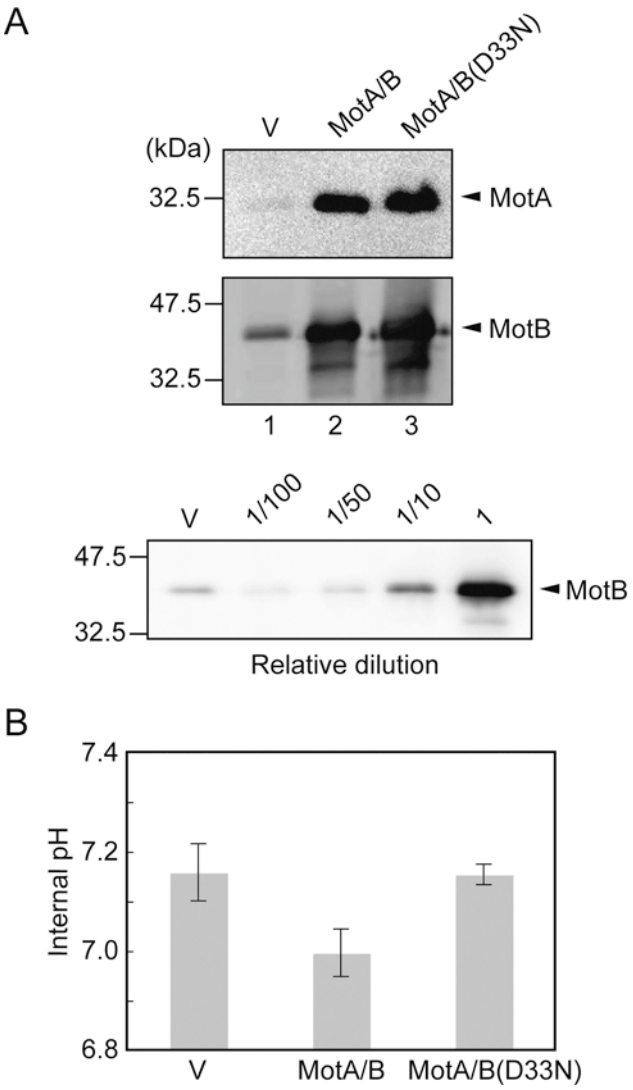

Fig. 1-3. Effect of different levels of MotA/B expression on intracellular pH changes. (A) Immunoblotting, using polyclonal anti-MotA and anti-MotB antibodies, of whole-cell proteins of MMPH001 (Δ*araBAD*::*pHluorin*) harboring pKK223-3 (V), pKSS13 (MotA/B) or pKSS13(D33N) (MotA/B(D33N)). To estimate the level of MotA/B, samples of MMPH001 with pKSS13 were diluted at 1/10, 1/50, and 1/100 (lower panel). (B) Measurements of intracellular pH for the same transformants at external pH 5.5.

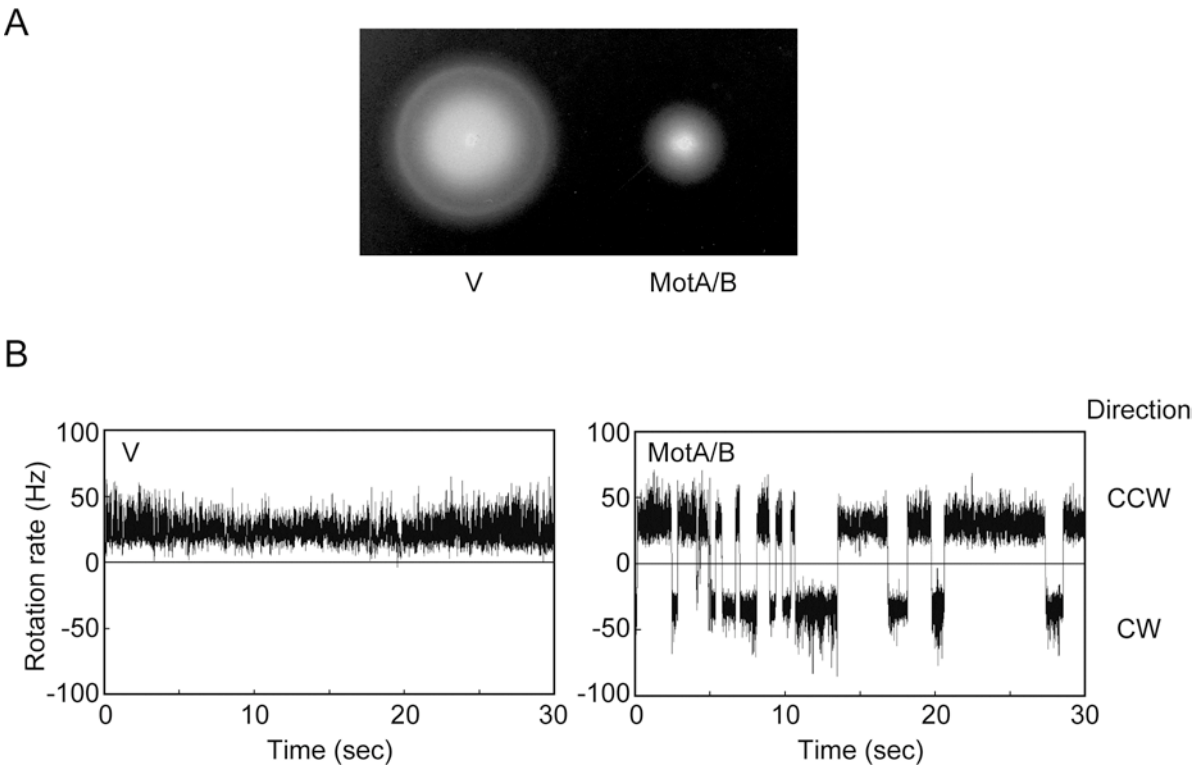

Fig. 1-4. Multicopy effect of MotA/B on motility of wild-type cells. (A) Motility of MMPH001 cells transformed with pKK223-3 (V) and pKSS13 (MotA/B) in tryptone semi-solid agar. Plates were incubated for 6 h at 30°C. (B) Measurement of CCW and CW rotation of a flagellar motor using the bead assays with 1.5 μm polystyrene beads.

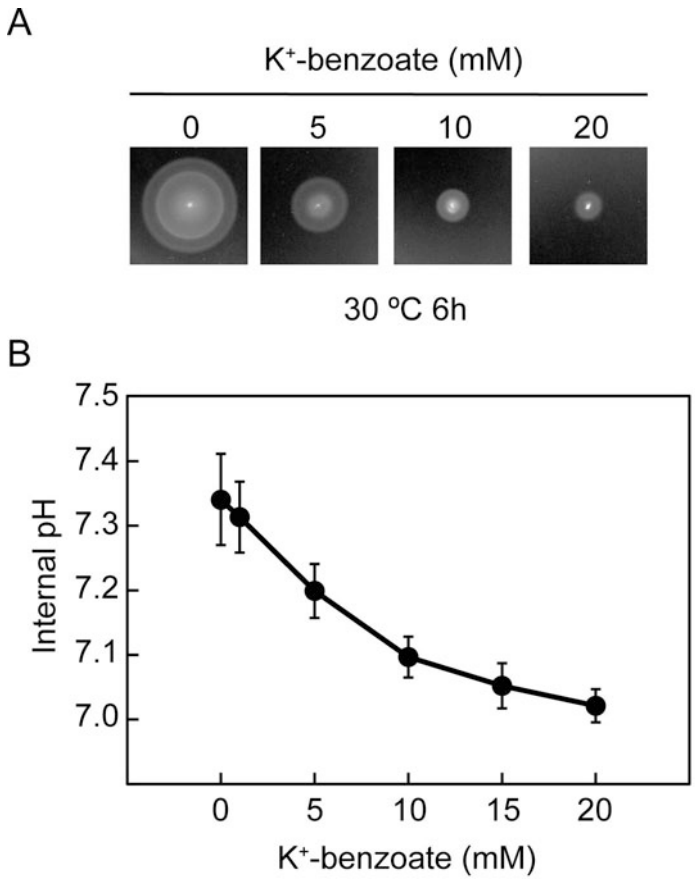

Fig. 1-5. Effects of motility and intracellular pH on wild-type cells in the presence of various concentrations of potassium benzoate at external pH 7.0. (A) Colonies of MMPH001 cells in tryptone semi-solid agar at pH 7.0 with 0, 5, 10, and 20 mM potassium benzoate. Plates were incubated at 30ºC for 6h. (B) Intracellular pH was measured with the pHluorin probe.

Table 1-1. Strains used in Chapter 1

Strains	Relevant characteristics	Source or reference
E. coli		
NovaBlue	Recipient for cloning experiments	Novagen
BL21(DE3) pLysS	T7 expression host	Novagen
Salmonella		
JR501	For converting plasmids to *Salmonella* compatibility	Ryu and Hartin (1990)
SJW1103	Wild type for motility and chemotaxis	Yamaguchi *et al*. (1984)
SJW46	*fliC*(Δ204-292)	Yoshioka *et al*. (1995)
SJW2241	Δ(*motA-motB*)	Komoriya *et al*. (1999)
SJW3076	Δ(*cheA-cheZ*)	Osawa and Imae (1983)
MMPH001	Δ*araBAD::pHluorin*	Morimoto *et al*. (2010a)
YVM021	Δ*fliC::pHluorin*	Morimoto *et al*. (2010a)

Table 1-2. Plasmids used in Chapter 1

Plasmids	Relevant characteristics	Source or reference
pKK223-3	Cloning vector	GE Healthcare
pTrc99A	Cloning vector	GE Healthcare
pBAD24	Cloning vector	Guzman *et al*. (1995)
pKSS13	pKK223-3 / MotA+MotB	Morimoto *et al*. (2010a)
pKSS13(D33N)	pKK223-3 / MotA+MotB(D33N)	Morimoto *et al*. (2010a)
pYC001	pKK223-3 / pHluorin	Nakamura *et al*. (2009a)
pNSK9	pTrc99A / MotA+MotB	Che *et al*. (2008)
pTSK30	pTrc99A / MotA+MotB(Δ51-100)	Kojima *et al*. (2009)
pTSK30(L119P)	pTrc99A / MotA+MotB(Δ51-100/L119P)	Kojima *et al*. (2009)
pTSK30(L119E)	pTrc99A / MotA+MotB(Δ51-100/L119E)	Kojima *et al*. (2009)
pYC20	pBAD24 / MotA+MotB	Morimoto *et al*. (2010a)
pYC109	pBAD24 / MotA+MotB(Δ52-71)	Morimoto *et al*. (2010a)
pGST-pHluorin	pGEX2T / GST-pHluorin	Miesenböck *et al*. (1998)

Table 1-3. Primers used in Chapter 1

Primers	Sequence
FliC-tetR	gcaacagcccaataacatcaagttgtaattgataaggaaattaagacccactttcacatt
FliC-tetA	cgctgccttgattgtgtaccacgtgtcggtgaatcaatcgctaagcacttgtctcctg
FliC-pH-Fw	cagcccaataacatcaagttgtaattgataaggaaaagatcatgagtaaaggagaagaac
FliC-pH-Rv	gccttgattgtgtaccacgtgtcggtgaatcaatcgccggattatttgtatagttcatcc

Chapter 2. Charged residues in the cytoplasmic loop of MotA are required for stator assembly into the bacterial flagellar motor

Introduction

The proton channel of the MotA/B complex is also regulated to open only upon stator assembly by the plug segment consisting of residues 53-66 of MotB, which is just after its single transmembrane segment. The deletion of the plug segment results in proton leakage through free MotA/B complexes not assembled into the motor and thereby impairs cell growth [Hosking *et al*., 2006; Morimoto *et al*., 2010a]. Interestingly, however, the deletion of residues 51-100 of *Salmonella* MotB still allows a functional stator to be formed with MotA [Muramoto and Macnab, 1998; Kojima *et al*., 2009]. But the crystal structure of a $MotB_C$ fragment corresponding to residues 99-276 of MotB indicates that it is too small to reach the PG layer if connected directly to the transmembrane helix by the deletion of residues 51-100, suggesting that a relatively drastic conformational change in the N-terminal portion of $MotB_C$ should occur upon stator assembly to allow the stator to be anchored and open the proton channel [Kojima *et al*., 2009]. Therefore, it is quite possible that an interaction between MotA and FliG initiates the binding of the MotA/B complex to the motor and trigger conformational changes in $MotB_C$.

Although the structures of the entire basal body containing the stators have been visualized by electron cryotomography [Murphy *et al.*, 2006; Liu *et al.*, 2009; Kudryashev *et al.*, 2010], the resolution is still limited. Since the stator is missing in highly purified flagellar basal bodies [Minamino *et al*., 2008], relatively high-resolution structures of the basal body by electron cryomicroscopy and single particle image analysis do not show the binding mode of the stators [Thomas *et al.*, 2006]. Therefore,

it is still unclear how the MotA/B complex is localized to the basal body to be the stator.

To understand the localization mechanism of the MotA/B complex, I investigated the subcellular localization of GFP-MotB and MotA-mCherry by fluorescence microscopy. I show that over-expression of MotA inhibits wild-type motility due to the reduced number of functional stators in the flagellar motor. This suggests that MotA can be installed into the motor even in the absence of MotB. I also show that the R90E mutation in the cytoplasmic loop of MotA significantly affects the subcellular localization of GFP-MotB, suggesting that the electrostatic interaction between the cytoplasmic loop of MotA and FliG is required for the efficient assembly of the stators around the rotor.

Materials and Methods

Media

L-broth (LB), semi-solid agar plates and motility medium were used as described in Chapter 1. Ampicillin was added to LB at a final concentration of 50 μg/ml.

Bacterial strains

All strains used in this chapter are listed in Table 2-1. All the *Salmonella* mutant strains were derived from SJW1103 (wild type for motility and chemotaxis). P22-mediated transduction was carried out as described [Yamaguchi *et al*., 1986]. To construct *Salmonella gfp-fliG, motA-mCherry or gfp-motB strains, the fliG, motA* or *motB* gene on the chromosome was replaced by the *gfp-fliG, motA-mCherry or gfp-motB* allele, respectively, by using the λ Red homologous recombination system developed by Datsenko and Wanner (2000). The *gfp-fliG, motA-mCherry and gfp-motB* alleles are placed under the control of their native promoters. PCR primers used in construction of strains were listed in Table 2-3.

Plasmids construction

All plasmid vectors used in this chapter are listed in Table 2-2. Plasmid expression vectors, pKK223-3 were used for overproduction of proteins, and pTrc99A and pBAD24 for complementation analysis. To construct plasmids carrying point mutations of *motA* and *motB*, site-directed mutagenesis was carried out by the QuikChange Site-directed mutagenesis method as described in the manufacturer's instruction (Stratagene). PCR primers used in site-directed mutagenesis were listed in Table 2-3. Mutations were confirmed by DNA sequencing.

Preparation of whole cell proteins and immunoblotting

Salmonella cells were grown overnight at 30ºC in LB with shaking. Cell pellets were suspended in a SDS-loading buffer and normalized by cell density to give a constant amount of cells. After sodium dodecyl sulfate-polyacrylamide gel electrophoresis (SDS-PAGE), immunoblotting with polyclonal anti-MotA, anti-MotB, anti-GFP (MBL) and anti-RFP (MBL) antibodies was carried out as described in Chapter 1.

Swarming motility assay in semi-solid agars

Fresh colonies were inoculated onto soft tryptone agar plates and incubated at 30°C.

Swimming speed measurement

Salmonella cells were grown at 30°C in LB until the cell density reached an OD_{600} of ca. 1.0. Motility of the cells was observed at ca. 23ºC under a phase contrast microscope (CH40, Olympus) and recorded on hard disk drive. The positions of individual cells were identified using Move-tr/2D software (Library Co., Ltd.) and swimming speed was determined.

Fluorescence microscopy

To observe bacterial cell bodies and epi-fluorescence of GFP, mCherry and tetramethyl rhodamine methyl ester (TMRM), I used an inverted fluorescence microscope (IX-71, Olympus) with a 150× oil immersion objective lens (UApo150XOTIRFM, NA 1.45, Olympus) and an EMCCD camera (C9100-02, Hamamatsu Photonics). Epi-fluorescence was excited by a 100 W ultra-high-pressure mercury lamp (USHIO) with the following fluorescence mirror units: U-MGFPHQ (Olympus) for GFP; U-DM-CY3-2 (Olympus) for TMRM; and mCherry-A (Semrock) for

mCherry. Fluorescence images of GFP and mCherry were captured by the EMCCD camera with every 1-sec exposure. Sequential fluorescence images were also acquired every 100 ms. Fluorescence image processing was done with the ImageJ version 1.42 software (National Institutes of Health).

Labeling of flagellar filaments with a fluorescent dye.

Salmonella cells were attached to a cover slip (Matsunami glass, Japan), and unattached cells were washed away with motility medium. A 1 μl aliquot of polyclonal anti-FliC antibody and 1 μl of anti-rabbit IgG conjugated with Alexa Fluor® 594 (Invitrogen) were suspended in 100 μl of motility medium. A 50 μl aliquot of the buffer containing the fluorescent dye was applied to the cells attached to the cover slip. After washing with motility medium, cells were observed by a fluorescence microscope (Axio Observer, Carl Zeiss Microimaging) with a 100× oil immersion objective lens (αPlan-Apo 100x, NA 1.46, Carl Zeiss Microimaging) and a CCD camera (AxioCam MRm, Carl Zeiss Microimaging).

Measurement of intensities of fluorescent spots of GFP-MotB.

The fluorescence images of GFP-MotB before and after a CCCP treatment for 30 min were subjected to 10 iterations of 2D blind deconvolution using the AutoDeblur software (Media Cybernetics). Then, the intensity of each fluorescent spot was determined by fitting a two-dimensional Gaussian function with an image processing program developed based on the Igor Pro 6 software (WaveMetrics).

Measurement of the membrane potential across the cytoplasmic membrane.

The membrane potential was measured as described by Lo *et al* (2007). Cells were

suspended in motility medium plus 10 mM EDTA for 10min. Cells were washed with motility medium and were incubated in motility medium containing 0.1 μM TMRM (Invitrogen) for 10 min at room temperature. Calculation of the membrane potential was carried out as described [Lo *et al.,* 2007] with minor modifications.

Measurement of intracellular pH.

Intracellular pH measurement with a ratiometric fluorescent pH indicator protein, pHluorin [Miesenböck *et al*., 1998], was carried out at an external pH of 7.0 as described Chapter 1. The fluorescence-excitation spectra of MMPH001 (Δ*araBAD*::*pHluorin*) expressing MotA were recorded by a fluorescence spectrophotometer (RF-5300PC, Shimadzu).

Bead assays

Salmonella MM3076iC cells harboring pKK223-3 or pKSS12 were grown in LB containing ampicillin for 4 hours at 30ºC with shaking. Bead assays with polystyrene beads with diameters of 1.0 and 0.8 μm (Invitrogen) or with fluorescent beads with diameters of 0.5 μm (FluoSpheres® 'yellow/green', excitation 470 nm, emission 518 nm; Invitrogen) and 0.1 μm (FluoSpheres® 'orange', excitation 540 nm, emission 560 nm; Invitrogen) were carried out in Chapter 1. In the measurements using 1.0-μm and 0.8-μm beads, phase contrast images were projected onto a quadrant photodiode and the signals were recorded at 1 msec intervals. In the measurements using 0.5-μm and 0.1-μm fluorescent beads, fluorescence images were captured by an EMCCD camera (iXon, Andor) every 0.4 msec. The torque produced by the flagellar motor was determined as described previously [Sowa *et al.*, 2003]. The frictional drag coefficients of a flagellar filament (f_f) and the bead attached to the filament (f_b) was

determined by the following equations.

$$f_{\mathrm{f}} = \frac{2\pi L r_{\mathrm{f}}^2 \left(2p^2 + 4\pi^2 r_{\mathrm{f}}^2\right)\eta}{\left(p^2 + 4\pi^2 r_{\mathrm{f}}^2\right)\left(\ln\left(2p/d\right) - 0.5\right)}$$

$$f_{\mathrm{b}} = 8\pi\eta r_{\mathrm{b}}^3 + 6\pi\eta r_{\mathrm{b}} r_{\mathrm{r}}^2$$

η = 9.6 x 10^{-4} Ns/m^2 (at 25ºC) , L = 4 μm, r_{f} = 200 nm, p = 2.3 μm, d = 10 nm, r_{b} and r_{r} are the viscosity of the motility media, the filament length, the helical radius, the helical pitch, the radius of the filament, the radius of the bead and the radius of bead rotation, respectively. As the frictional drag coefficient is the sum of f_{f} and f_{b}, the torque was calculated by $T = \omega(f_{\mathrm{f}} + f_{\mathrm{b}})$, where ω is the angular velocity. To produce speed histograms, the rotation rate of each cell was sampled at 1 kHz for 10 sec and the average speed was determined from a power spectrum using 1-sec long data windows (1024 points) at 0.1 sec intervals (speed resolution was about 1 Hz) as described by Reid *et al*. (2006). The data analyzed by a program developed based on the Igor Pro 6 software. All the experiments were done at ca. 23ºC.

Results

Effect of the motB(D33N) mutation on the subcellular localization of the stator complex

A highly conserved aspartic acid residue of *Vibrio* PomB, Asp-24, is thought to be a Na^+-binding site. The D24N mutation in PomB abolishes polar localization of the PomA/B complex, suggesting that the binding of Na^+ to Asp-24 is critical for stator assembly into the motor [Fukuoka *et al*., 2009]. In contrast, the *E. coli motB*(D32N) and *motB*(D32A) alleles, which are non-functional, exert a strong negative-dominant effect on motility of wild-type cells, suggesting that the MotA/B(D32N) and MotA/B(D32A) complexes can be installed into the motor [Zhou *et al*., 1998b; Kojima and Blair, 2001]. Therefore, to investigate whether analogous D33N and D33A mutations of *Salmonella* MotB affect stator assembly, I constructed *Salmonella* strains that encode either GFP-MotB, GFP-MotB(D33N) or GFP-MotB(D33A) on the chromosome under the control of the promoter of the *motAB* operon and analyzed their subcellular localization by fluorescence microscopy (Fig. 2-1). In agreement with a previous report [Leake *et al*., 2006], GFP-MotB was partially functional (Fig. 2-1A). Most of the GFP-MotB molecules were intact in the cells as judged by immunoblotting with polyclonal anti-MotB antibody although a very faint band of MotB was seen as a cleaved product (Fig. 2-1B). To examine the subcellular localization of GFP-MotB, cells expressing GFP-MotB were observed by epi-illumination fluorescence microscopy (Fig. 2-1C). I used a *Salmonella* strain encoding GFP-FliG as a positive control because FliG forms part of the C ring [Francis *et al*., 1994]. This strain was also partially functional (Fig. 2-1A) and GFP-FliG was mostly intact in the cell (Fig. 2-1B). Fluorescent spots of GFP-FliG and GFP-MotB were observed within the cell bodies of each strain (Fig. 2-1C). Some spots of GFP-FliG and GFP-MotB were

observed at the center of rotation of cells tethered to a cover slip by a single flagellar filament. In agreement with this, the fluorescent spots of GFP-FliG and GFP-MotB were observed at the base of the filament labeled with a fluorescent dye (Fig. 2-1D). In contrast, when GFP-MotB was expressed in the *fliF flgM* double mutant, which allows GFP-MotB to be expressed from the *motAB* promoter even in the presence of the *fliF* mutation [Kutsukake and Iino, 1994], no spots were detected, and only diffuse fluorescent signals were observed throughout the cell body (Fig. 2-9A). These results demonstrate that the GFP-labelled MotA/B complex can be installed into the motor. The D33N and D33A mutations caused a loss-of-function of GFP-MotB (Fig. 2-1A), in agreement with a previous report [Zhou et al., 1998b]. However, these mutations did not affect the subcellular localization of GFP-MotB (Fig. 2-1C and D). These results suggest that proton binding to Asp-33 of MotB is not critical for stator assembly around the rotor.

Na^+ motive force across the cytoplasmic membrane is critical for polar localization of the PomA/B complex [Fukuoka *et al*., 2009]. Therefore, I investigated whether PMF is required for the subcellular localization of GFP-labeled stators. Since PMF can be collapsed by a protonophore, CCCP, I analyzed the effect of CCCP on stator assembly (Fig. 2-2). In the presence of 50 μM CCCP, the rotation of tethered cells expressing GFP-MotB was totally inhibited (Fig. 2-2B), indicating that PMF is totally collapsed. However, the number and the intensity of the fluorescent spots of GFP-MotB were both mostly unchanged by a CCCP treatment for 30 min (Fig. 2-2A, Table 2-4). Interestingly, new fluorescent spots occasionally appeared over the treatment period. When CCCP was removed by replacing the motility buffer, the tethered cells rotated again (Fig. 2-2B). These results suggest that PMF is not required for stator assembly around the rotor in the proton-driven flagellar motor.

Multicopy effect of MotA on motility of wild-type cells

To test if MotA alone can be installed into a motor, I first analyzed the multicopy effect of MotA on motility of wild-type cells in semi-solid agar plates. When MotA was overproduced (Fig. 2-3A, lane 2), the swarming size decreased significantly compared to the vector control (Fig. 2-3B). I also measured free-swimming motility in liquid media by phase contrast microscopy and found that the swimming speed of the cells over-expressing MotA was significantly reduced (Fig. 2-3C). In agreement with a previous report [Wilson and Macnab, 1988], cell growth was not impaired by the over-expression of MotA (Fig. 2-4A). Consistently, neither membrane potential nor intracellular pH was changed by the over-expression (Fig. 2-4B), indicating that PMF across the cytoplasmic membrane was not affected either. Therefore, I conclude that the poor motility of the cells over-expressing MotA is not a consequence of either growth impairment or reduced PMF.

MotA interacts with FliG, which is not only responsible for torque generation and the switching of rotational direction of the motor but is also needed for export of flagellar proteins [Yamaguchi *et al*., 1986; Minamino and Macnab, 1999]. To test whether excess MotA might titrate FliG away from the motor, resulting in the inhibition of flagellar protein export, I observed wild-type cells over-expressing MotA by high-intensity dark-field light microscopy and found that the number of flagellar filaments was not affected (data not shown). Chemotactic behavior was also not changed (data not shown). These results indicate that the reduced motility is neither due to reduction in the flagellar protein export activity nor increase in the probability of CW-biased rotation.

To investigate whether the poor motility is due to a reduced torque, I next carried out bead assays of motor rotation with polystyrene and fluorescent beads (Fig.

2-5 and Table 2-5). The torque-speed relationships of *Salmonella* MM3076iC cells over-expressing MotA are shown in Fig. 2-5A in comparison with a vector control. Rotation rates of the motors of the cells over-expressing MotA were reduced over the entire range of observation under various amounts of load. The zero-speed torque, as obtained by zero-speed extrapolation of the torque-speed curve, was ca. 60% of the vector control. The zero-torque speeds as deduced by extrapolation of the regression lines also decreased from 225 Hz of the vector control to 145 Hz when MotA was over-produced. The torque at high load is dependent on the number of stators while the motor speed near zero load is independent of the number of functional stators. [Ryu *et al*., 2000; Reid *et al*., 2006; Yuan and Berg, 2008]. These results suggest that free MotA can be installed into the motor to reduce torque even without forming the MotA/B complex and also inhibit high-speed rotation at near zero load. It is also possible that excess MotA may induce the formation of anomalous stator complexes, thereby disturbing motor function.

Multicopy effect of MotA on the subcellular localization of GFP-labeled stators

To test whether over-expression of MotA actually reduces the number of functional stators in a rotating flagellar motor, I analyzed the multicopy effect of MotA on the subcellular localization of GFP-MotB (Fig. 2-6A). When both MotA and MotB were expressed in the GFP-MotB encoding strain (Fig. 2-6B, lane 3), the fluorescent spots of GFP-MotB drastically decreased (Fig. 2-6A, top right) compared to the vector control (Fig. 2-6A, top left), indicating that non-labeled MotB molecules assembles into the motor along with MotA. Over-expression of MotA also reduced not only the number of fluorescent spots of GFP-MotB but also their fluorescence intensity although not to the levels seen in the cells over-expressing MotA/B (Fig. 2-6A, top

middle). In contrast, when MotA alone or MotA/B was over-expressed in the GFP-FliG encoding strain, the number of GFP-FliG spots was not changed (Fig. 2-6A, bottom row). These results suggest that a certain number of the MotA/GFP-MotB complexes are replaced with MotA in the motor.

To estimate the number of functional stators in the motor of *Salmonella* cells over-expressing MotA, the position of the bead was determined at a sampling rate of 1 kHz for 10 sec, and the rotation rates were determined from the power spectra calculated from 1-sec long data windows that were shifted every 0.1 sec over the entire 10 sec data (Fig. 2-5B). The vector control showed a relatively narrow distribution in the speed histogram with the speed ranging from 40 to 80 Hz (Fig. 2-5B, left). Since a single stator unit can drive the proton-driven flagellar motor labeled with 1.0-μm beads at ca. 7 Hz (Reid *et al*., 2006; Nakamura *et al*., 2010), the maximum number of stators in the fully functional motor is estimated to be 11, in agreement with a previous report [Ryu *et al*, 2000]. In contrast, the motor speeds of MotA-expressing cells were distributed over a wide range from 15 to 70 Hz and also showed several distinct peaks separated by a roughly equal interval of around 7 Hz in the histogram (Fig. 2-5B, right). These results let us assume that the number of functional stators decreased to 5 ± 3 by the over-expression of MotA.

Fluorescence microscopy observation of MotA-mCherry

To obtain more direct evidence that MotA can assemble into the motor even in the absence of MotB, I constructed *Salmonella* YVM018 strain (*gfp-fliG*, *motA-mCherry,* Δ*motB*) with or without MotB expressed from a pTrc99A-based plasmid, and analyzed the subcellular co-localization of MotA-mCherry and GFP-FliG by epi-fluorescence microscopy (Fig. 2-7). MotA-mCherry was not functional (data not shown). However,

fluorescent spots of MotA-mCherry were occasionally observed at the same position as those of GFP-FliG whether MotB is present or not (Fig. 2-7A and 7B), although the probability of fluorescent-spot observation of MotA-mCherry was much less than that of GFP-MotB, presumably due to its-loss-function phenotype. When MotA-mCherry was expressed in the *fliF flgM* double mutant background, only diffuse fluorescent signals were observed throughout the cell body (Fig. 2-9B). These results suggest that MotA can be incorporated into the flagellar motor to some extent even without MotB and that the localization of MotA is dependent on its interaction with other components of the flagellar motor.

Effect of the MotA(R90E) mutation on the motility

Two charged residues, Arg-90 and Glu-98, which are in the cytoplasmic loop of MotA, are thought to interact with charged residues of FliG for torque generation [Zhou and Blair, 1997; Zhou *et al*., 1998]. It has been reported that the *motA*(R90E) and *motA*(E98K) alleles are recessive, although the MotA(R90E) and MotA(E98K) proteins are as stable as wild-type MotA [Zhou and Blair, 1997]. These results suggest that these mutant proteins are not efficiently incorporated into the motor. Since it has been shown that there is fundamental difference between *E. coli* and *Salmonella* flagellar motors [Nakamura *et al*., 2009b], I analyzed the effects of the *Salmonella* MotA(R90E) and MotA(E98K) mutations on the motility in liquid media (Fig. 2-8A and B). When the expression levels of MotA(R90E) and MotB was almost the same as those expressed from the chromosome of wild-type cells, almost all of the cells expressing the MotA(R90E)/B complex was nonmotile. However, an increment of the expression level of MotA(R90E)/B allowed about 70% of the cells to become motile, and their swimming speed reached about 60% of the wild-type levels. To test whether

no motility of the *motA*(R90E) mutant under low induction condition is due to the poor assembly of the MotA(R90E)/B complex around the rotor, I constructed the *Salmonella motA*(R90E), *gfp-motB* strain and analyzed the subcellular localization of GFP-MotB. The MotA(R90E) substitution drastically decreased both the number and intensity of the fluorescent spots of GFP-MotB (Fig. 2-8C), although the expression level of GFP-MotB was not changed (Fig. 2-8D). These suggest that the R90E mutation just reduces the binding affinity of the stator to the rotor. In contrast, the *motA*(E98K) allele was non-functional even under high-induction condition and did not exert any dominant negative effect on wild-type motility (data not shown), in agreement with a previous report [Zhou and Blair, 1997]. This indicates that Glu-98 is critical for the assembly of the MotA/B complex into the motor.

Discussion

MotB consists of the N-terminal cytoplasmic region, one transmembrane helix, and the C-terminal periplasmic region named $MotB_C$, which contains the PG-binding motif [Berg, 2003; Kojima and Blair, 2004; Sowa and Berry, 2008]. Since the $MotB_C$ fragment inhibits motility of wild-type cells when exported into the periplasm, $MotB_C$ is proposed to be required for proper targeting and stable anchoring of the MotA/B complex to the motor [Kojima *et al*., 2008]. The stators can be replaced even during motor rotation, indicating that the stator does not permanently bind to the motor and the peptidoglycan layer [Leake *et al*., 2006]. The proton-conductivity of free MotA/B complexes is suppressed by the plug segment in the $MotB_C$ region when they are not associated with the motor as described in Chapter 1[Hosking *et al*., 2006; Morimoto *et al*., 2010a]. However, since the MotA/B complex is not co-purified with the hook-basal body [Minamino *et al*., 2008], it remains unclear how the MotA/B complex finds and assembles into the motor and activates its proton-conductivity to become a functional stator. In the present study, I analyzed the multicopy effect of MotA on the torque-speed relationships of the flagellar motor and the subcellular localization of GFP-labeled stators and obtained evidence suggesting that MotA can be installed into the flagellar motor even in the absence of MotB.

MotA/B(D33N) and MotA/B(D33A) can assemble into the motor

Stator assembly in a Na^+-driven flagellar motor responds to Na^+ concentration [Fukuoka *et al*., 2009; Paulick *et al*., 2009]. Mutations in the amino acid residues of PomB involved in the Na^+-relay mechanism significantly interfere with the polar localization of the PomA/B complex [Fukuoka *et al*., 2009]. In this study, I found that the *motB*(D33N) and *motB*(D33A) mutations, which abolish proton translocation

through the proton channel [Zhou *et al*., 1998b; Morimoto *et al*., 2010a], does not affect the localization of GFP-MotB at the base of the flagellar filament (Fig. 2-1). This is in agreement with previous data showing that *E. coli* MotB(D32N) and MotB(D32A) exert a negative dominant effect on wild-type motility [Zhou *et al*., 1998b; Kojima and Blair, 2001]. Therefore, stator assembly in the proton-driven motor is not dependent on the proton conductive activity of the MotA/B complex.

It has been reported that the stators of the Na^+-driven motor detach from the rotor when motor is de-energized and stopped [Sowa *et al*., 2005; Fukuoka *et al*., 2009]. In this study, the treatment of the proton-driven motor by 50 μM CCCP, which totally inhibited the rotation of tethered cells, did not affect the subcellular localization of GFP-MotB (Fig. 2-2), suggesting that the GFP-labeled stators remain to exist around the rotor even in the absence of PMF. In agreement with this, it has been shown that the stator actually switches its functional state between the active and inactive ones without detaching from the rotor completely when PMF is largely reduced [Nakamura *et al*., 2010]. Therefore, I conclude that the assembly of the MotA/B complex into the motor is not obligatorily linked to the process of the proton translocation through the proton channel of the MotA/B complex.

Over-expression of MotA inhibits motility of wild-type cells

It has been shown that the in-frame deletion of residues 51-100 in *Salmonella* MotB does not markedly impair motility [Muramoto and Macnab, 1998; Kojima *et al*., 2009]. In agreement with this, the flagellar motors produced torque at wild-type level upon full induction of the MotA/B(Δ51-100) complex from an IPTG-inducible promoter [S. Nakamura, unpublished data], suggesting that MotA/B(Δ51-100) can be properly incorporated into the motor. However, the crystal structure of a $MotB_C$ fragment

corresponding to residue 99-276 of MotB is so small that MotB(Δ51-100) cannot reach the PG layer if the fragment is directly connected to the transmembrane helix by the deletion of residues 51-100 [Kojima *et al*., 2009], raising the question of how the MotA/B complex finds the stator-binding site on the motor. Here, I showed that over-expression of MotA greatly reduces wild-type motility both in semi-solid agar plates and in liquid media (Fig. 2-3). Neither the growth rate (Fig. 2-4A), flagellation (data not shown), nor chemotactic behavior (data not shown) was changed by over-expression of MotA. However, the torque-speed relationship of the flagellar motor was significantly affected (Fig. 2-5). The rotation rate of the proton-driven motor at a given load is proportional to PMF [Gabel and Berg, 2003]. Since neither the membrane potential nor the transmembrane proton gradient was changed by over-expression of MotA (Fig. 2-4B), the approximately 40% reduction in the zero-speed torque by over-production of MotA is not the consequence of reduced PMF. Since the zero-speed torque is dependent on the number of functional stators in the motor [Ryu *et al*., 2000; Reid *et al*., 2006], this suggests that MotA occupies the stator-binding sites of the motor and reduces the number of functional stators. This is further supported by my data showing that over-expression of MotA reduces not only the number of the fluorescent spots of GFP-MotB but also their fluorescence intensity compared to the vector control (Fig. 2-6) and that MotA-mCherry is localized at the base of the flagellum to some extent even in the absence of MotB (Fig. 2-7). I therefore conclude that MotA alone can be installed into the motor. Interestingly, high-speed rotation at near zero load was also decreased by over-expression of MotA (Fig. 2-5). Since one stator unit can spin the motor at the same speed as many stators do at near zero load [Ryu *et al*., 2000; Yuan and Berg, 2008], I suggest that MotA incorporated into the motor may attach to the rotor and somehow interfere with

high-speed rotation.

Two charged residues of *E. coli* MotA, Arg-90 and Glu-98, are involved in electrostatic interactions with charged residues of FliG for torque generation [Zhou and Blair, 1997; Zhou *et al*., 1998]. It has been reported that the *motA*(R90E) and *motA*(E98K) alleles are recessive [Zhou and Blair, 1997], suggesting that these mutant proteins are not efficiently incorporated into the motor. Consistently, I also found that *Salmonella motA*(R90E) and *motA*(E98K) mutants displayed essentially the same phenotype as those of *E. coli* when their expression levels were the same as those of wild-type cells (Fig. 2-8). Interestingly, however, an increase in the expression level of the MotA(R90E)/B complex by more than 10-fold allowed 70% of the cells to swim in liquid media. It was confirmed by markedly decreased number and intensity of fluorescent spots of GFP-MotB (Fig. 2-8C and D) that no motility of the *motA*(R90E) mutant results from poor stator assembly around the rotor when the expression level of MotA(R90E)/MotB was the same as that of MotA/B expressed from the chromosome. Since the loss-of-function phenotype of the *motA*(R90E) and *motA*(E98K) alleles are considerably suppressed by the *fliG*(D289K) and *fliG*(R281V) mutations, respectively [Zhou *et al*., 1998], my present results suggest that the interactions between MotA Arg-90 and FliG Asp-289 and between MotA Glu-98 and FliG Arg-281 are critical not only for torque generation but also for the assembly of the stators into the motor.

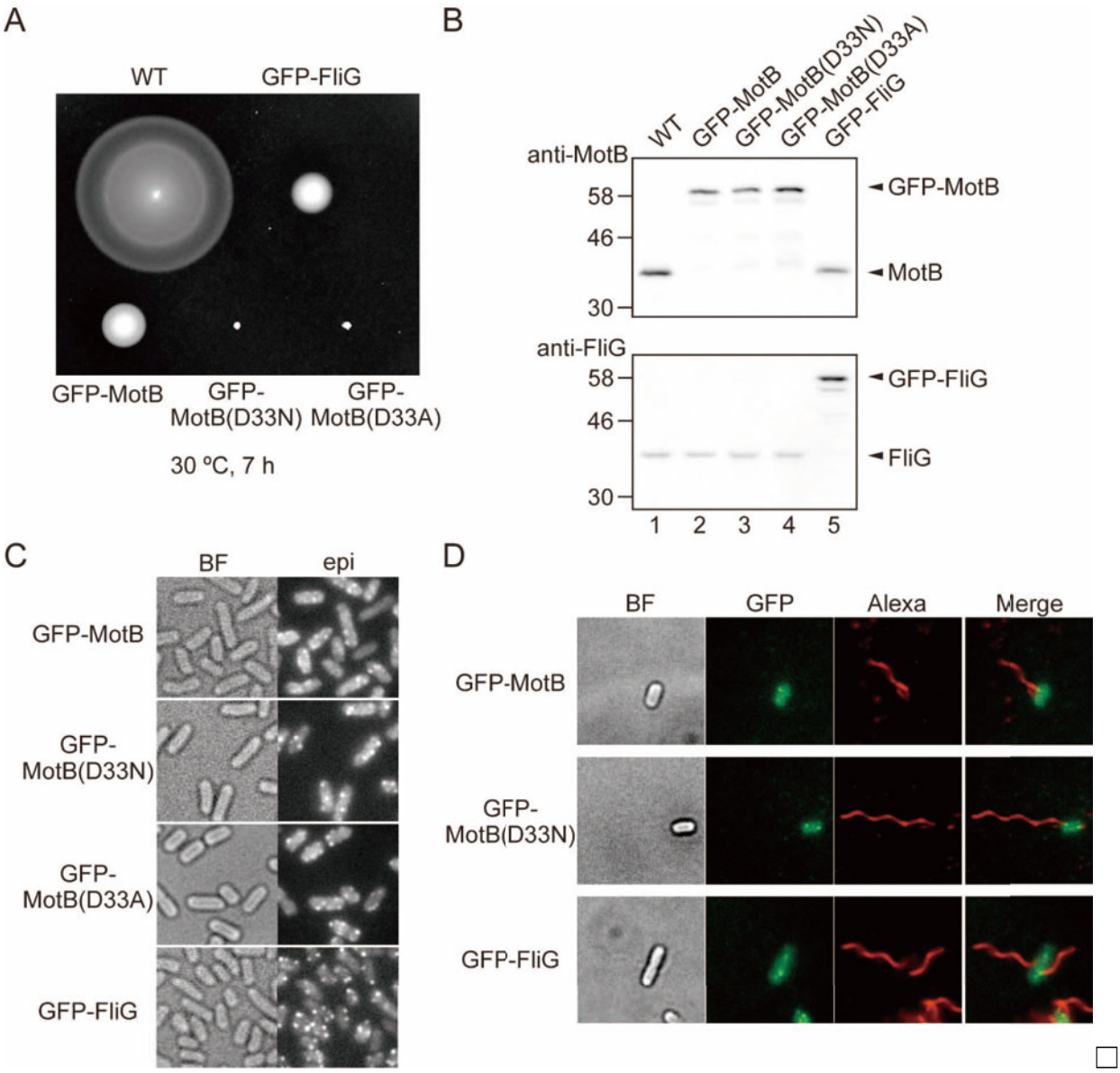

Fig. 2-1. Effect of the motB(D33N) mutation on the subcellular localization of GFP-MotB. (A) Swarming motility of SJW1103 (wild-type, indicated as WT), YVM003 (GFP-MotB), YVM004 (GFP-FliG), YVM007 (GFP-MotB(D33N)) and YVM030 (GFP-MotB(D33A)) in semi-solid agar plates. Plates were incubated at 30ºC for 7 h. (B) Immunoblotting, using polyclonal anti-MotB (upper panel) and anti-FliG (lower panel) antibodies, of whole cellular proteins prepared from the same cells. The positions of molecular mass markers (kDa) are shown on the left. Arrowheads indicate the positions of MotB, GFP-MotB, FliG and GFP-FliG. (C) Fluorescence (epi) and bright field images (BF) of YVM003 (GFP-MotB), YVM004 (GFP-FliG), YVM007 (GFP-MotB(D33N)) and YVM030 (GFP-MotB(D33A)). The cells were grown overnight in LB at 30ºC and observed by fluorescence microscopy. (D) Co-localization of GFP-MotB, GFP-MotB(D33N) and GFP-FliG with the flagellar filaments labeled with the Alexa fluorescent dye. The cells were treated with polyclonal anti-FliC antibody and Alexa Fluor 594-conjugated anti-rabbit secondary antibody. The fluorescence images of GFP-MotB, GFP-MotB(D33N) and GFP-FliG (green) and the filament labeled with Alexa (red) were merged in the right panel.

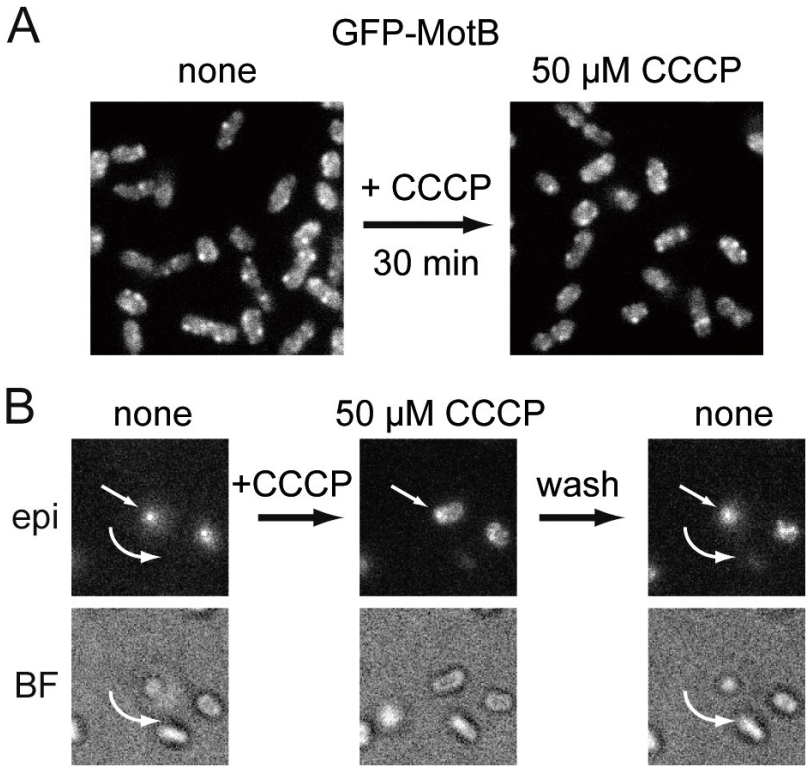

Fig. 2-2. Effect of CCCP on the subcellular localization of GFP-MotB. (A) Fluorescence images of YVM003 (GFP-MotB) before and after the treatment with 50 μM CCCP for 30 min at room temperature. (B) Bright field (BF) and fluorescence (epi) images of tethered rotational GFP-MotB cell. When the tethered cell was treated with 50 μM CCCP, and the rotation immediately stopped. After washing by the motility medium without CCCP, the rotation restarted. White straight arrows indicate the fluorescent spot at the center of rotation. Arc-shaped arrows indicate the rotation of the cell by which the image of the cell body is blurred.

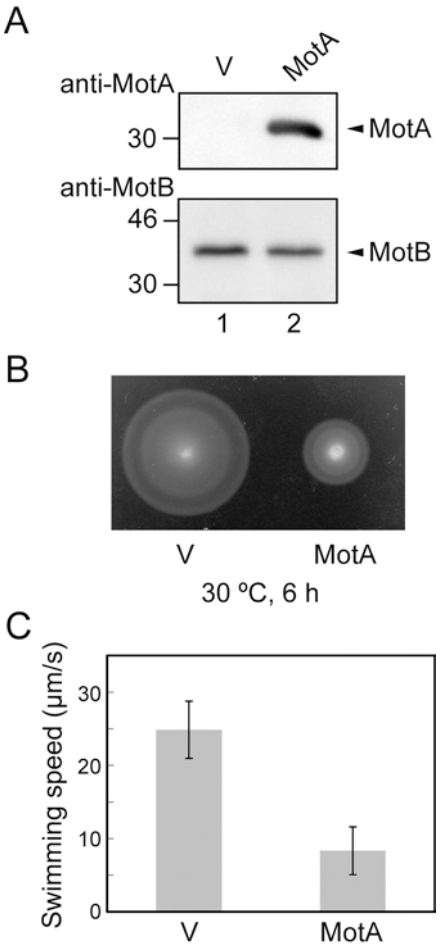

Fig. 2-3. Multicopy effect of MotA on motility of wild-type cells. (A) Immunoblotting, using polyclonal anti-MotA and anti-MotB antibody, of whole cell proteins prepared from the same transformants. The positions of molecular mass markers (kDa) are shown on the left. Arrowheads indicate the positions of MotA and MotB. Since our polyclonal anti-MotA antibody cannot detect the chromosomal expression level of MotA, no band of MotA was seen in lane 1. (B) Swarming motility assay of SJW1103 (wild-type) transformed with pKK223-3 (Vector, V) and pKSS12 (MotA) on soft agar plates. The plates were incubated at 30ºC for 6 h. (C) Free-swimming speed measured by phase contrast microscopy. Measurements were done at ca. 23ºC. Vertical bars are standard errors.

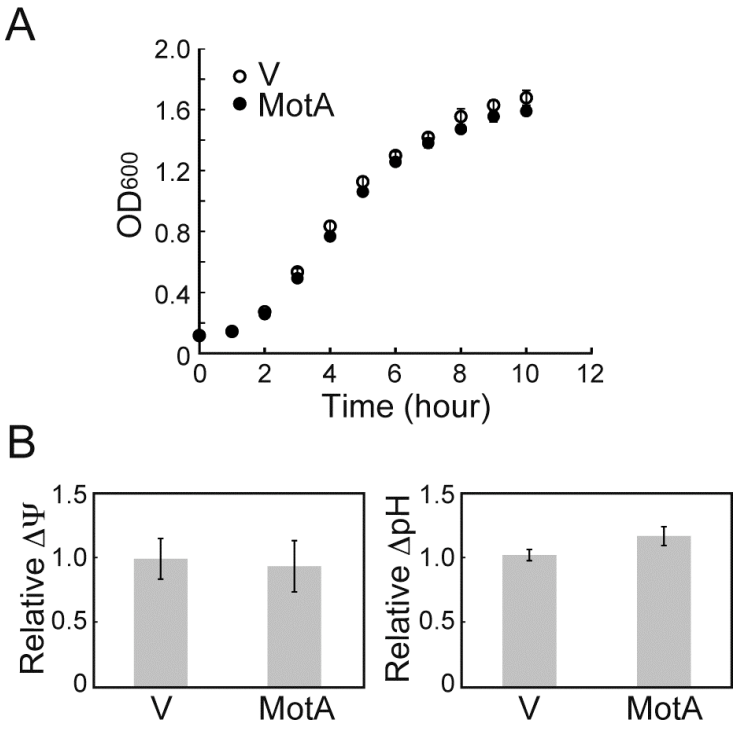

Fig. 2-4. Effect of MotA-overproduction on growth rate and the proton motive force across the cytoplasmic membrane. (A) Growth curve of the wild-type strain SJW1103 transformed with pKK223-3 (V) (open circles) or pKSS12 (MotA) (closed circles). The cells were grown in T-broth at 30° C with shaking. The optical density at 600 nm (OD_{600}) was measured. (B) Relative membrane potential ($\Delta\psi$) and transmembrane proton gradient (ΔpH). The membrane potential was measured using TMRM. Intracellular pH was measured with pHluorin at an external pH of 7.0. Both $\Delta\psi$ and ΔpH are normalized to those of the vector control. The $\Delta\psi$ of the cells harboring pKK223-3 or pKSS12 is the average of 135 cells and 111 cells, respectively. The data of ΔpH is the average of 6 independent experiments. Vertical bars indicate standard errors.

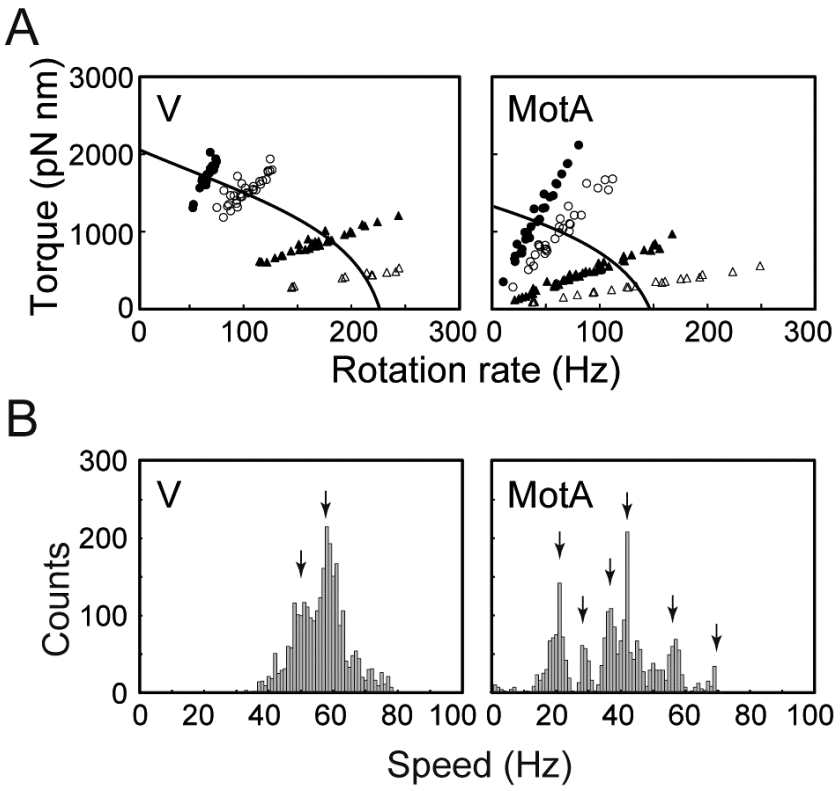

Fig. 2-5. Effect of MotA-overproduction on the torque-speed relationship of the flagellar motor. (A) Torque-speed curve of MM3076iC [Δ(*cheA-cheZ*), *fliC*(Δ204-292)] carrying pKK223-3 (left panel) or pKSS12 (MotA) (right panel). Rotation measurements of individual flagellar motors were carried out by tracking the position of 1.0-μm (closed circle), 0.8-μm (open circle), 0.5-μm (closed triangle) and 0.1-μm beads (open triangle) attached to the sticky flagellar filament. All the measurements were done at ca. 25ºC. (B) Speed histogram of MM3076iC carrying pKK223-3 (left) or pKSS12 (right). Rotation rates of single flagellar motors labeled with 1.0-μm beads were determined from the power spectrum using 1 sec data windows (1024 points) at an interval of 0.1 sec (Table 2-5). Arrows indicate peaks of rotation rates that are likely to correspond to different numbers of functional stators in the motor (Reid *et al.*, 2006).

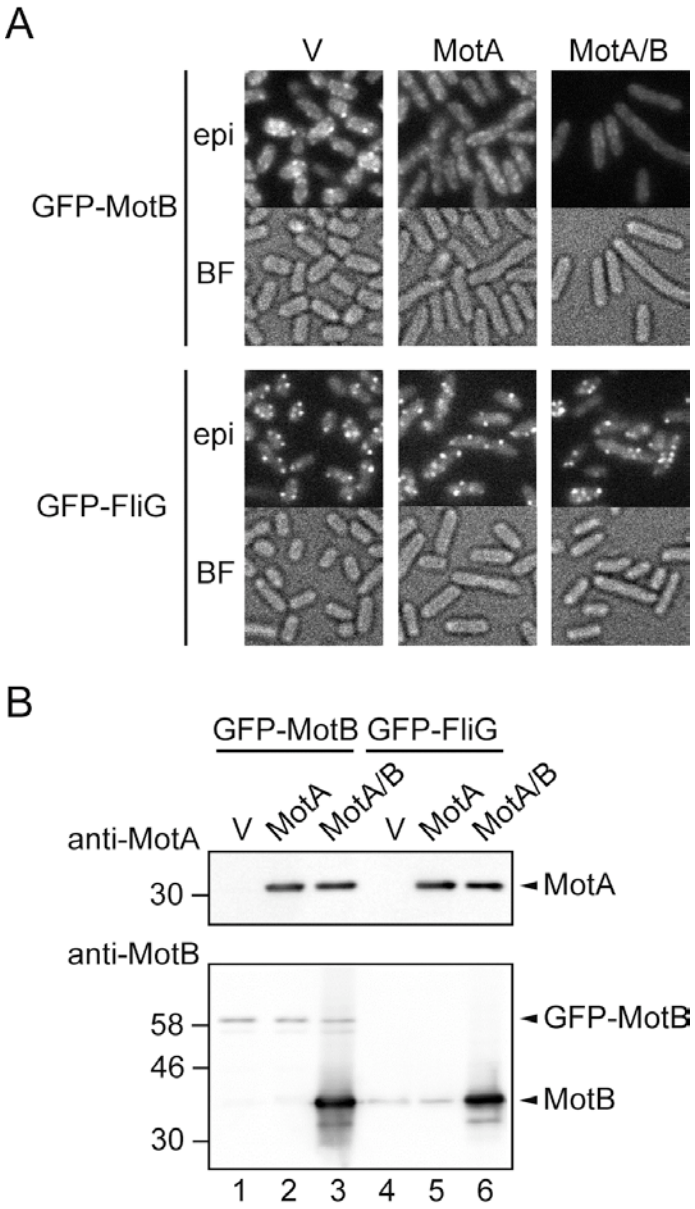

Fig. 2-6. Multicopy effect of MotA on the subcellular localization of GFP-MotB and GFP-FliG. (A) Fluorescence (epi) and bright field images (BF) of the *Salmonella* YVM003 (*gfp-motB*) and YVM004 (*gfp-fliG*) strains transformed with pKK223-3 (V), pKSS12 (MotA) and pKSS13 (MotA/B). The cells were grown overnight at 30ºC and observed by fluorescence microscopy. (B) Immunoblotting, using polyclonal anti-MotA (upper panel) and anti-MotB (lower panel) antibodies, of whole cell proteins prepared from the same transformants. Lane 1, YVM003 carrying pKK223-3; lane 2, YVM003 harboring pKSS12; lane 3, YVM003 carrying pKSS13; lane 4, YVM004 carrying pKK223-3; lane 5, YVM004 harboring pKSS12; lane 6, YVM004 carrying pKSS13. Arrowheads indicate the positions of MotA, MotB and GFP-MotB.

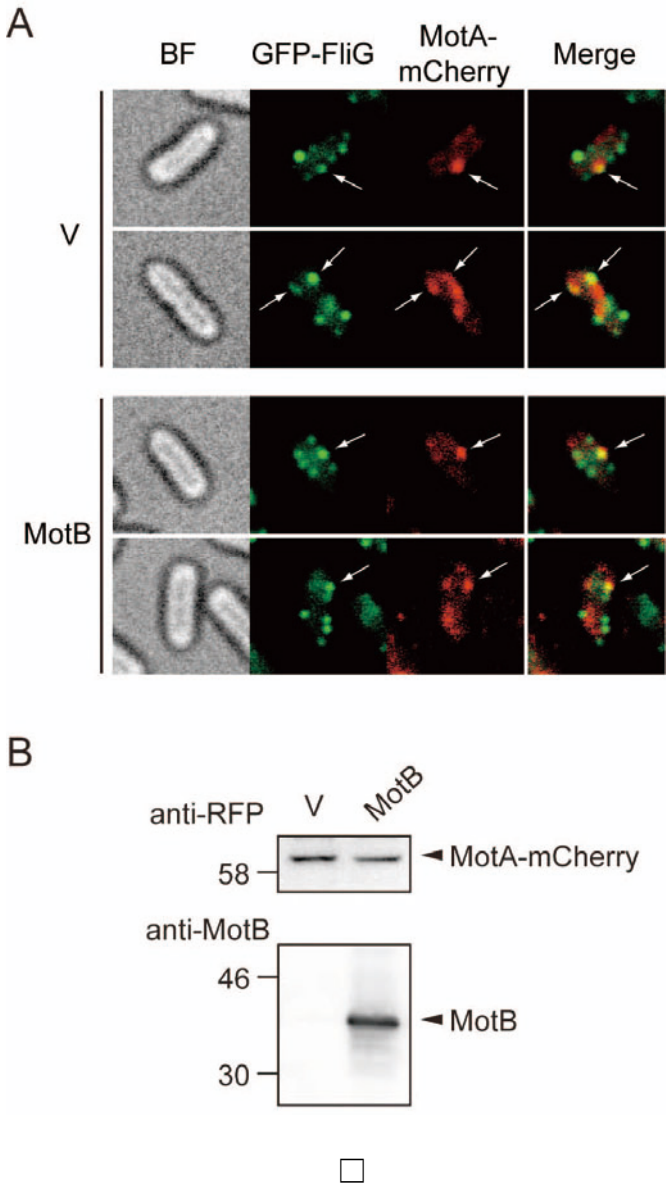

Fig. 2-7. Subcellular localization of MotA-mCherry. (A) Fluorescence images of YVM018 (*gfp-fliG, motA-mCherry, ΔmotB*) transformed with pTrc99A (V) or pHMK1602 (MotB). The cells were grown in LB at 30ºC for 5 hours and observed by fluorescence microscopy. The fluorescence images of GFP-FliG (green) and MotA-mCherry (red) were merged in the right panel. (B) Immunoblotting, using polyclonal anti-RFP (upper panel) and anti-MotB (lower panel) antibodies, of whole cell proteins prepared from the same transformants. Arrowheads indicate the positions of MotA-mCherry and MotB.

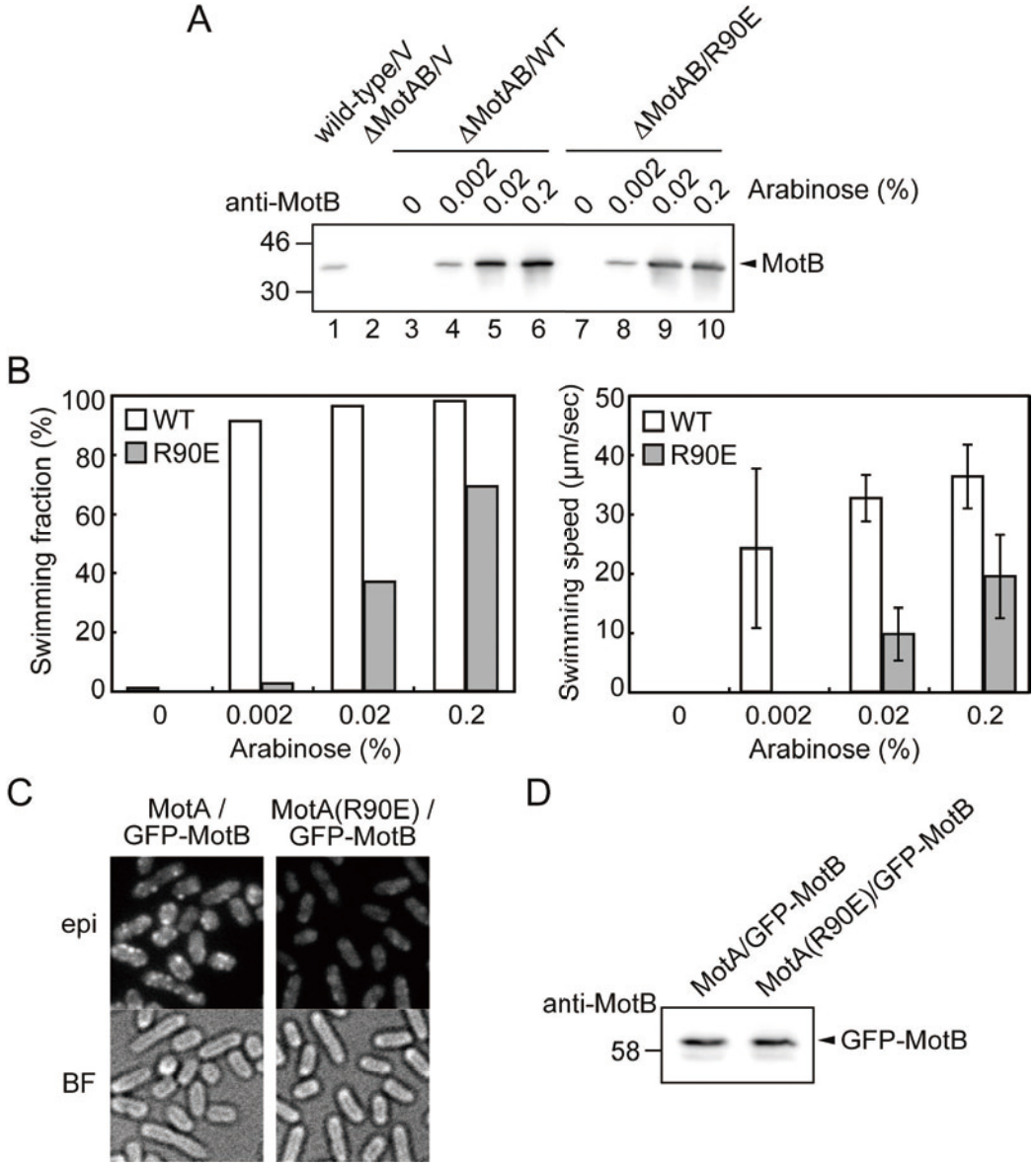

Fig. 2-8. Motility of cells producing MotA(R90E) and MotB in liquid media. (A) Immunoblotting, using polyclonal anti-MotB antibody, of whole cell proteins prepared from SJW1103 (wild-type) harboring pBAD24 (V), and SJW2241(*ΔmotAB*) carrying pBAD24 (V), pYC20 (WT) or pYC20(R90E) (R90E) were incubated at 30ºC for 5 hours in LB with 0, 0.002, 0.02, 0.2% arabinose. Arrowhead indicates the positions of MotB. (B) Free-swimming fraction and speed of SJW2241(*ΔmotAB)* carrying pYC20 (WT) (open bar) and pYC20(R90E) (R90E) (shaded bar) measured by phase contrast microscopy. Swimming fraction is the number fraction of swimming cells. Swimming speed is the average of more than 20 cells, and vertical lines are standard errors. If the fraction of motile cells was less than 5% of total cells, the swimming speed is presented as zero. Measurements were done at ca. 23ºC. (C) Bright field (BF) and fluorescence (epi) images of YVM003 (MotA/GFP-MotB) and YVM031 (MotA(R90E)/GFP-MotB). The cells were grown overnight in LB at 30ºC and observed by fluorescence microscopy. (D) Immunoblotting, using polyclonal anti-MotB antibodies, of whole cell proteins prepared from the same strains. Arrowheads indicate the positions of GFP-MotB.

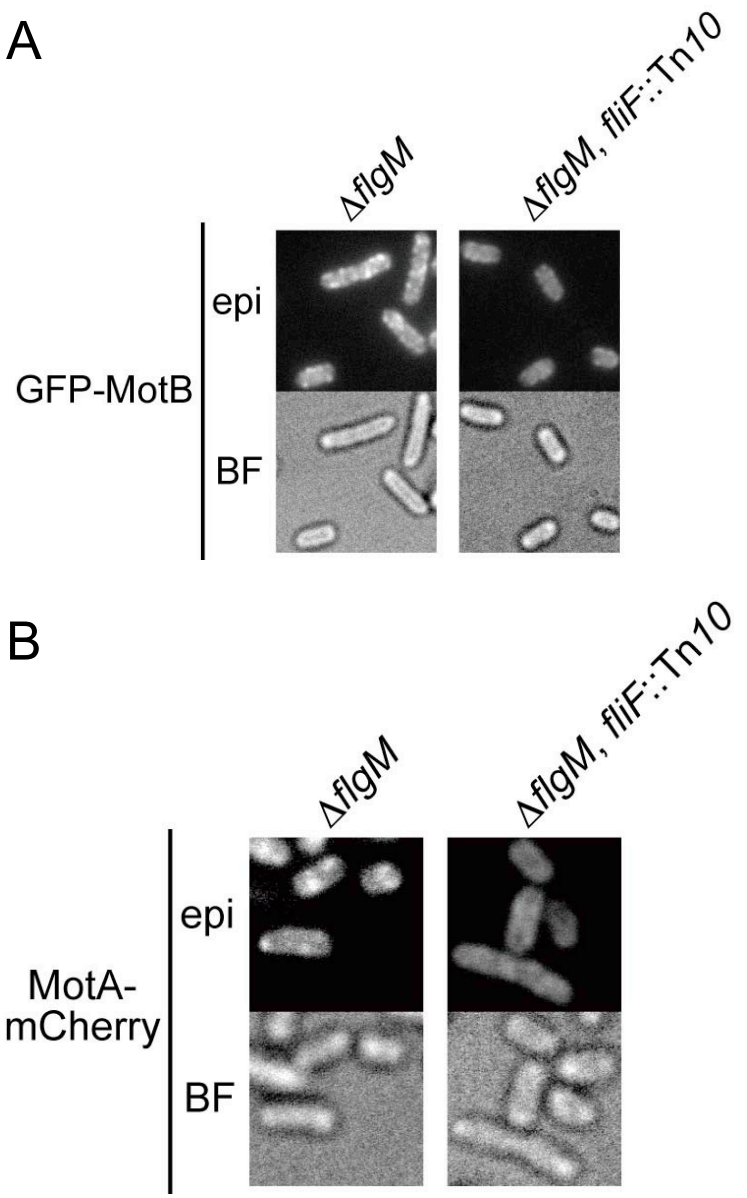

Fig. 2-9. Effect of the defect of basal body on subcellular localization of stator complex. (A) Fluorescence (epi) and bright field images (BF) of YMM002 (GFP-MotB, Δ*flgM*) and YMM010 (GFP-MotB, Δ*flgM, fliF*::Tn*10*). The cells were grown overnight in LB at 30ºC and observed by fluorescence microscopy. (B) Fluorescence (epi) and bright field images (BF) of YMM019 (MotA-mCherry, Δ*flgM*) and YMM020 (MotA-mCherry, Δ*flgM, fliF*::Tn*10*). The cells were grown in LB at 30ºC for 5 hours and observed by fluorescence microscopy.

Table 2-1. Strains used in Chapter 2

Strains	Relevant characteristics	Source or reference
Salmonella		
SJW1103	Wild type for motility and chemotaxis	Yamaguchi *et al*. (1984)
SJW2241	Δ(*motA-motB*)	Komoriya *et al*. (1999)
SJW3076iC	Δ(*cheA-cheZ*), *fliC*(Δ204-292)	Nakamura *et al*. (2009b)
MMPH001	Δ*araBAD::pHluorin*	Morimoto *et al*. (2010a)
YVM003	*gfp-motB*	Morimoto *et al*. (2010b)
YVM004	*gfp-fliG*	Morimoto *et al*. (2010b)
YVM007	*gfp-motB*(D33N)	Morimoto *et al*. (2010b)
YVM018	*gfp-fliG*, *motA-mCherry*, Δ*motB*	Morimoto *et al*. (2010b)
YVM030	*gfp-motB*(D33A)	Morimoto *et al*. (2010b)
YVM031	*motA*(R90E), *gfp-motB*	Morimoto *et al*. (2010b)
YMM002	*gfp-motB, Δflg*M::*kan*	Morimoto *et al*. (2010b)
YMM010	*gfp-motB, Δflg*M::*kan, fliF*::Tn*10*	Morimoto *et al*. (2010b)
YMM019	*gfp-fliG, motA-mCherry, ΔmotB, Δflg*M::*kan*	Morimoto *et al*. (2010b)
YMM020	*gfp-fliG, motA-mCherry, ΔmotB, Δflg*M::*kan, fliF*::Tn*10*	Morimoto *et al*. (2010b)

Table 2-2. Plasmids used in Chapter 2

Plasmids	Relevant characteristics	Source or reference
pKK223-3	Cloning vector	GE Healthcare
pTrc99A	Cloning vector	GE Healthcare
pBAD24	Cloning vector	Guzman *et al*. (1995)
pKSS12	pKK223-3 / MotA	Morimoto *et al*. (2010b)
pKSS13	pKK223-3 / MotA+MotB	Morimoto *et al*. (2010a)
pNSK9	pTrc99A / MotA+MotB	Che *et al*. (2008)
pHMK1602	pTrc99A / MotB	Morimoto *et al*. (2010b)
pYC20	pBAD24 / MotA+MotB	Morimoto *et al*. (2010a)
pYC20(R90E)	pBAD24 / MotA(R90E)+MotB	Morimoto *et al*. (2010b)
pYC20(E98K)	pBAD24 / MotA(E98K)+MotB	Morimoto *et al*. (2010b)

Table 2-3. Primers used in Chapter 2

Primers	Sequence
$MotB_N$-tetR	cagtgagaaacccaaaccagcagcagacgactgaggaagcttaagacccactttcacatt
$MotB_N$-tetA	ctgcggcgttttacgacgacaatgggatgagcctgattttctaagcacttgtctcctg
$MotB_N$-GFP-Fw	gcagtgagaaacccaaaccagcagcagacgactgaggaagcatgagtaaaggagaagaacttttc
$MotB_N$-GFP-Rv	ctgcggcgttttacgacgacaatgggatgagcctgatttttttttgtatagttcatccatgccatg
$FliG_N$-tetR	gtggtggcgctggtcattcgccagtggatgagtaacgatcttaagacccactttcacatt
$FliG_N$-tetA	ggtcatcaacaaaatgacgcttttatcggtaccgctaagactaagcacttgtctcctg
$FliG_N$-GFP-Fw	gcgcgtggtggcgctggtcattcgccagtggatgagtaacgatcatgagtaaaggagaagaacttttc
$FliG_N$-GFP-Rv	ggtcatcaacaaaatgacgcttttatcggtaccgctaagattacttttgtatagttcatccatgccatg
MotB-ΔD33-tetR	cggcggcggggcgcacggttcctggaaaattgcctacgccttaagacccactttcacatt
MotB-ΔD33-tetA	gccacatcaccagaaaaaaagccatcatcgccgtcataaactaagcacttgtctcctg
MotB(D33N)-short	gccacatcaccagaaaaaaagcc
MotB(D33N)-long	cggcggcggggcgcacggttcctggaaaattgcctacgccaattttatgacggcgatgatggctttttttctggtgatgtggc
MotB(D33A)-long	cggcggcggggcgcacggttcctggaaaattgcctacgccgcttttatgacggcgatgatggctttttttctggtgatgtggc
$MotA_C$-tetR	cgcgcagtgagaaacccaaaccagcagcagacgactgaggttaagacccactttcacatt
$MotB_C$-tetA	tcaaaaaatgtctgataaaaatcgctaatatccatgctcactaagcacttgtctcctg
$MotA_C$-mCherry-Fw	agtgagaaacccaaaccagcagcagacgactgaggaagcaatggtgagcaagggcgagga
$MotA_C$-mCherry-Rv	aaaatcgctaatatccatgctcacgctatcacctcggttccgcttctacttgtacagctcgtcca
flgM::kan-Fw	atggtagctggccgctacaacgtaaccctcgatgaggataaataaatgagccatattcaacgggaaa
flgM::kan-Rv	agtatttctgacaaacgagtcatacgcttatttactctgtaagtattagaaaaactcatcgagcatc
MotA-R90E-Fw	atcgcctgatggccaaatcagaacagcaggggatgttctccct
MotA-R90E-Rv	agggagaacatcccctgctgttctgatttggccatcaggcgat
MotA-E98K-Fw	agcaggggatgttctcccttaaacgcgatattgaaaatccaaa
MotA-E98K-Rv	tttggattttcaatatcgcgtttaagggagaacatcccctgct

Table 2-4. Effect of CCCP on the localization of GFP-MotB.

	GFP-MotB	
50 μM CCCP	Number of spots / cell	Fluorescence intensity (A.U.)
-	1.9 ± 0.9 (n=176)	1486 ± 257 (n=40)
+	2.3 ± 0.8 (n=149)	1439 ± 301 (n=40)

Table 2-5. Effect of MotA-overproduction on flagellar motor rotation.

Bead	Vector		MotA	
	Rotation rate (Hz)	Torque (pN nm)	Rotation rate (Hz)	Torque (pN nm)
1.0 μm	65 ± 7	1705 ± 190 n = 17	40 ± 18	1122 ± 440 n = 27
0.8 μm	101 ± 15	1519 ± 172 n = 32	61 ± 24	960 ± 355 n = 29
0.5 μm	169 ± 32	854 ± 152 n = 38	81 ± 38	424 ± 198 n = 48
0.1 μm	218 ± 57	449 ± 115 n = 13	130 ± 62	270 ± 130 n = 20

Chapter 3. M153R mutation in a pH-sensitive green fluorescent protein stabilizes its fusion proteins

Introduction

The flagellar motor can spin stably at 300 Hz [Yuan and Berg, 2008]. The rotation-dependent proton influx has been estimated to be about 1,200 protons per revolution [Meister *et al*., 1987]. Since a decrease in intracellular pH significantly reduces flagellar motor rotation [Minamino *et al*., 2003; Nakamura *et al*., 2009], the proton release from the stator channel to the cytoplasm appears to play an important role in the torque generation process, and local pH near the motor must be tightly controlled. Interestingly, an in-frame deletion of the plug segment of MotB (MotB$_{\Delta plug}$) causes considerable proton leakage, thereby arresting cell growth, even when the expression level of MotA/B$_{\Delta plug}$ is the same as that of MotA/B expressed from the chromosome as shown in Chapter 1 [Hosking *et al*., 2006; Morimoto *et al*., 2010b]. This raises the interesting question of how a change in local pH near the flagellar motor is minimized.

GFP and related fluorescent proteins have been utilized to monitor and analyze a wide range of biological processes such as gene expression, protein localization and cell motility. These fluorescent proteins can also be used as the indicator of Ca^{2+} or ATP concentration or pH because they provide a high sensitivity in detection and are not toxic to living cells [Nagai *et al*., 2001; Imamura *et al*., 2009; Miesenböck *et al*., 1998]. The relative emission intensity of ratiometric pHluorin at the two excitation wavelengths show a remarkable pH dependence, thereby pH can be measured by the 410/470 nm excitation ratio, $R_{410/470}$ [Miesenböck *et al*., 1998]. The

$R_{410/470}$ ratio changes in less than 0.5 ms when the pH is changed, indicating that the ratiometric measurement by pHluorin can detect a rapid pH change [Hess *et al*., 2004]. Since ratiometric methods, in which dual-wavelength measurements detect changes in the fluorescence absorption or emission spectra upon ion-binding, are independent of the concentration of the indicator, a precise and quantitative pH measurement of living cells can be easily carried out using pHluorin.

In this chapter, I constructed *Salmonella* cells expressing pHluorin fusion proteins such as pHluorin-FliG and pHluorin-MotB. I show that the M153R mutation in pHluorin improves the stability of the fusion proteins. I also show that pHluorin(M153R)-FliG can be used as a pH sensor.

Materials and Methods

Bacterial strains, plasmids, DNA manipulations and media

Bacterial strains and plasmids used in this chapter are listed in Table 3-1 and 3-2. DNA manipulations were carried out as described in Chpater 1. PCR primers were listed in Table 3-3. *Salmonella* strains expressing pHluorin-fusion proteins were constructed using the λ Red homologous recombination system [Datsenko *et al*., 2000]. Mutations were confirmed by DNA sequencing. L broth, T broth, soft agar plates and motility medium were prepared as described in Chpater 1. Ampicillin was added to the medium at a final concentration of 100 μg/ml.

Preparation of whole cell proteins and immunoblotting

Salmonella cells were grown overnight at 30ºC in LB with shaking. Cell pellets were suspended in a SDS-loading buffer and normalized by cell density to give a constant amount of cells. After SDS-PAGE, immunoblotting with polyclonal anti-FliG, anti-MotB and anti-GFP (MBL) antibodies was carried out as described in Chapter 1.

Purification of proteolytic products of pHluorin-MotB-His_8

Membranes containing overproduced pHluorin-MotB-His_8 fusion proteins were solubilized by 0.2% (w/v) of dodecylphosphocholine (Anatrace) and their proteolytic cleavage products were purified by Ni-NTA affinity chromatography as described [Minamino and Macnab, 2000]. Molecular mass of the cleavage products was analyzed by a mass spectrometer (Voyager DE/PRO, Applied Biosystems) as described [Saijo-Hamano *et al*., 2004].

Fluorescence microscopy

Epi-fluorescence of pHluorin fusion proteins was observed by an inverted fluorescence microscope (IX-71, Olympus) with a 150× oil immersion objective lens (UApo150XOTIRFM, NA 1.45, Olympus) and an Electron-Multiplying Charged-Coupled Device (EMCCD) camera (C9100-02, Hamamatsu Photonics) as described in Chapter 2.

Purification and Spectroscopy of pHluorin, pHluorin(M153R) and pHluorin(M153R)-FliG-His_6.

pHluorin and pHluorin(M153R) were purified as described in Chapter 1. pHluorin(M153R)-FliG-His_6 was purified from the soluble fractions of BL21(DE3)pLysS carrying pYVM013, by affinity chromatography with a HisTrap™HF column (GE Healthcare). pHluorin(M153R)-FliG-His_6 was purified by gel-filtration chromatography with a Hiload 26/60 Suprerdex 75 pg column (GE Healthcare) Fluorescence excitation spectra of purified pHluorin, pHluorin(M153R), and pHluorin-FliG-His_6 in buffers of defined pH were recorded on a fluorescence spectrophotometer (RF-5300PC, Shimadzu), and the 410/470-nm excitation ratios of pHluorin fluorescence intensities were determined at different pH values to generate a calibration curve.

For measurements of intracellular pH, wild-type cells carrying pYC001 or pYVM001 were grown with shaking in T-broth at 30 ºC until the cell density had reached an OD_{600} of 1.0. The cells were washed twice with motility buffer and resuspended in motility buffer. The cells were diluted 1:100 into motility buffer, and the fluorescence excitation spectra of the cells were recorded on a fluorescence spectrophotometer. The 410/470-nm excitation ratios were calculated and converted to pH values based on the calibration curve previously generated.

Results

Effect of the M153R mutation on the stability of pHluorin-fusion proteins

To investigate local pH near the bacterial flagellar motor, the ratiometric pHluorin probe must be localized to the flagellar motor. Since it has been reported that the GFP-FliG and GFP-MotB fusion proteins are partially functional described in Chapter 2 [Morimoto *et al*., 2010b; Leake *et al*., 2006], I fused pHluorin to the N-termini of FliG and MotB to produce *Salmonella pHluorin-fliG* and *pHluorin-motB* strains, respectively. However, these fusion proteins were unstable, and about a half of them were cleaved into a 47 kDa fragment as shown on the immunoblots (Fig. 3-1A, lane 2 in both panels). Neither intact FliG nor MotB was observed, suggesting that the cleavage must occur within pHluorin. To identify the cleavage sites, a His_8 tag was attached to pHluorin-MotB at its C terminus to facilitate protein purification. The cleavage product of pHluorin-MotB-His8 was purified by Ni-NTA affinity chromatography and its molecular mass was measured by matrix-assisted laser desorption ionization time-of-flight mass spectrometry. The molecular mass was around 43.2 – 44.8 kDa. In search of possible proteolytic fragments having these masses, we identified possible cleavage sites to be at Met-153, Ala-154, Lys-162 or Ala-163 of pHluorin. Therefore, I carried out site-directed mutagenesis of these residues to see if any of such mutations have a stabilizing effect on the fusion proteins. The M153R mutation markedly stabilized both pHluorin-FliG and pHluorin-MotB fusion protein (Fig. 3-1A, right panel, lane 3 in both panels) while the other mutations showed no improvement.

We next investigated whether the M153R mutation increases the signal to noise (S/N) ratio. Since the turnover of GFP-FliG between the cytoplasmic pool and functional motors does not occur [Fukuoka *et al*., 2010], I analyzed the subcellular localization of pHluorin-FliG and pHluorin(M153R)-FliG by epi-illumination

fluorescence microscopy. The M153R mutation substantially increased the number of fluorescent spots of pHluorin-FliG (Fig. 3-1B). The fluorescence intensities of the pHluorin-FliG and pHluorin(M153R)-FliG spots were 1,065 ± 278 A.U. (n = 109) and 3,560 ± 1322 A.U. (n = 126), respectively, indicating that the M153R mutation resulted in a remarkable improvement in the S/N ratio of the fluorescent images.

Effect of the M153R mutation on brightness and 410/470-nm ratio

To test whether the M153R mutation affects the brightness of pHluorin alone in vivo, I transformed a *Salmonella* wild-type strain, SJW1103, with a plasmid encoding pHluorin(M153R) on pKK223-3 and analyzed the fluorescent intensity of pHluorin(M153R) with a spectrophotometer (Fig. 3-2A). I used SJW1103 expressing wild-type pHluorin as a control. Immunoblotting with polyclonal GFP antibody revealed that the expression level of pHluorin(M153R) was the same as that of pHluorin (Fig. 3-2A, inset). Interestingly, the fluorescent intensity of pHluorin(M153R) was approximatly 2.5-fold brighter than that of pHluorin. When the fluorescence intensities of purified pHluorin and pHluorin(M153R) were measured at the same protein concentration, there was no difference in the fluorescence intensity (Fig. 3-2B). This result indicates that the M153R mutation does not increase the intrinsic brightness of properly matured pHluorin molecules. Therefore, I conclude that the M153R mutation improves the folding efficiency of pHluorin in vivo.

It has been reported that the M153A mutation shifts the excitation wavelength of GFP(S65T) to a longer wavelength [Heim and Tsien, 1996]. We therefore measured the excitation spectra of purified pHluorin and pHluorin(M153R) (Fig. 3-3). The M153R mutation changed neither the excitation wavelengths nor the relative emission intensity ratios at the excitation wavelengths of 410 and 470 nm over

a pH range from 5.5 to 8.5.

We next examined whether pHluorin(M153R)-FliG can be used as a ratiometric pH sensor. The $R_{410/470}$ ratio of purified pHluorin(M153R)-FliG-His_6 showed a pH-dependence from 0.3 at pH 5.5 to 1.2 at pH 8.5, which is as large as that of pHluorin(M153R) (Fig. 3-4), indicating that pHluorin(M153R)-FliG can be a useful tool to measure local pH near the flagellar motor.

Discussion

GFP has been used to determine subcellular protein localization. A peptide linker between GFP and the target protein is required for the stability and function of fusion proteins. However, GFP is often removed from fusion proteins by proteolytic cleavage. Here, I directly fused the ratiometric pHluorin probe to the N-termini of *Salmonella* FliG and MotB and found that these fusion proteins are also unstable in vivo (Fig. 3-1A). As pHluorin itself is stable (Fig. 3-2, inset), the fusion to target proteins presumably induces a conformational change in pHluorin, resulting in proteolytic cleavage of the fusion proteins. Site-directed mutagenesis revealed that the M153R mutation in pHluorin considerably improved the protein stability of its fusion proteins (Fig. 3-1A). The M153R mutation also increased not only the number of fluorescent spots of pHluorin-FliG in *Salmonella* cells but also their fluorescence intensity, improving the S/N ratio of the images (Fig. 3-1B).

It has been reported that the L99Q, M153R and V163A triple substitutions increases the brightness of TagGFP [Subach *et al*., 2008]. In this study, I found that the M153R mutation alone increases the brightness of pHluorin by about 2.5-fold in vivo (Fig. 3-2A). In contrast, the fluorescence intensity of purified pHluorin(M153R) was the same as that of pHluorin in solution (Fig. 3-2B). Met-153 is located on the surface of the crystal structure of the GFP molecule (Fig. 3-5) and is known to be important for the proper folding of GFP [Tsien, 1998]. The M153T mutation is called a folding mutation that improves folding at 37ºC, reduces aggregation at high protein concentrations, and increases protein diffusion inside the cells [Tsien, 1998]. Therefore, I conclude that the M153R mutation increases the efficiency of protein folding of pHluorin *in vivo*, thereby stabilizing its fusion proteins significantly.

The M153R mutation did not change the 410/470-nm excitation ratios of

pHluorin (Fig. 3-3), indicating that pHluorin(M153R) can be used as a pH sensor. The 410/470-nm excitation ratios of pHluorin(M153R)-FliG-His_6 also showed a similar pH-dependence (Fig. 3-4). Therefore, I believe that the pHluorin(M153R) probe can be used as a potentially powerful tool for local pH measurement in living cells. I am currently developing a high-resolution pH imaging system using pHluorin(M153R) as a probe.

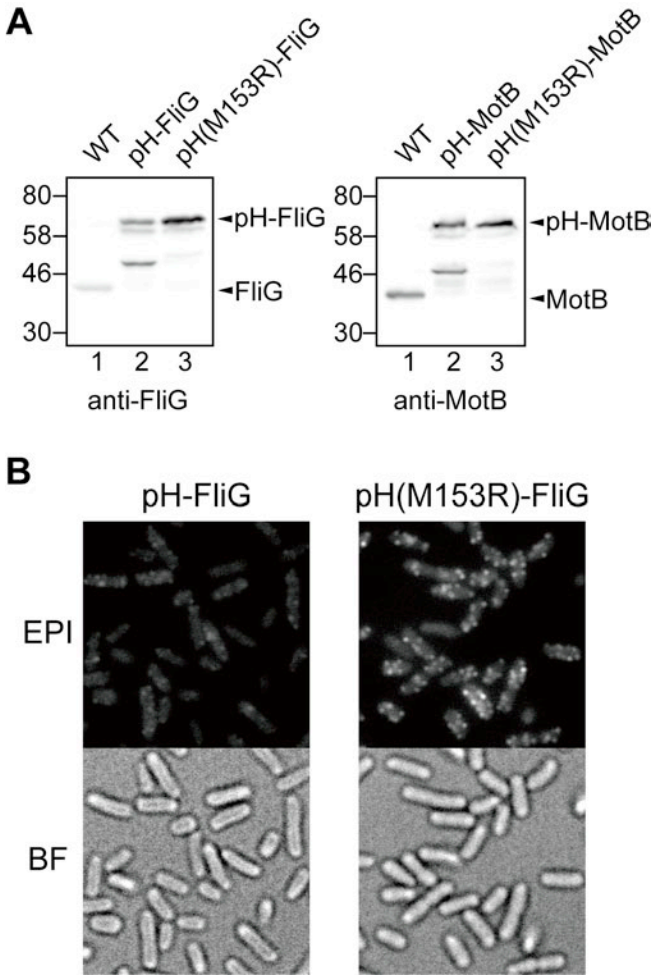

Fig. 3-1. Effects of the M153R mutation in pHluorin on the protein stability of its fusion products. (a) Immunoblotting, using polyclonal anti-FliG (left panel) or anti-MotB antibody (right panel), of whole cell proteins prepared from SJW1103 (WT), YVM1002 (pHluorin-FliG, indicated as pH-FliG), YVM1004 (pHluorin(M153R)-FliG, indicated as pH(M153R)-FliG), YVM1001 (pHluorin-MotB, indicated as pH-MotB) and YVM1003 (pHluorin(M153R)-MotB, indicated as pH(M153R)-MotB). The positions of molecular mass markers (kDa) are shown on the left. (b) Fluorescence images (EPI) and bright field images (BF) of YVM1002 and YVM1004. The cells were grown overnight in LB at 30ºC and observed by fluorescence microscopy.

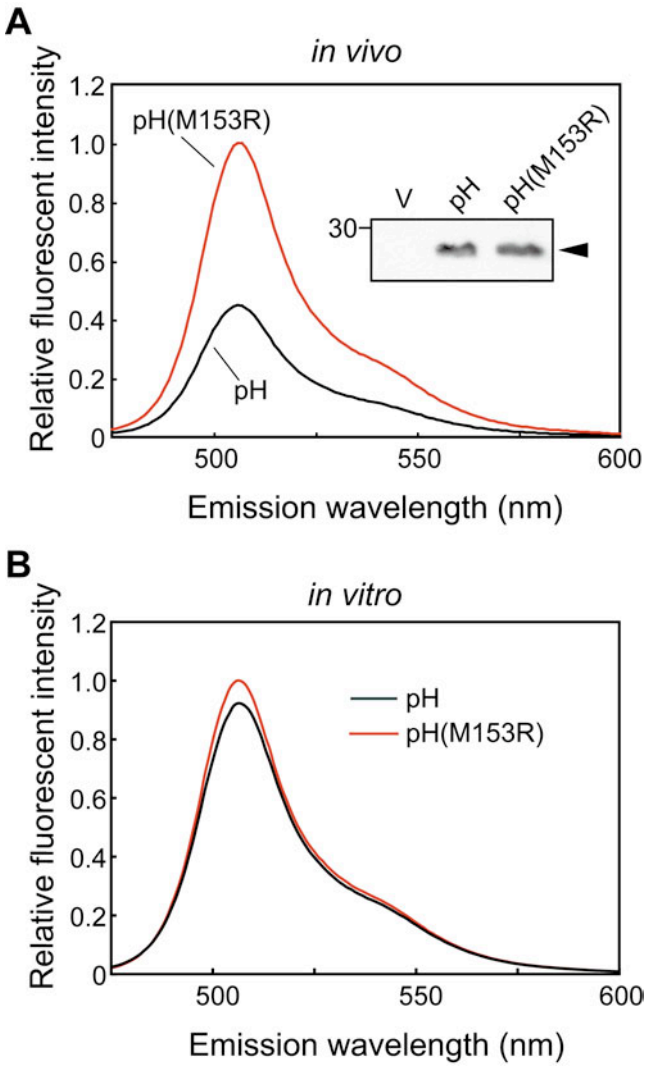

Fig. 3-2. Effect of the M153R mutation on $R_{410/470}$. (A) Fluorescent intensities of SJW1103/pYC001 (pHluorin) and SJW1103/pYVM001 (pHluorin(M153R)) cells grown in T-broth at 30 ºC. Emission spectra with 395 nm excitation were measured by a fluorescence spectrophotometer. The measurements were done at 23ºC. Inset: Immunoblotting, using polyclonal GFP antibody, of whole cell proteins. (B) Fluorescent intensities of purified pHluorin and pHluorin(M153R).

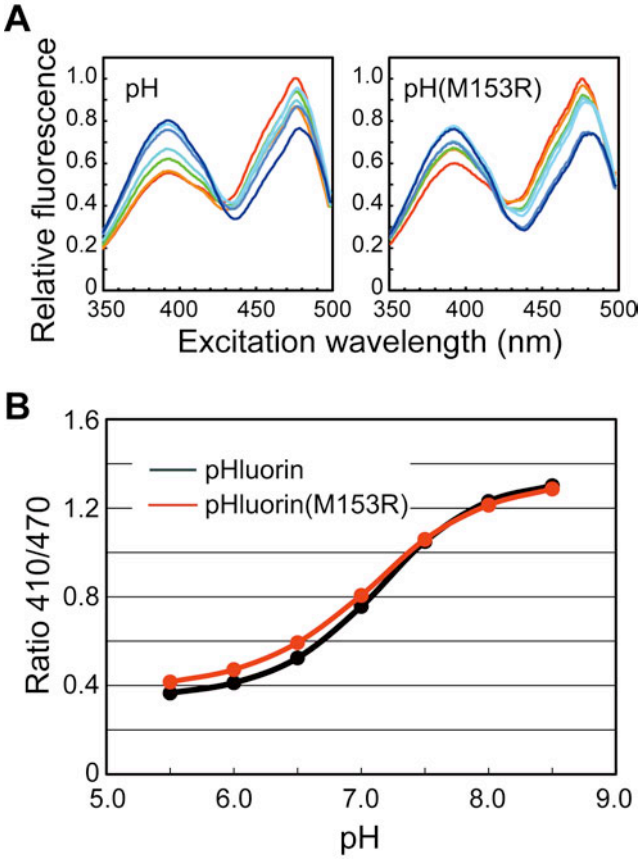

Fig. 3-3. pH dependence of fluorescence excitation spectra and $Ratio_{410/470}$ of pHluorin and pHluorin(M153R). (A) Fluorescence excitation spectra of pHluorin and pHluorin(M153R). (B) $Ratio_{410/470}$. The fluorescence excitation spectra of purified proteins were recorded on a fluorescence spectrophotometer. The measurements were done at 23ºC.

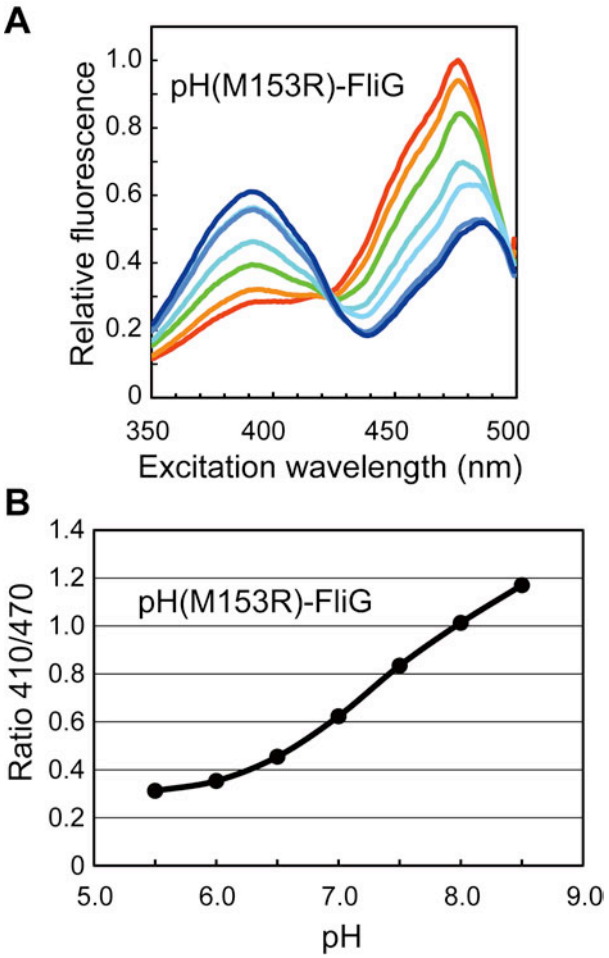

Fig. 3-4. pH dependence of fluorescence excitation spectra and $Ratio_{410/470}$ of pHluorin(M153R)-FliG-His_6. (A) Fluorescence excitation spectra. (B) $Ratio_{410/470}$. The fluorescence excitation spectra of purified proteins were recorded on a fluorescence spectrophotometer. The measurements were done at 23ºC.

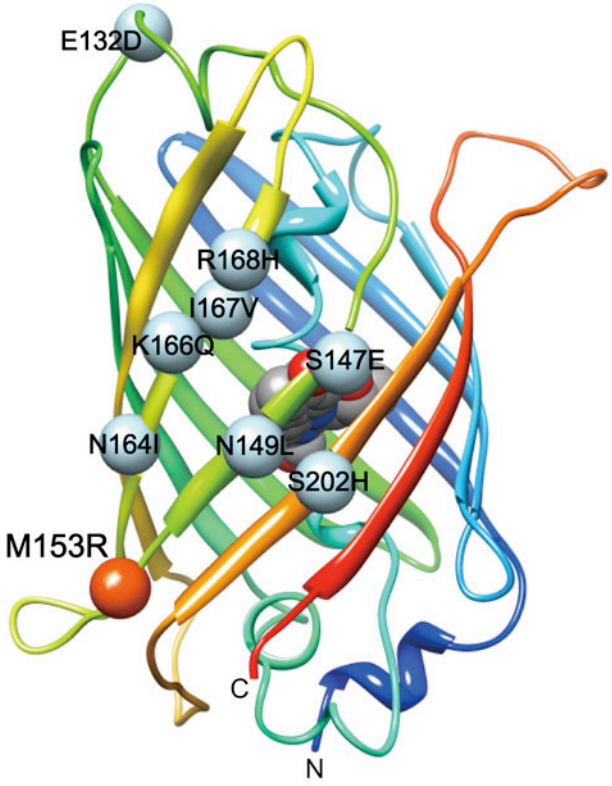

Fig. 3-5. Atomic model of GFP (PDB ID: 1EMA) and the mutations that generate the ratiometric pH probe pHluorin. The mutation sites are shown by balls: orange, for M153R; light blue, for E132D, S147E, N149L, N164I, K166Q, I167V, R168H and S202H.

Table 3-1. Strains used in Chapter 3

Strains	Relevant characteristics	Source or reference
E. coli		
BL21(DE3) pLysS	T7 expression host	Novagen
Salmonella		
SJW1103	Wild type for motility and chemotaxis	Yamaguchi *et al*. (1984)
YVM1001	*pHluorin-motB*	Y. Morimoto, unpublished
YVM1002	*pHluorin-fliG*	Y. Morimoto, unpublished
YVM1003	*pHluorin*(M153R)-*motB*	Y. Morimoto, unpublished
YVM1004	*pHluorin*(M153R)-*fliG*	Y. Morimoto, unpublished

Table 3-2. Plasmids used in Chapter 3

Plasmids	Relevant characteristics	Source or reference
pGST-pHluorin	pGEX2T / GST-pHluorin	Miesenböck *et al*. (1998)
pYC001	pKK223-3 / pHluorin	Nakamura *et al*. (2009)
pNSK22pH	pTrc99A / MotA + pHluorin-MotB-His_8*	S. Kojima, unpublished
pNSK22pH(M153R)	pTrc99A / MotA + pHluorin(M153R)-MotB-His_8*	S. Kojima, unpublished
pYVM001	pKK223-3 / pHluorin(M153R)	Y. Morimoto, unpublished
pYVM007	pGEX2T / GST-pHluorin(M153R)	Y. Morimoto, unpublished
pYVM013	pTrc99A / pHluorin(M153R)-FliG-His_6	Y. Morimoto, unpublished

*In this pHluorin-MotB-His_8 fusion construct, N-terminal 28 residues of MotB (Met1-Lys28) are attached to the N-terminus of pHluorin as described by Leake *et al.,* 2006.

Table 3-3. Primers used in Chapter 3

Primers	Sequence
$MotB_N$-tetR	cagtgagaaacccaaaccagcagcagacgactgaggaagcttaagacccactttcacatt
$MotB_N$-tetA	ctgcggcgttttacgacgacaatgggatgagcctgattttctaagcacttgtctcctg
$MotB_N$-pH-Fw	gcagtgagaaacccaaaccagcagcagacgactgaggaagcatgagtaaaggagaagaactttc
$MotB_N$-pH-Rv	ctgcggcgttttacgacgacaatgggatgagcctgatttttttgtatagttcatccatgccatg
$FliG_N$-tetR	gtggtggcgctggtcattcgccagtggatgagtaacgatcttaagacccactttcacatt
$FliG_N$-tetA	ggtcatcaacaaaatgacgcttttatcggtaccgctaagactaagcacttgtctcctg
$FliG_N$-pH-Fw	gcgcgtggtggcgctggtcattcgccagtggatgagtaacgatcatgagtaaaggagaagaactttc
$FliG_N$-pH-Rv	ggtcatcaacaaaatgacgcttttatcggtaccgctaagattacttttgtatagttcatccatgccatg
XbaI-fliG-SD	aatctagatggtggcgctggtcattcgccagt
FliG-HindIII	aaaagcttttagacataggtatcctcgc
FliG-XhoI	aactcgaggacataggtatcctcgccgc
His-HindIII	aaaagctttcagtggtggtggtggtggtgctc

Chapter 4. High-resolution pH measurement of live *Salmonella* cells by a pH-sensitive GFP and a new pH imaging system

Introduction

So far, I have clarified the regulatory mechanism of the proton-conductivity of the MotA/B complex, and the characteristics of stator protein MotA/B, but it remains unknown how the stator complex couples the proton flow to torque generation. To understand the energy coupling mechanism of the proton-driven flagellar motor, pH changes near the motor should be measured, desirably near the exit of the proton pathway. In Chpter 3, I introduced the M153R mutation to pHluorin to improve the stability of the fusion proteins. I also showed that pHluorin(M153R)-FliG can be used as a retiometric pH probe. I used this pHluorin(M153R) mutanat to develop an intracellular pH imaging system with high spatial and temporal resolution. This system can measure the intracellular pH distribution at a pH resolution of 0.02. Here, I describe the results using this mutation and discuss a new intracellular pH imaging system that has the ability to measure pH in single cells at unprecedented temporal and spatial resolution, offering new insight into local pH around the motor.

Materials and Methods

Bacterial strains, plasmids, DNA manipulations and media

Bacterial strains and plasmids used in this chapter are listed in Table 4-1 and 4-2. DNA manipulations were carried out as described in Chpater 1. PCR primers used were listed in Table 4-3. Mutations were confirmed by DNA sequencing. L broth, T broth, soft agar plates and motility medium were prepared as described in Chpater 1. Ampicillin was added to the medium at a final concentration of 50 μg/ml. Cells were grown in T-broth at 30°C until the optical density at 600 nm (OD_{600}) reached 1.0. The bacteria were washed two times by centrifugation (15000 rpm, 1 min.) and resuspended in motility medium.

Purification of pHluorin and pHluorin fusion proteins

pHluorin and pHluorin(M153R) were purified as described in Chapter 1. pHluorin(M153R)-FliG-His_6 were purified as described in Chapter 3. GST-Tar_C-pHluorin(M153R) was purified from the soluble fractions of BL21(DE3)pLysS carrying pYVM003, by affinity chromatography with a GSTrap™HP column (GE Healthcare). GST-Tar_C-pHluorin(M153R) was purified by gel-filtration chromatography with a Hiload 26/60 Suprerdex 200 pg column (GE Healthcare).

Fluorescence spectroscopy

Excitation spectra of pHluorin were measured using the fluorescent spectrophotometer RF-5300PC (Shimadzu) as described in Chapter 1. The standard curve was determined for each fluorophore with purified protein (pHluorin, pHluorin(M153R)-FliG-His_6 and GST-Tar_C-pHluorin(M153R)) by fluorescence measurements of samples resuspended at pH over a range of 5.5 – 8.5. A standard

curve was used to convert the 410/470 intensity ratio ($R_{410/470}$) to pH units.

Fluorescence microscopy

Cells expressing pHluorin were observed under a custom-built microscope (Fig. 4-1A). An optical system was built on an inverted fluorescence microscope (IX-71, Olympus). The microscope was equipped with the UApo 150×/ 1.45 oil TIRFM objective lens (Olympus) with ×1.6 variable inserts. I employed two methods of excitation.

(i) When a xenon lamp was used as an excitation light source, I used a high speed wavelength switcher (LAMBDA DG-4, Sutter) capable of switching the two excitation filters, 410 nm (400AF30, Omega Optical) and 470 nm (BP470-490, Olympus), in 1.2 ms. Fluorescence emission was passed through the dichroic mirror (FF510-Di01-25x36, Semrock) and an emission filter (520DF40, Omega Optical). Images were acquired with an EMCCD camera (C9100-02, Hamamatsu Photonics) and controlled by the MetaMorph 3.6 software (Molecular Devices).

(ii) Diode pumping solid state lasers of 405 nm (Compass 405-25, COHERENT) and 473 nm (Cobolt blues 473 nm, Cobolt AB) excitation wavelengths were used as the excitation light sources. The 405 nm laser aperture was narrowed by using two collimator lenses (f = 48 mm and f = 8 mm, CVI MellesGriot). Two lasers were combined with a dichroic mirror (DM450, Olympus). Images were acquired with a frame-transfer mode of ~1000 Hz by using a 128x128-pixel, cooled, back-illuminated EMCCD camera (iXon DU860-BV, Andor Technology). The on/off switching of the excitation laser and camera were controlled by an electrical stimulator (SEN-8203, Nihon Kohden) and the Andor Solis software (Andor Technology). The 405 nm laser can be controlled directly, while the 473 nm laser was gated by a high-speed mechanical shutter (Uniblitz UHS1T2, Vincent Associates).

Image processing

Calculation of cytoplasmic pH

Intracellular pH distribution within a single cell was determined from the ratio of fluorescece intensity distribution in the two excitation wavelength images (Fig. 4-2). I analyzed fluorescent images with an image processing program I developed based on the Igor Pro 6 (WaveMetrics). The fluorescence intensity of pHluorin was determined as

$$I_{pH} = I_{all} - I_{bg} - I_{af}$$

where I_{pH} is the intensity for calculation of pH, I_{all} is the total intensity, I_{bg} is the background intensity, and I_{af} is the autofluoresence intensity. The raw data includes the background noise of the detector and autofluorescence values of the cells. First I defined the intensity of the cell regions (I_{all}), which was the average value of the threshold determined by the image profile. I then subtracted background noise (I_{bg}) and autofluorescence values (I_{af}). The background value (I_{bg}) was the average of an arbitrary 100 x 100 pixel region absent of any cells. Autofluorescence values (I_{af}) were the mean pixel intensities of 50 wild-type cells containing no GFP.

Due to the optical resolution limited by the wavelength and numerical aperture, the spatial resolution of the pH imaging system is 214 nm. Taking this into consideration, I introduced a smoothing procedure by processing over 3×3 pixels for images acquired by iXon DU860-BV, and over 7×7 pixels for images acquired by C9100-02. The pH was determined by using the standard curve for each fluorophores (Fig. 4-1B). I performed these steps separately for each image.

Determination of local pH around the motor

The fluorescence intensity of a single fluorescent spot of pHluorin-FliG was determined by fitting the intensity distribution with a 2D-Gaussian function by using the Igor Pro 6 software (WaveMetrics) (Fig. 4-3). Local pH was determined from $R_{410/470}$ of the fluorescent spot by the standard curve (Fig. 4-1B).

Results

pH resolution of the pH imaging system.

The intracellular pH imaging system is based on an inverted fluorescence microscope (Fig. 4-1A). High spatial and temporal resolution was achieved by using an EMCCD camera. The fluorescence intensity of purified pHluorin was measured at different protein concentrations at pH 7.0 (Fig. 4-4) to estimate the pH resolution of the system. The pH value was determined with $R_{410/470}$, the fluorescent intensity ratio by excitation at 410 and 470 nm (Fig. 4-1B). The standard deviation of the pH was defined as the pH resolution of the system. The fluorescence intensity depended on the concentration of purified pHluorin in the buffer. By considering the 508 nm emission peak of pHluorin and using a NA1.45 objective lens, a spatial resolution of 214 nm was achieved, as given by resolution = 0.61 * wavelength / NA. pHluorin was imaged either with a xenon lamp or with laser excitation used for high spatial resolution and high-speed imaging. Image data by the xenon lamp wxcitation were acquired by an EMCCD, Hamamatsu C9100-02 (33 nm / pixel in my system), with smoothing over 7 × 7 pixels. Image data by laser excitation were acquired by another EMCCD, Andor iXon (100 nm / pixel in my system), with smoothing over 3 × 3 pixels. Spatial smoothing of images over multiple pixels improved the pH resolution. The result shows that the pH imaging system can measure intracellular pH at a pH resolution of 0.02 when the fluorescence intensity is adequate (Fig. 4-4).

Time-lapse measurement of intracellular pH of a single cell

It is important that time-lapse observations with high temporal resolution be made to observe the dynamics of the cell. Because weak acids such as acetate and benzoate in the extracellular solution are able to cross the cytoplasmic membrane in their

neutral forms and then dissociate in the cytoplasm, intracellular pH can be measured by lowering the external pH without significantly changing the total PMF. Previous data showed that 20 mM benzoate greatly reduced intracellular pH to nearly the external pH value [Kihara *et al.*, 1981; Minamino *et al.*, 2003; Nakamura *et al.*, 2009a; Morimoto *et al.*, 2010a]. I measured intracellular pH over an external pH range of 6.0 – 7.5 with or without benzoate using either a fluorescence spectrophotometer or the pH imaging system (Fig. 4-5). In the absence of benzoate, intracellular pH changed only by 0.3 units (Fig. 4-5). In contrast, in the presence of benzoate, intracellular pH changed more or less linearly and approached to the external pH (Fig. 4-5), in agreement with previous observations in Chapter 1 [Kihara *et al.*, 1981; Minamino *et al.*, 2003; Morimoto *et al.*, 2010a]. This suggests that the pH values obtained by the pH imaging system are comparable to those obtatained by a fluorescence spectrophotometer when a large number of cells were measured.

I measured the intracellular pH of *Salmonella* cell upon lowering the external pH from 7.0 to 6.0 with or without benzoate at every 30 ms (Fig. 4-6). At pH 6.0 in weak acid, the intracellular pH shifted also to 6.0. Without the weak acid, intracellular pH changed from 7.5 only to 7.3, demonstrating the high pH resolution of the system. Intracellular pH shifted to 6.0 within about 2 seconds after the external pH was shifted from 7.0 to 6.0 in a medium with 20 mM benzoate. When the external pH was brought back to 7.0 by using the original medium without benzoate, intracellular pH recovered to the original pH within about 2 seconds. The gradual changes in intracellular pH were largely due to the speed of medium change.

Effects of the overproduction of the unplugged MotA/B complex on intracellular pH and cell growth

As described in Chapter 1, cell growth is impaired due to proton leakage by the induction of the unplugged MotA/B complex from the plasmid (Fig. 1-1) [Hosking *et al.*, 2006; Morimoto *et al.*, 2010a]. By using the pH imaging system I measured the cytoplasmic pH of single *Salmonella* cells transformed with pYC20 before and after the induction with arabinose (Fig. 4-7). Cytoplasmic pH decreased by 0.6 units within 20 min after the induction and stayed constant at that level, in agreement with the data obtained by a spectrophotometer [Morimoto *et al.*, 2010a].

Rapid and sensitive response of the directional switching of motor rotation to a decrease in intracellular pH

It has been shown that a decrease in intracellular pH results in a strong CW bias in motor rotation as described in Chapter 1 and previous reports [Kihara and Macnab, 1981; Morimoto *et al.*, 2010a]. I carried out single-cell pH imaging upon shifting external pH from 7.0 to 6.0 in the presence of benzoate and recorded intracellular pH and flagellar motor rotation simultaneously using a split-imaging system (Fig. 4-8A). Motor rotation changed from CCW to CW bias within 10 ms of a 0.1 decrease in internal pH (Fig. 4-8B). The results show that *Salmonella* cells have the potential to respond to quite small pH changes in the environment.

Local pH measurement

There are reports on the fluorescence imaging of flagellar motor components by fusing them to fluorescent proteins [Leake *et al.*, 2006; Fukuoka *et al.*, 2007, 2010]. Although these studies revealed the localization and dynamics of fusion proteins,the temporal resolution was unsatisfactory. To watch the dynamics of internal pH, high-speed imaging is needed. The pHluorin(M153R)-FliG fusion protein made it

possible to improve the S/N ratio of fluorescence images significantly, enabling local pH measurements in single cells (Fig. 3-4).

The N-terminal region of FliG, which forms part of the C-ring close to the cytoplasmic membrane, is responsible for binding to the MS-ring, which is comosed of FliF and spans the membrane [Kihara *et al.*, 2000]. FliG interacts with the MotA/B complex for torque generation, and the MotA/B complex forms a proton channel upon its attachment to the flagellar basal body to become a functional stator. Therefore, pHluorin was fused to the N-terminus of FliG (YVM1004 strain) to monitor the local pH around FliG and the MotA/B complex during the process of torque generation. The pH probe is located about 3 nm away from the cytoplasmic membrane in this case. In the *Salmonella* SJW1368 *flhDC* mutant cells lacking flagellar master regulator, pHluorin-FliG was distributed homogeneously over the cytoplasm and showed no localization (lower left panel of Fig. 4-9A). In the YVM1004 strain, however, many distinct fluorescent spots are observed clearly, with the number of spots per cell close to that of the flagellum. Thus, local pH around the torque generating unit can be monitored with the cells of this strain. Cytoplasmic and local pHs were measured at external pH of 5.5 and 7.0. Cytoplasmic pH was around 7.4 at external pH 7.0, while it was about 7.3 at external pH 5.5 (Fig. 4-9B). There were no significant differences between local pH near the motor and bulk pH of the cytoplasm at both external pH 5.5 and 7.0 (Fig. 4-9B), indicating that intracellular pH is more or less uniform throughout the cell body, including the membrane peripheral.

In Tar-pHluorin strain, pHluorin was fused to the C-terminus of Tar to monitor local pH around the cytoplasmic domain of the Tar receptor. The C-terminus of Tsr, which is Tar homologue, is known to be located near the cytoplasmic membrane [Kim *et al.*, 1999]. The C-terminal regions of Tar and Tsr are thought to be flexible from

cryoEM images [Francis *et al.*, 2002, 2004]. Therefore, Tar-pHluorin is considered to measure cytoplasmic pH within about 5 nm from the membrane. The fluorescence image of the YVM009 strain cells with Tar-pHluorin showed fluorescent intencities localized to the cell poles, indicating the localization of the Tar receptors. Local pHs measured by Tar-pHluorin at external pH 5.5 and 7.0 were almost the same as those in the cytoplasm and those measured by pHluorin-FliG, respectively, indicating again that intracellular pH is uniform in the cytoplasmic space and the membrane peripheral.

Discussion

Calibration of ratiometric pH measurements

Many experimental techniques have been developed to measure intracellular pH [Slonczewksi *et al.*, 1982; Zilberatein *et al.*, 1984; Kneen *et al.*, 1998]. However, only fluorescence techniques currently offer the sensitivity required for accurate measurements at the single cell level of bacteria. Currently, there exist two methods for determining ion concentrations by using fluorescent indicators [Kneen *et al.*, 1998; Llopis *et al.*, 1998; Miesenböck *et al.*, 1998]. Monochromatic indicators have spectra that change little upon ion binding and therefore rely instead on differences in fluorescence intensity [Kneen *et al.*, 1998; Wilks and Slonczewski, 2007]. This type of measurement depends strongly on the experimental conditions such as the indicator concentration. In contrast, ratiometric methods such as pHluorin probes avoid such problems [Miesenböck *et al.*, 1998]. Using this method, I was able to acquire calibration curves for different types of purified proteins, which allowed accurate pH measurement as well as high temporal and spatial resolution.

Photobleaching

The number of successive measurements that can be made on a single cell is limited due to photobleaching. Wild-type GFP has multiple states [Chattoraj *et al.*, 1996; Tsien, 1998]. The specificity of pHluorin is due to two states of its chromophore, both of which are susceptible to photobleaching compromising pH measurements [Hess *et al.*, 2004]. To avoid photobleaching, pH was measured at low excitation intensity by ND filters. The pH imaging system I developed proved that intracellular pH could be measured stably for more than 1 min (data not shown). However, further modifications to the technique are necessary for stable local pH measurement.

Comparison to other pH measurement methods

The pH imaging system has a temporal resolution of 3 ms. While similar systems have been developed in previous studies, they operated only on the second time scale at maximum and were not able to examine rapid pH homeostasis [Sankaranarayanan *et al.*, 2000]. Because of the high temporal resolution of the present system, it has the potential to investigate the molecular mechanism that regulates proton conduction employed by various protein complexes.

Previous kinetic studies of intracellular pH regulation used ^{31}P NMR, a method that requires highly concentrated cell suspensions [Olsen *et al.*, 2002; Wilks and Slonczewski, 2007]. In these experiments, cells were harvested in the late log phase and resuspended at high density, leading to experimental errors. One important advantage of single cell measurements is that they provide explicit information on individual cell variation, avoiding the type of errors caused by ensamble average. I previously found that there are considerable cell-to-cell variations. For example, the number of flagellar motors per cell varies from 4 to 8 [Turner *et al.*, 2000]. Such variation would in turn affect proton influx through the stators of the motors, which could result in misinterpretations of the data when the average of multiple cells is monitored.

Local pH measurement

In this study, local pH in single *Salmonella* cell was measured with Tar-pHluorin and pHluorin-FliG fusion proteins (Fig. 4-9). Tar-pHluorin is considered to measure cytoplasmic pH within about 5 nm from the cytoplasmic membrane [Kim *et al.*, 1999]. Although Tar was localized at the cell poles, as shown by previous data [Shiomi *et al.*, 2005], there were no marked differences between local pH measured by Tar-pHluorin

and bulk pH of the cytoplasm (Fig. 4-9). This result indicates that Tar senses local polar pH that has quite similar value to that throughout the cytoplasm.

Proton influx through the flagellar motor

The local pH measured by pHluorin-FliG is thought to indicate the pH around the torque generation unit formed by FliG and the MotA/B complex, which is 2–3 nm away from the cytoplasmic membrane based on cryo-EM images of the flagellar basal body [Thomas *et al.*, 2001]. The number of protons that flows into the cytoplasm through the motor per revolution was estimated to be about 1200 [Meister *et al*, 1987]. The proton-driven flagellar motor rotates at around 300 Hz [Berg, 2003]. Therefore, the number of protons that enters into the cytoplasm through a single flagellar motor is about 360,000 per second. Despite this relatively large number, there were no significant differences between local pH near the motor and bulk pH of the cytoplasm (Fig. 4-9), suggesting that the pH homeostasis of the bacterial cell has a strong pH buffering capacity, probably by strong proton pumping by complex machinery, such as H^+-ATPase, ATP synthase, H^+ antiporters and respiratory complexes.

High-resolution pH imaging in the future

Flagellar rotation, which corresponds to the output of the flagellar motor, has been studied in many bacteria using various methods. On the contrary, a far less number of studies have been made on the proton influx, which is the input. Meister *et al.* estimated that the number of influx protons per motor per revolution was ca. 1200 [Meister *et al*, 1987]. However this value is questionable since it was determined by using cell suspensions. I constructed a functional fusion protein of pHluorin(M153R) with FliG to measure local pH around the torque generation unit of the flagellar motor

(Fig. 4-9). The pH imaging system, combining with this construct, will allow the motor rotation and local pH change to be monitored at high temporal resolution (Fig. 4-8). I will fully utilize the capability of this sytem to investigate the energy conversion mechanism of the flagellar motor by simultaneously measuring proton influx and motor rotation at the single-motor level. By combining with different fusion proteins that localize distinct cellular locations to exert distinct functions, the pH imaging system will also be sensitive enough to allow measurements of activities of various energy transduction systems at single molecule levels *in vivo* at high spatial and temporal resolution.

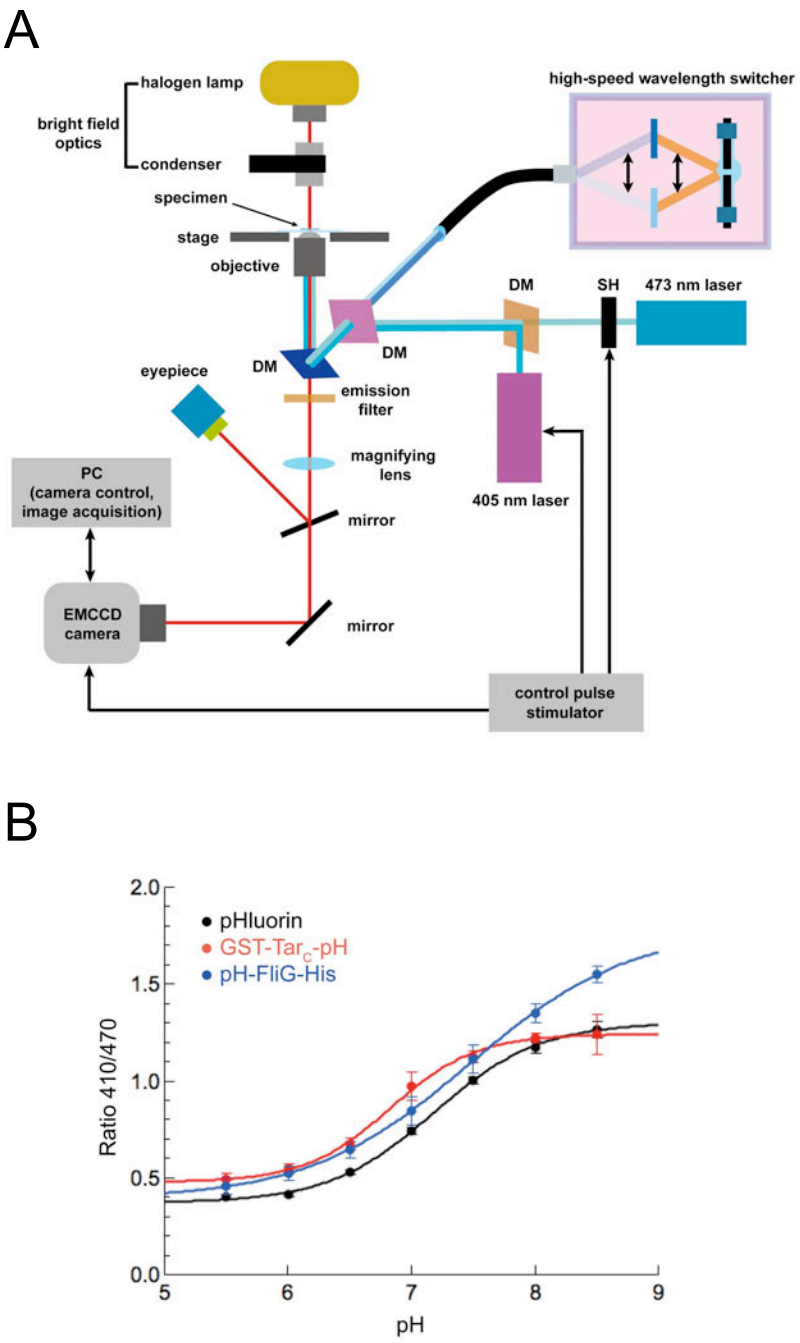

Fig. 4-1. Intracellular pH imaging system (A) Schematic illustration of the intracellular pH imaging system built on an inverted fluorescence microscope. 'DM': dichroic mirror; 'SH': mechanical shutter. (B) Calibration curve between pH and $Ratio_{410/470}$. Calibration curves were presented as a sigmoid plot of the fluorescence excitation ratio versus pH. Fluorescent intensities of purified protein; pHluorin, GST-Tar_c-pHluorin and pHluorin(M153R)-FliG-His_6 were acquired by pH imaging system.

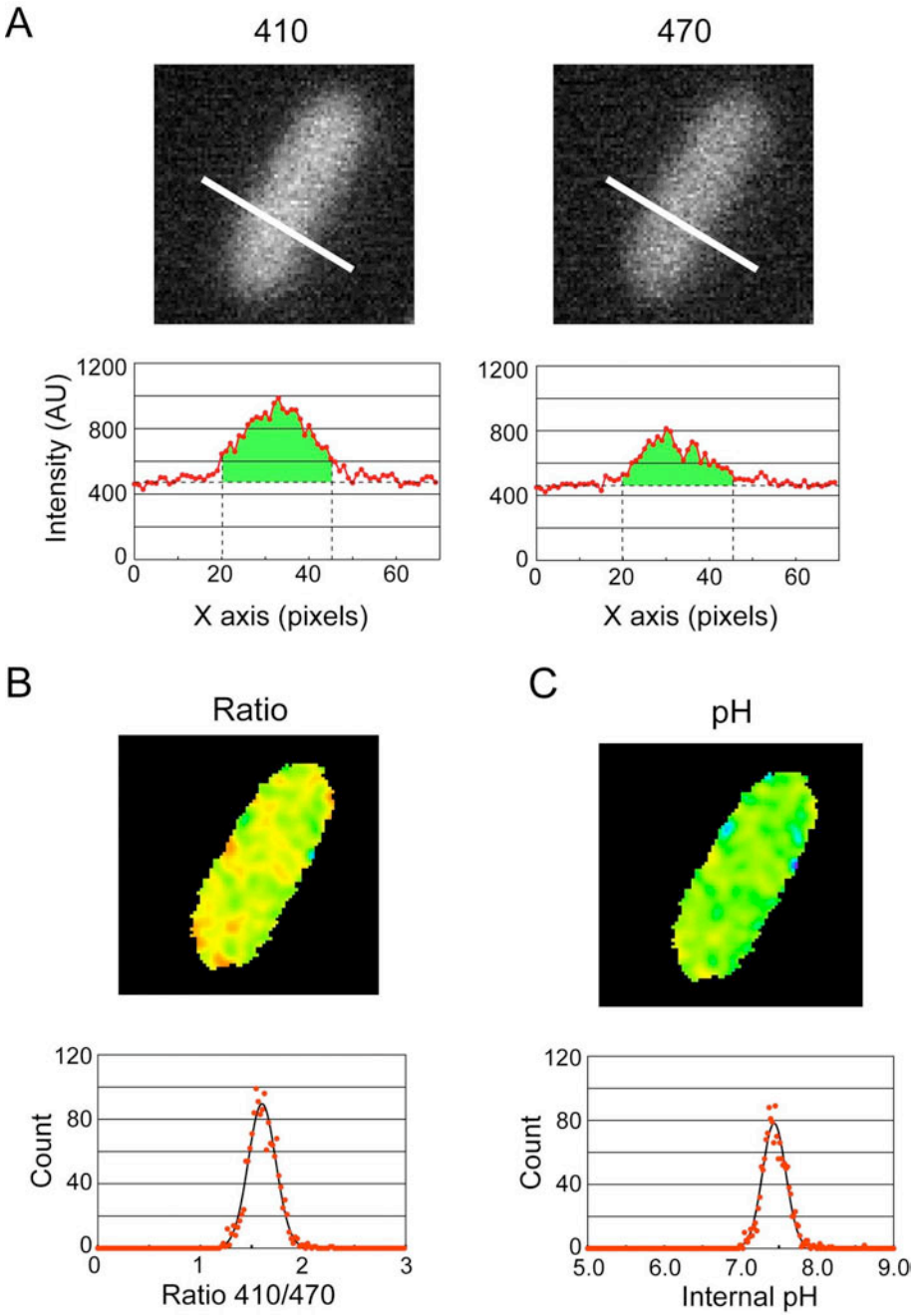

Fig. 4-2. Typical pH imaging of a single cell. (A) Upper images: fluorescence images of MMPH001, excited with 410 nm and 470 nm by a xenon lamp, respectively. Lower graphs: fluorescence intensity profile along the line indicated in the upper images. The green area under the peak is used to determine the intracellular pH. (B) $Ratio_{410/470}$ of MMPH001 was calculated by 3 x 3 gaussian smoothing. (C) Intracellular pH was determined from $Ratio_{410/470}$ for each pixels.

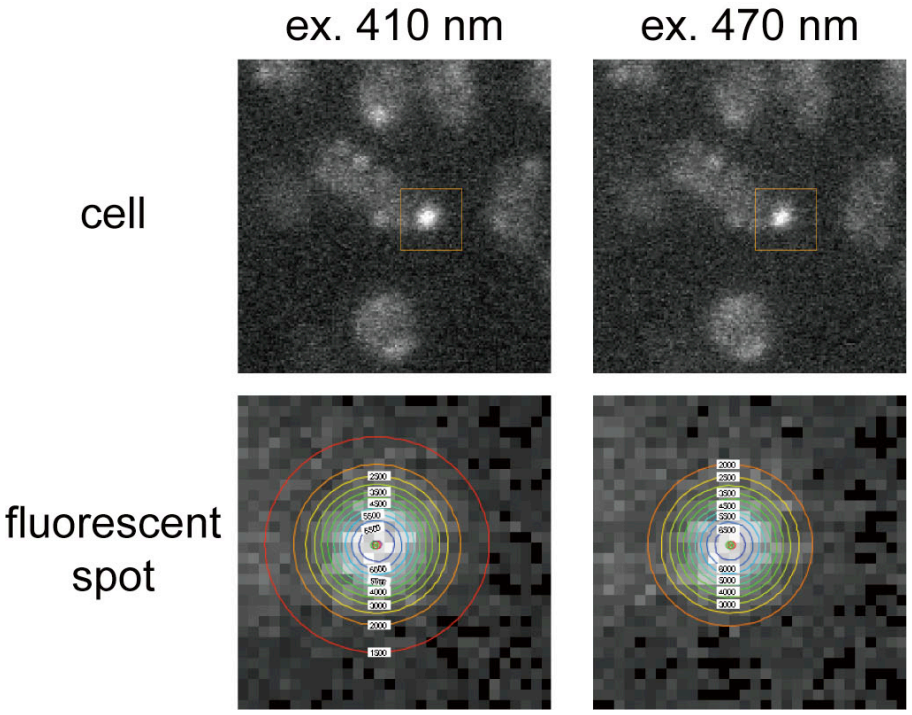

Fig. 4-3. Typical example of local pH measurement by a fluorescent spot of pHluorin-FliG. Upper images: fluorescence images of YVM1004, excited with 410 nm and 470 nm by a Xenon lamp, respectively. Lower images: magnified images of the fluorescent spots within the orange box in the upper images. The intensity of single fluorescent spot of pHluorin-FliG was identified and extracted by fitting with a 2D-Gaussian, which is presented as concentric circles. Local pH was determined from the ratio of integrated intensities of fluorescent spots.

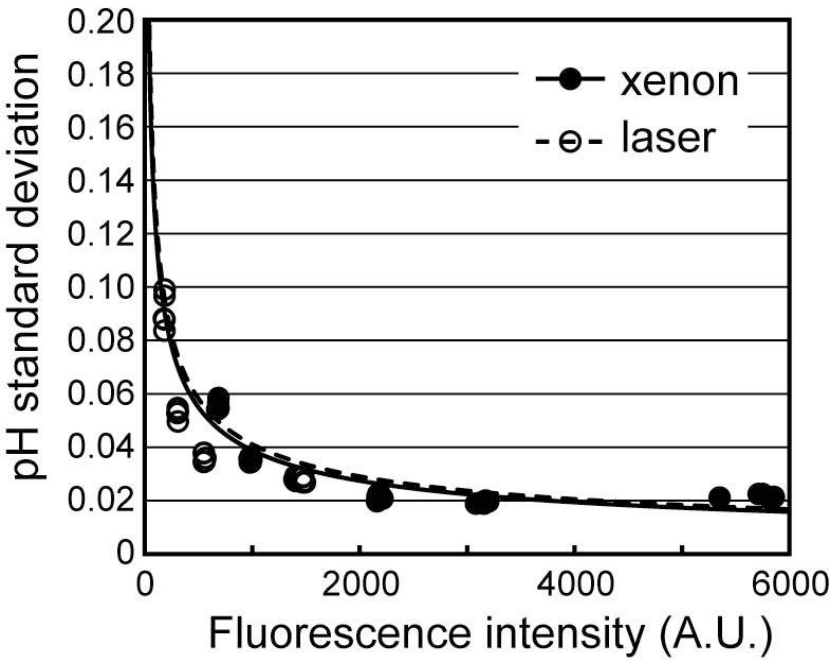

Fig 4-4. pH resolution of the pH imaging system. pH was measured with purified pHluorin at pH 7.0 by either xenon lamp or laser excitation. The standard deviations of pH are plotted as a function of the fluorescence intensity. The data obtained by the xenon lamp were acquired by the EMCCD Hamamatsu C9100-02 with 7 × 7 pixel smoothing (xenon). The data obtained by lasers was acquired by the EMCCD Andor iXon with 3 × 3 pixel smoothing (laser). A best-fit curvilinear power regression curve was selected with Kaleida Graph (Synergy Software).

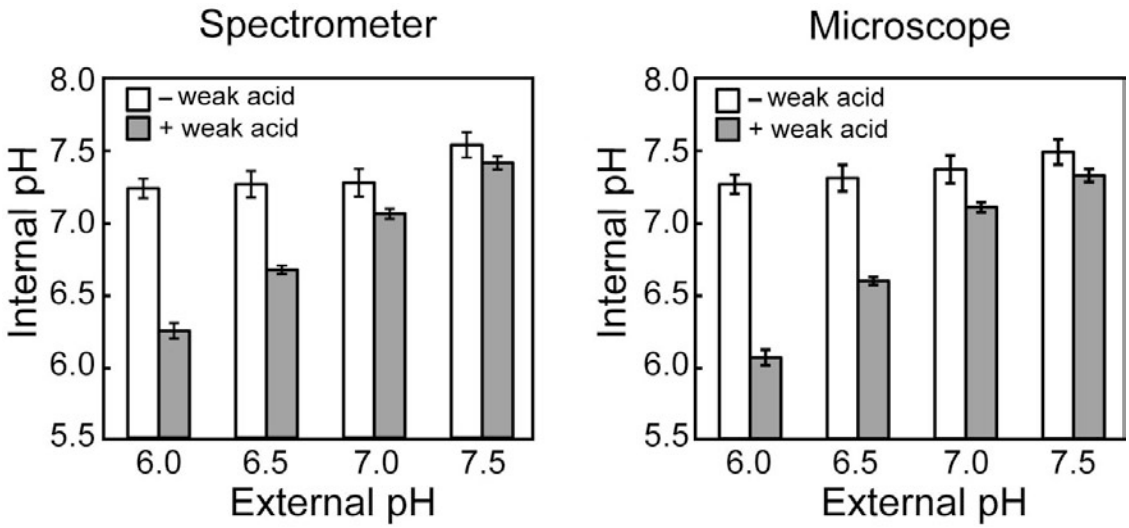

Fig. 4-5. Effect of weak acid on intracellular pH. Intracellular pH of MMPH001 was measured by a spectrophotometer (Spectrometer) or the pH imaging system (Microscope) at external pH range 6.0 – 7.5 with or without 20 mM benzoate. Each set of data is the average of more than 100 cells. The measurements were done at ca. 23ºC.

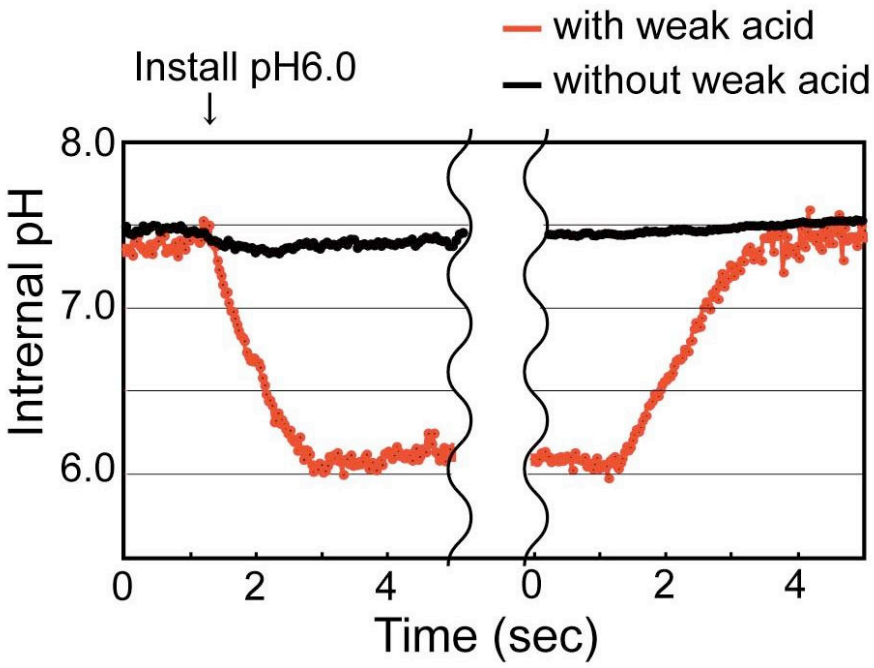

Fig. 4-6. Time-lapse measurement of intracellular pH change. The intracellular pH of SJW1103/pYVM001 was measured with changing intracellular pH by changing the external medium pH from 7.0 to 6.0 with or without benzoate. The external pH was brought back to 7.0 with the original buffer without benzoate. The change in intracellular pH was measured at 30 ms intervals by DPSS laser excitation. The measurements were done at ca. 23ºC.

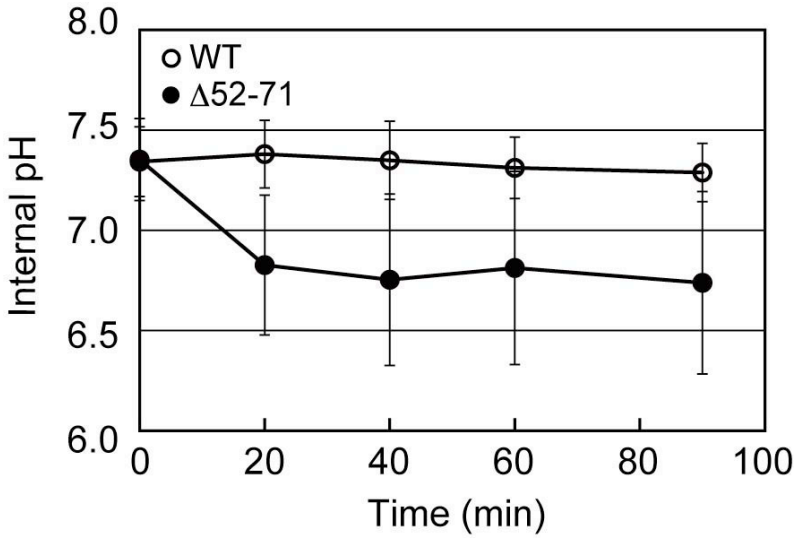

Fig. 4-7. Effects of deletion of the plug segment of *Salmonella* MotB on proton leakage. Measurement of the intracellular pH of YVM021 cells (Δ*fliC*::*pHluorin*) transformed with the pBAD24-based plasmids pYC20 (WT) or pYC109 (Δ52-71) using the pHluorin probe after induction of MotA/B or MotB(Δ52-71) expression at an external pH of 5.5.

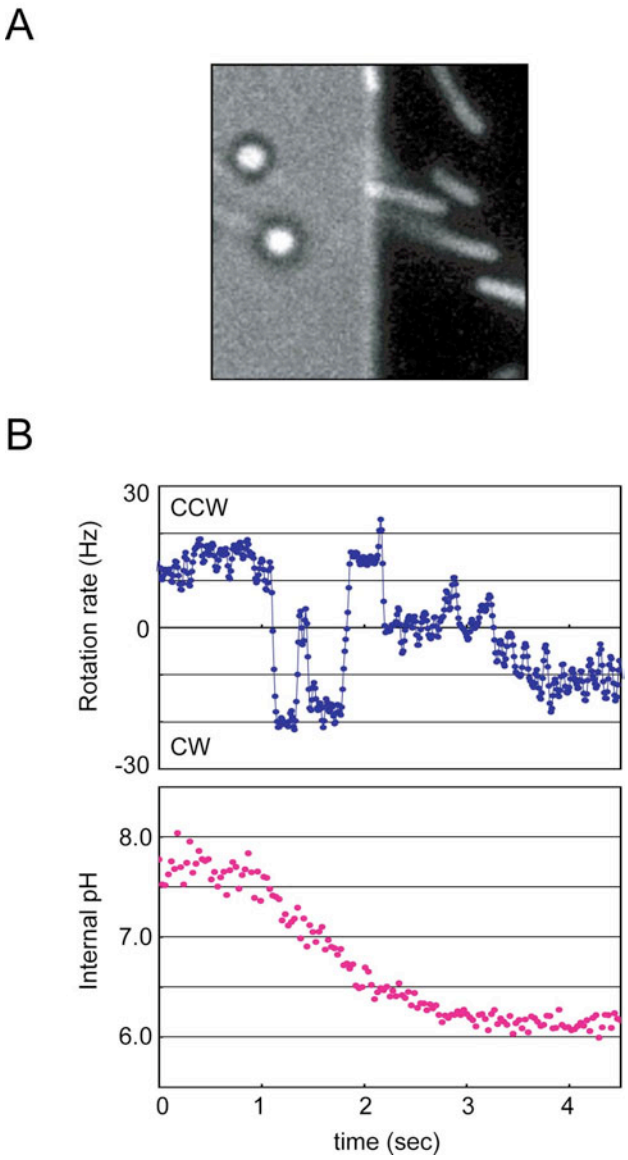

Fig. 4-8. Rapid responses to a decrease in intracellular pH. Intracellular pH and the rotation rate of a 1.5 μm diameter bead attached to the sticky flagellar filaments were measured in a single cell. (A) Simultaneous measurement carried out with a split-image microscope unit. Left half is the bright field image for detecting the rotation of polystyrene beads attached to a filament. Right half region is the fluorescent image used to calculate pH with pHluorin. (B) Intracellular pH and the rotation rate were measured at 30 ms and at 10 ms intervals, respectively. External pH was shifted from 7.0 to 6.0 by a 20 mM benzoate medium.

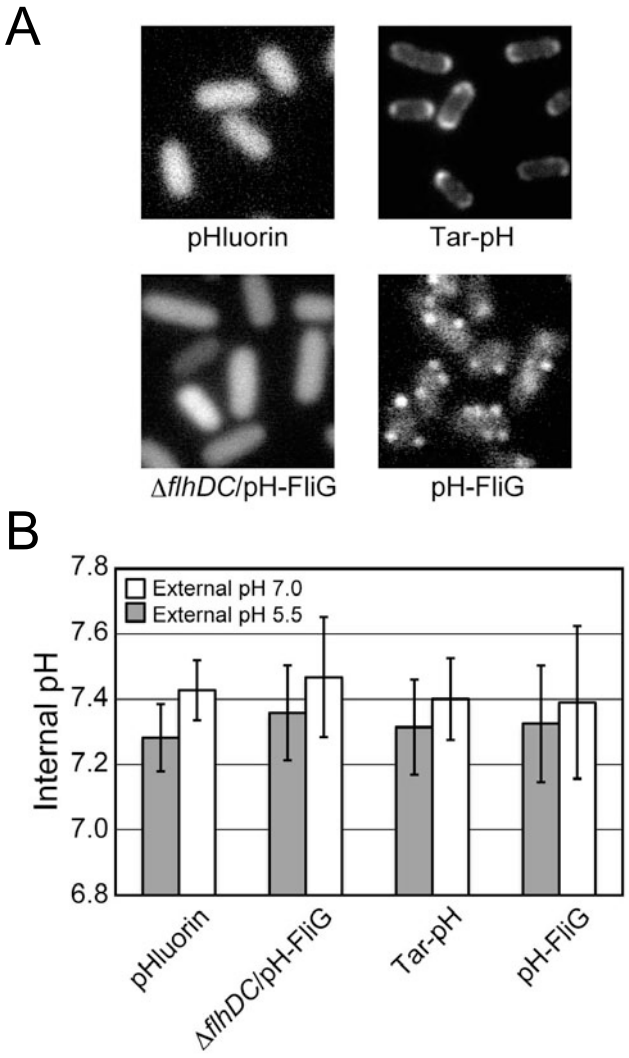

Fig. 4-9. Local pH measurements of a single cell. (A) MMPH001 (pHluorin), SJW1368/pYVM008 (Δ*flhDC*/pH-FliG), YVM009 (Tar-pH) and YVM1004 (pH-FliG) were observed under a fluorescence microscope. Cells were incubated at 30ºC for 6 hours. (B) pH was measured using the pH imaging system with a pH 5.5 or 7.0 motility medium. pH was determined by the standard curves obtained from purified pHluorin (for MMPH001), GST-Tar_C-pHluorin(M153R) (for YVM009) and pHluorin(M153R)-FliG-His_6 (for SJW1368/pYVM008 and YVM1004). The measurements were done at ca. 23ºC.

Table 4-1. Strains used in Chapter 4

Strains	Relevant characteristics	Source or reference
E. coli		
BL21(DE3) pLysS	T7 expression host	Novagen
Salmonella		
SJW1103	Wild type for motility and chemotaxis	Yamaguchi *et al*. (1984)
SJW46	*fliC*(Δ204-292)	Yoshioka *et al*. (1995)
SJW1368	Δ(*cheW-flhD*)	Ohnishi *et al*. (1994)
SJW2241	Δ(*motA-motB*)	Komoriya *et al*. (1999)
MMPH001	Δ*araBAD::pHluorin*	Morimoto *et al*. (2010a)
YVM009	*tar-pHluorin*(M153R)	Y. Morimoto, unpublished
YVM1004	*pHluorin*(M153R)-*fliG*	Y. Morimoto, unpublished

Table 4-2. Plasmids used in Chapter 4

Plasmids	Relevant characteristics	Source or reference
pKK223-3	Cloning vector	GE Healthcare
pTrc99A	Cloning vector	GE Healthcare
pBAD24	Cloning vector	Guzman *et al*. (1995)
pKSS13	pKK223-3 / MotA+MotB	Morimoto *et al*. (2010a)
pYC001	pKK223-3 / pHluorin	Nakamura *et al*. (2009a)
pYC20	pBAD24 / MotA+MotB	Morimoto *et al*. (2010a)
pYC109	pBAD24 / MotA+MotB(Δ52-71)	Morimoto *et al*. (2010a)
pGST-pHluorin	pGEX2T / GST-pHluorin	Miesenböck *et al*. (1998)
pYVM001	pKK223-3 / pHluorin(M153R)	Y. Morimoto, unpublished
pYVM003	pGEX6p-1 / GST-$Tar_{286–553}$-pHluorin(M153R)	Y. Morimoto, unpublished
pYVM007	pGEX2T / GST-pHluorin(M153R)	Y. Morimoto, unpublished
pYVM008	pTrc99A / pHluorin(M153R)-FliG	Y. Morimoto, unpublished
pYVM013	pTrc99A / pHluorin(M153R)-FliG-His_6	Y. Morimoto, unpublished

Table 4-3. Primers used in Chapter 4

Primers	Sequence
Tar_C-tetR	ccgcagtcattagccgccagggatgatgcgaactgggaaattaagacccactttcacatt
Tar_C-tetA	cgggttcgcaaattaatcgataaccgacagcgcacgtcgactaagcacttgtctcctg
Tar_C-pH_Fw	gcagtcattagccgccagggatgatgcgaactgggaaaccttcatgagtaaaggagaagaacttttc
Tar_C-pH_Rv	cggcgggttcgcaaattaatcgataaccgacagcgcacgtcgattatttgtatagttcatccatgcc
BamHI-Tar286	aaggatccaataccgacctctcttccc
pH_EcoRI	aagaattcttatttgtatagttcatccatgcca
XbaI-fliG_SD	aatctagatggtggcgctggtcattcgccagt
fliG-HindIII	aaaagcttttagacataggtatcctcgc
fliG_ds-XhoI	aactcgaggacataggtatcctcgccgc
His-HindIII	aaaagctttcagtggtggtggtggtggtgctc

Conclusion

This study has been carried out towards the goal of understanding the molecular mechanisms of the activation and localization of the MotA/B proton channel complex of the proton-driven bacterial flagellar motor. Summary of my new finding throughout the work is described below.

(1) *Salmonella* MotB has the plug region, which acts in a similar way to the corresponding region of *E. coli* MotB.

(2) The proton-conductivity of the MotA/B complex not incorporated into the motor is two orders of magnitude lower than that of a complex that was incorporated and activated.

(3) The process of proton translocation through the channel is not required for the MotA/B assembly.

(4) The electrostatic interaction of the cytoplasmic loop of MotA with FliG is required for the efficient assembly of the stators around the rotor but not for torque generation.

(5) The M153R mutation in pHluorin improves the stability of its fusion proteins.

(6) A pH imaging system has been developed to measure local pH near the motor using pHluorin with a pH resolution of 0.02 and a temporal resolution of 3 msec.

The proton-conductivity of the MotA/B complex

The MotA/B stator complex acts as a proton channel of the proton-driven flagellar motor. Since an in-frame deletion of residues 51-70 in *E. coli* MotB, which corresponds to residues 52-71 in *Salmonella* MotB, causes significant proton leakage and arrests cell growth, the deleted region has been proposed to act as a plug that prevents the MotA/B complex from leaking protons before it assembles into the motor [Hosking et al., 2006]. In Chapter 1, I measured the proton-conductivity of the

unplugged and plugged MotA/B complex of *Salmonella* by a ratiometric pH indicator protein, pHluorin, and found that the proton-conductivity of the MotA/B complex not incorporated into the motor is small but large enough to change the cytoplasmic pH to a level at which the chemotactic signal transduction system responds. Approximately 50-fold over-expression of MotA/B compared to the chromosome expression level was necessary to cause such small proton leakage, indicating that the conserved plug segment in MotB does not tightly suppress proton leakage. There are two possible reasons: 1) the plug may breathe in and out of the cytoplasmic membrane, as suggested previously [Hosking *et al.*, 2006], or 2) even with the plug place in there is some leakage.

Because the change in the intracellular pH as small as ca. 0.2 units can be detected either by pHluorin expressed in the cell or by the chemotaxis signal transduction system of *Salmonella* using motility assay, I suggest that the proton conductivity of potential, but unproven, transmembrane proton channels and conductors may be examined easily and quickly by expressing the proteins in *Salmonella* cells expressing cytoplasmic pHluorin and by swarming motility assay. This will be a convenient and high-throughput method for examining proton conductivity of membrane protein complexes.

Subcellular localization of the MotA/B complex

MotB consists of the N-terminal cytoplasmic region, one transmembrane helix, and the C-terminal periplasmic region named $MotB_C$, which contains the PG-binding motif [Kojima and Blair, 2004; Kojima *et al.*, 2009]. $MotB_C$ is thought to be required for proper targeting and stable anchoring of the MotA/B complex to the motor [Kojima *et al.*, 2008]. The stators can be exchanged with the membrane pool even during motor

rotation, indicating that the stator does not stably bind to the motor and the peptidoglycan layer [Leake *et al*., 2006]. The plug segment in the $MotB_C$ region suppresses the proton-conductivity of free MotA/B complexes diffusing in the cytoplasmic membrane when they are not installed into the motor [Hosking *et al*., 2006; Morimoto *et al*., 2010a]. In Chapter 2, I showed that the process of proton translocation through the channel is not required for stator assembly and that MotA alone can be installed into the flagellar motor in the absence of MotB. The results suggested that two charged residues of MotA, Arg-90 and Glu-98, which are important for electrostatic interactions with FliG, were critical not only for torque generation but also for the assembly of the stators into the motor. However, the roles of these two residues were slightly different. I have to work out this mechanism. Further single molecule imaging analysis of MotA and MotB by fluorescent microscopy and carrying out high-resolution structural analyses by electron cryomicroscopy and single particle analysis of the basal body with stators are required to clarify the localization mechanism of the MotA/B complex. Dynamic behavior of the MotA/B complex must be investigated by single molecule detection technique combined with molecular genetics.

High-resolution pH imaging

I analyzed the proton-conductivity and the subcellular localization mechanism of the MotA/B complex to understand the energy coupling mechanism of the bacterial flagellar motor. However, I was not able to clarify the energy conversion mechanism. To do this, I must establish the system to measure the proton flow coupled with motor rotation. Many methods for the rotation analyses of the rotary motor with high spatial and temporal resolutions have been developed [Yuan and Berg, 2008; Ueno *et al.*,

2010]. In contrast to F_oF_1-ATPsynthase [Noji *et al.*, 1997], *in vitro* reconstruction of the flagellar motor has not been succeeded. Furthermore, in the proton-driven motor, manipulations of the energy input is quite difficult compared with the sodium-driven motor. For these reasons, a far less number of studies have been made on the proton influx through the flagellar motor, although Meister *et al.* roughly estimated that the number of influx protons per revolution is ca. 1200 [Meister *et al.*, 1987]. But this value is questionable since it was determined by using cell suspensions.

pH-sensitive red fluorescent protein has been developed, and used for monitoring the nucleoside transport-coupled proton flow in the investigation of a human concentrative transporter [Johnson *et al.*, 2009]. The number of proton co-transported with nucleoside by the transporter has been estimated. This report supports the view that the pH imaging technique is capable of monitoring proton flux through the proton channel.

I have developed a pH imaging system that can measure local pH near the motor using pHluorin. This system can measure the intracellular pH distribution with a pH resolution of 0.02 and a temporal resolution of 3 msec. I also measured local pH around the motor with the cell having its flagellar motor components fused to the pHluorin(M153R) mutant. The local pH around the torque generation unit of the motor, which is 2–3 nm away from the cytoplasmic membrane, were almost same with bulk cytoplasmic pH, probably because of a strong pH homeostasis throughout the cell. This tequnique for measuring local pH near the membrane is expected to give us critical insights into the energy conversion mechanism of the flagellar motor by simultaneously measuring local pH and motor rotation at the single-motor level.

pH imaging is becoming an efficient and usuful method in various fields, such as a medicine, because local pH is one of the most important parameters of live

cells. A pH probe has been developed for *in vivo* cancer imaging by taking advantage of the lysosome that holds low pH (pH 5.0–6.0) relative to the cytoplasmic pH (pH ~7.4) [Urano *et al.*, 2008]. This technique can be helpful in detecting early cancer. Additionally, it is suggested that for oxidative phosphorylation, alkaliphilic *Bacillus* uses the proton movement laterally along membrane surface, which is rapid enough to support the ATP synthesis before protons are lost to the bulk [Heberle *et al.*, 1994; Guffanti and Krulwich, 1994]. Because of the high resolution, the pH imaging system developed here will be usefully applied to diverse areas of biological sciences.

Acknowledgements

This study has been carried out in the Protonic NanoMachine Laboratory, Graduate School of Frontier Biosciences, Osaka University.

I would like to express my sincere gratitude to my supervisor, Prof. Keiichi Namba for stimulating discussion and encouragement throughout my Ph.D study. I am deeply grateful to Associate Prof. Tohru Minamino for teaching me a lot including the experimental methods as well as his continuous support, helpful advices and discussion. I wish to express my sincere thanks to Prof. Yasushi Hiraoka, Prof. Masahiro Ueda and Prof. Hiroyuki Noji for evaluating this work.

I am also grateful to Dr. Nobunori Kami-ike for technical advices and developing analysis programs. I thank Dr. Yong-Suk Che and Dr. Shuichi Nakamura for helpful comments and technical advices for experiments. I acknowledge Prof. J.E. Rothman, Dr. Seiji Kojima and Dr. Hideyuki Matsunami for a gift of plasmid. I also thank to all the members of the Protonic NanoMachine Laboratory for their professional and personal help.

This study was supported by the Predoctoral Fellowship from the Japan Society for the Promotion of Science and the Global COE Program “System Dynamics of Biological Function” of the Graduate School of Frontier Biosciences, Osaka University.

Finally, I thank my family and my friends for their kind support.

March, 2011 Y.V. Morimoto

References

Armitage, J.P. (1999) Bacterial tactic responses. *Adv Microb Physiol* **41**: 229–289.

Asai, Y., Kawagishi, I., Sockett, R.E. and Homma, M. (2000) Coupling ion specificity of chimeras between H^+- and Na^+-driven motor proteins, MotB and PomB, *Vibrio* Polar flagella. *EMBO Journal* **19**: 3639–3648.

Asai, Y., Yakushi, T., Kawagishi, I. and Homma, M. (2003) Ion-coupling determinants of Na+-driven and H^+-driven flagellar motors. *J Mol Biol* **327**: 453–463.

Berg, H.C. (2000) Constraints on models for the flagellar motor. *Phil Trans Roy Soc B* **335**: 491–502.

Berg, H.C. (2003) The rotary motor of bacterial flagella. *Annu Rev Biochem* **72**: 19–54.

Berg, H.C. and Brown, D.A. (1972) Chemotaxis in *Escherichia coli* analysed by three-dimensional tracking. *Nature* **239**: 500–504.

Berg HC, and Anderson R.A. (1973) Bacteria swim by rotating their flagellar filaments. *Nature* **245**: 380–382.

Berg, H.C. and Turner, L. (1993) Torque generated by the flagellar motor of Escherichia coli. *Biophys J* **65**: 2201–2216.

Berry, R.M. and Berg, H.C. (1999) Torque generated by the flagellar motor of Escherichia coli while driven backward. *Biophys J* **76**: 580–587.

Blair, D.F., and Berg, H.C. (1988) Restoration of torque in defective flagellar motors. *Science* **242**: 1678–1681.

Blair, D.F., and Berg, H.C. (1990) The MotA protein of *E. coli* is a proton-conducting component of the flagellar motor. *Cell* **60**: 439–449.

Blair, D. F. (2003) Flagellar movement driven by proton translocation. *FEBS Lett* **545**: 86–95.

Block, S.M., and Berg, H.C. (1984) Successive incorporation of force-generating units in the bacterial rotary motor. *Nature* **309**: 470–472.

Braun, T. and Blair, D.F. (2001) Targeted Disulfide Cross-Linking of the MotB Protein of *Escherichia coli*: Evidence for Two H+ Channels in the Stator Complex. *Biochemistry* **40**: 13051–13059.

Braun, T., Poulson, S., Gully, J.B., Empey, J.C., Van Way, S., Putnam, A., and Blair, D.F. (1999) Function of proline residues of MotA in torque generation by the flagellar motor of Escherichia coli. *J Bacteriol* **181**: 3542–3551.

Braun, T.F., Al-Mawasawi, L.Q., Kojima, S. and Blair, D.F. (2004) Arrangement of core membrane segments in the MotA/MotB protein-channel complex of *Escherichia coli*. *Biochemistry* **43**: 35–45.

Chattoraj, M., B. A. King, G. U. Bublitz and S. G. Boxer. (1996) Ultra-fast excited state dynamics in green fluorescent protein: multiple states and proton transfer. *Proc Natl Acad Sci USA* **93**: 8362–8367.

Che, Y-S., Nakamura, S., Kojima S., Kami-ike, N., Namba, K. and Minamino, T. (2008) Suppressor analysis of the MotB(D33E) mutation to probe the bacterial flagellar motor dynamics coupled with proton translocation. *J Bacteriol* **190**: 6660–6667.

Chen, X. and Berg, H. C. (2000a) Torque-speed relationship of the flagellar motor of *Escherichia coli*. *Biophys J* **78**: 1036–1041.

Chen, X. and Berg, H. C. (2000b) Solvent-isotope and pH effects on flagellar rotation in *Escherichia coli*. *Biophys J* **78**: 2280–2284.

Crameri, A., Whitehorn, E.A., Tate, E. and Stemmer, W.P.C. (1996) Improved green fluorescent protein by molecular evolution using DNA shuffling. *Nat Biotechnol* **14**: 315–319.

Datsenko, K.A. and Wanner B.L. (2000) One-step inactivation of chromosomal genes in *Escherichia coli* K-12 using PCR products. *Proc Natl Acad Sci USA* **97**: 6640–6645.

Delalez, N. and Armitage, J.P. (2009) Parts exchange: tuning the flagellar motor to fit the conditions. *Mol Microbiol* **71**: 807–810.

De Mot, R. and Vanderleyden, J. (1994) The C-terminal sequence conservation between OmpA-related outer membrane proteins and MotB suggests a common function in both gram-positive and gram-negative bacteria, possibly in the interaction of these domains with peptidoglycan. *Mol Microbiol* **12**: 333–334.

DePamphilis, M. L. and Adler, J. (1971a) Purification of intact flagella from E*scherichia coli* and *Bacillus subtilis*. *J Bacteriol* **105**: 376–383.

DePamphilis, M. L. and Adler, J. (1971b) Fine structure and isolation of the hook-basal body complex of flagella from *Escherichia coli* and *Bacillus subtilis*. *J Bacteriol* **105**: 384‒395

DeRosier, D. (2006) Bacterial Flagellum: Visualizing the Complete Machine In Situ. *Current Biology* **16**: 928–930.

Francis, N.R., Sosinsky, G.E., Thomas, D. and DeRosier, D.J. (1994) Isolation, characterization, and structure of bacterial flagellar motors containing the switch complex. *J Mol Biol* **235**: 1261–1270.

Fukuoka H., Sowa, Y. Kojima, S. Ishijima, A. and Homma, M. (2007) Visualization of functional rotor proteins of the bacterial flagellar motor in the cell membrane. *J Mol*

Biol **367**: 692–701.

Fukuoka, H., Wada, T., Kojima, S., Ishijima, A. and Homma M. (2009) Sodium-dependent dynamic assembly of membrane complexes in sodium-driven flagellar motors. *Mol Microbiol* **71**: 825–835.

Fung, D.C. and Berg, H.C. (2005) Powering the flagellar motor of *Escherichia coli* with an external voltage source. *Nature* **375**: 809–812.

Fukuoka, H., Inoue, Y., Terasawa, S., Takahashi, H. and Ishijima, A. (2010) Exchange of rotor components in functioning bacterial flagellar motor. *Biochem Biophys Res Commun* **394**: 130–135.

Gabel, C.V. and Berg, H.C. (2003) The speed of the flagellar rotary motor of *Escherichia coli* varies linearly with protonmotive force. *Proc Natl Acad Sci USA* **100**: 8748–8751.

Gosink, K.K. and Häse, C.C. (2000) Requirements for conversion of the Na(+)-driven flagellar motor of Vibrio cholerae to the H(+)-driven motor of *Escherichia coli*. *J Bacteriol* **182**: 4234–40.

Guffanti, A.A. and Krulwich, T.A. (1994) Oxidative phosphorylation by ADP + P(i)-loaded membrane vesicles of alkaliphilic *Bacillus firmus* OF4. *J Biol Chem* **269**: 21576–21582

Guzman, L.M., Belin, D., Carson, M.J. and Beckwith J. (1995) Tight regulation, modulation, and high-level expression by vectors containing the arabinose PBAD promoter. *J Bacteriol* **177**: 4121–4130.

Heberle, J., Riesle, J., Thiedemann, G., Oesterhelt, D. and Dencher, N.A. (1994) Proton migration along the membrane surface and retarded surface to bulk transfer. *Nature* **370**: 379-382.

Heim, R. and Tsien, R.Y. (1996) Engineering green fluorescent protein for improved brightness, longer wavelengths and fluorescence resonance energy transfer. *Curr. Biol*. **6**: 178–182.

Heberle, J., Riesle, J., Thiedemann, G., Oesterhelt, D. and Dencher, N.A. (1994) Proton migration along the membrane surface and retarded surface to bulk transfer. *Nature* **370**: 379–382.

Hess, S.T., Heikal, A.A. and Webb, W.W. (2004) Fluorescence Photoconversion Kinetics in Novel Green Fluorescent Protein pH Sensors (pHluorins). *J Phys Chem B* **108**: 10138–10148.

Hirota, N. and Imae, Y. (1983) Na+-driven flagellar motors of an alkalophilic *Bacillus* strain Yn-1. *J Biol Chem* **258**: 10577–10581.

Hirota, N., Kitada, M. and Imae, Y. (1981) Flagellar motors of alkalophilic *Bacillus* Are powered by an electrochemical potential gradient of Na+. *FEBS Lett* **132**: 278–280.

Hizukuri, Y., Kojima, S. and Homma, M. (2010) Disulfide cross-linking between the stator and the bearing components in the bacterial flagellar motor. *J Biochem* **148**: 309–318.

Hosking, E.R., Vogt, C., Bakker, E.P. and Manson, M.D. (2006) The *Escherichia coli* MotAB proton channel unplugged. *J Mol Biol* **364**: 921–937.

Imamura, H., Nhat, K.P., Togawa, H., Saito, K., Iino, R., Kato-Yamada, Y., Nagai, T. and Noji, H. (2009) Visualization of ATP levels inside single living cells with fluorescence resonance energy transfer-based genetically encoded indicators. *Proc Natl Acad Sci USA* **106**: 15651–15656.

Ito, M., Terahara, N., Fujinami, S., and Krulwich, T.A. (2005) Properties of Motility in Bacillus subtilis Powered by the H^+-Coupled MotAB Flagellar Stator, Na^+-Coupled MotPS or Hybrid Stators MotAS or MotPB. *J Mol Biol* **352**:396–408.

Kami-ike, N., Kudo, S. and Hotani, H. (1991) Rapid changes in flagellar rotation induced by external electric pulses. *Biophys J* **60**:1350–1355.

Khan, S., Khan, I.H. and Reese, T.S. (1991) New structural features of the flagellar base in Salmonella typhimurium revealed by rapid-freeze electron microscopy. *J Bacteriol* **173**: 2888–2896.

Kihara, M. and Macnab, R.M. (1981) Cytoplasmic pH mediates pH taxis and weak-acid repellent taxis of bacteria. *J Bacteriol* **145**: 1209–1221.

Kneen, M., J. Farinas, Li, Y. and Verkman, A. S. (1998) Green fluorescent protein as a noninvasive intracellular pH indicator. *Biophys J* **74**:1591–1599.

Kojima, S. and Blair, D.F. (2001) Conformational change in the stator of the bacterial flagellar motor. *Biochemistry* **40**: 13041–13050.

Kojima, S. and Blair, D.F. (2004) Solubilization and purification of the MotA/MotB complex of *Escherichia coli*. *Biochemistry* **43**: 26–34.

Kojima, S., Furukawa, Y., Matsunami, H., Minamino, T. and Namba, K. (2008) Characterization of the periplasmic domain of MotB and implications for its role in the stator assembly of the bacterial flagellar motor. *J Bacteriol* **190**: 2259–2266.

Kojima, S., Imada, K., Sakuma, M., Sudo, Y., Kojima, C., Minamino, T., Homma, M. and Namba, K. (2009) Stator assembly and activation mechanism of the flagellar motor by the periplasmic region of MotB. *Mol Microbiol* **73**: 710–718.

Komoriya, K., Shibano, N., Higano, T., Azuma, N., Yamaguchi, S. and Aizawa, S.-I. (1999) Flagellar proteins and type III-exported virulence factors are the predominant proteins secreted into the culture media of *Salmonella typhimurium*. *Mol Microbiol* **34:** 767–779.

Krulwich, T.A. (1995) Alkaliphiles: 'basic' molecular problems of pH tolerance and

bioenergetics. *Mol Microbiol* **15**: 403–410.

Kudryashev, M., Cyrklaff, M., Wallich, R., Baumeister, W. and Frischknecht, F. (2010) Distinct in situ structures of the Borrelia flagellar motor. *J Struct Biol* **169**:54–61.

Kutsukake, K. and Iino, T. (1994) Role of the FliA-FlgM regulatory system on the transcriptional control of the flagellar regulon and flagellar formation in *Salmonella typhimurium. J Bacteriol* **176**: 3598–3603

Larsen, S.H., Adler, J., Gargus, J.J. and Hogg, R.W. (1974) Chemomechanical coupling without ATP: the source of energy for motility and chemotaxis in bacteria. *Proc Natl Acad Sci USA* **71**: 1239–1243.

Leake, M.C., Chandler, J.H., Wadhams, G.H., Bai, F., Berry, R.M. and Armitage, J.P. (2006) Stoichiometry and turnover in single, functioning membrane protein complexes. *Nature* **443**: 355–358.

Liu, J., Lin, T., Botkin, D.J., McCrum, E., Winkler, H. and Norris, S.J. (2009) Intact Flagellar Motor of Borrelia burgdorferi Revealed by Cryo-Electron Tomography: Evidence for Stator Ring Curvature and Rotor/C-Ring Assembly Flexion. *J Bacteriol* **191**: 5026–5036.

Llopis, J., McCaffery, M. Miyawaki, A. Farquhar, M.G. and Tsien. R.Y. (1998) Measurement of cytosolic, mitochondrial, and Golgi pH in single living cells with green fluorescent proteins. *Proc Natl Acad Sci USA* **95**: 6803–6808

Lloyd, S.A. and Blair, D.F. (1997) Charged residues of the rotor protein FliG essential for torque generation in the flagellar motor of *Escherichia coli*. *J Mol Biol* **266**: 733–744.

Lo, C.J., Leake, M.C., Pilizota, T. and Beryy, R.M. (2007) Nonequivalence of membrane voltage and ion-gradient as driving forces for the bacterial flagellar motor at low load. *Biophys J* **93**: 294–302.

Manson, M.D., Tedesco, P, Berg, H.C., Harold, F.M. and Van der Drift, C. (1977) A protonmotive force drives bacterial flagella. *Proc Natl Acad Sci USA* **4**: 3060–3064.

Macnab, R.M. and Ornston MK (1977) Normal-to-curly flagellar transitions and their role in bacterial tumbling. Stabilization of an alternative quaternary structure by mechanical force. *J Mol Biol* **112**: 1–30

Macnab, R.M. (2003) How bacteria assemble flagella. *Annu Rev Microbiol* **57**: 77–100.

Matsura, S., Shioi, J. and Imae, Y. (1977) Motility in *Bacillus subtilis* driven by an artificial protonmotive force. *FEBS Lett* **82**: 187–190

McCarter, L.L. (1994a) MotX, The channel component of the sodium-type flagellar motor. *J Bacteriol* **176**: 5988–5998.

McCarter, L.L. (1994b) MotY, a component of the sodium-type flagellar motor. *J Bacteriol* **176**: 4219–4225.

Meister, M. and Berg, H.C.. (1987) The stall torque of the bacterial flagellar motor. *Biophys J* **52:** 413–419.

Meister, M., Lowe, G. and Berg, H.C. (1987) The proton flux through the bacterial flagellar motor. *Cell* **49**: 643–650.

Miesenböck, G., De Angelis, D.A., and Rothman, J.E. (1998) Visualizing secretion and synaptic transmission with pH-sensitive green fluorescent proteins. *Nature* **394**: 192–195.

Minamino, T. and Macnab, R.M. (1999) Components of the *Salmonella* flagellar export apparatus and classification of export substrates. *J Bacteriol* **181:** 1388–1394.

Minamino, T. and Macnab. R.M. (2000) Interactions among components of the Salmonella flagellar export apparatus and its substrates. *Mol Microbiol* **35**: 1052–1064.

Minamino, T., Imae, Y., Oosawa, F., Kobayashi, Y. and Oosawa, K. (2003) Effect of intracellular pH on the rotational speed of bacterial flagellar motors. *J Bacteriol* **185**: 1190–1194.

Minamino, T. and Namba, K. (2004) Self-assembly and type III protein export of the bacterial flagellum. *J Mol Microbiol Biotechnol* **7**: 5–17.

Minamino, T., Imada, K. and Namba, K. (2008) Molecular motors of the bacterial flagella. *Curr Opin Struct Biol* **18**:693–701.

Morimoto, Y.V., Che, Y-.S., Minamino, T. and Namba, K. (2010a) Proton-conductivity assay of plugged and unplugged MotA/B proton channel by cytoplasmic pHluorin expressed in *Salmonella*. *FEBS lett* **584**: 1268–1272.

Morimoto, Y.V., Nakamura, S., Kami-ike, N., Namba, K. and Minamino, T. (2010b) Charged residues in the cytoplasmic loop of MotA are required for stator assembly into the bacterial flagellar motor. *Mol Microbiol* **78**: 1117–1129

Muramoto, K. and Macnab, R.M. (1998) Deletion analysis of MotA and MotB, components of the force-generating unit in the flagellar motor of *Salmonella*. *Mol Microbiol* **29:** 1191–202.

Murphy, G.E., Leadbetter, J.R. and Jensen, G.J. (2006) In situ structure of the complete Treponema primitia flagellar motor. *Nature* **442**: 1062–1064.

Nagai, T., Sawano, A., Park, E.S. and Miyawaki, A. (2001) Circularly permuted green fluorescent proteins engineered to sense Ca2+. *Proc Natl Acad Sci USA* **98**: 3197–3202.

Nagai, T., Ibata, K., Park, E.S., Kubota, M., Mikoshiba, K. and Miyawaki, A. (2002) A

variant of yellow fluorescent protein with fast and efficient maturation for cell-biological applications. *Nat Biotech* **20**: 87–90.

Nakamura, S., Kami-ike, N., Yokota, P.J., Kudo, S., Minamino, T. and Namba, K. (2009a) Effect of intracellular pH on the torque-speed relationship of bacterial proton-driven flagellar motor. *J Mol Biol* **386**: 332–338.

Nakamura, S., Morimoto, Y.V., Kami-ike, N., Minamino, T. and Namba, K. (2009b) Role of a conserved prolyl residue (Pro-173) of MotA in the mechanochemical reaction cycle of the proton-driven flagellar motor of Salmonella. *J Mol Biol* **393**: 300–307.

Nakamura, S., Kami-ike, N., Yokota, J.P., Minamino, T. and Namba, K. (2010) Evidence for symmetry in the elementary process of bidirectional torque generation by the bacterial flagellar motor. *Proc Natl Acad Sci USA* **107**: 17616–17620.

Noji, H., Yasuda, R., Yoshida, M. and Kinosita, K. (1997) Direct observation of the rotation of F1-ATPase. *Nature*. **386**: 299–302.

Olsen, K.N., Budde, B.B. Siegumfeldt, H.K. Rechinger, B. Jakobsen, M. and Ingmer, H. (2002) Noninvasive measurement of bacterial intracellular pH on a single-cell level with green fluorescent protein and fluorescence ratio imaging microscopy. *Appl Environ Microbiol* **68**: 4145–4147

Orij, R., Postmus, J., Ter Beek, A., Brul, S. and Smits, G.J. (2009) In vivo measurement of cytosolic and mitochondrial pH using a pH-sensitive GFP derivative in Saccharomyces cerevisiae reveals a relation between intracellular pH and growth. *Microbiology* **155**: 268–78.

Padan, E., Bibi, E., Ito, M. and Krulwich, T.A. (2005) Alkaline pH homeostasis in bacteria: new insights. *Biochim Biophys Acta* **1717**: 67–88.

Paulick, A., Koerdt, A., Lassak, J., Huntley, S., Wilms, I., Narberhaus, F. and Thormann, K.M. (2009) Two different stator systems drive a single polar flagellum in Shewanella oneidensis MR-1. *Mol Microbiol* **71**: 836–850.

Ravid, S. and Eisenbach, M. (1984) Minimal requirements for rotation of bacterial flagella. *J Bacteriol* **158**: 1208–1210.

Reid, S.W., Leake, M.C., Chandler, J.H., Lo, C.J., Armitage, J.P. and Berry, R.M. (2006) The maximum number of torque-generating units in the flagellar motor of *Escherichia coli* is at least 11. *Proc Natl Acad Sci USA* **103**: 8066–8071.

Ryu, W.S., Berry, R.M. and Berg, H.C. (2000) Torque-generating units of the flagellar motor of *Escherichia coli* have a high duty ratio. *Nature* **403**: 444–447.

Saijo-Hamano, Y., Minamino, T., Macnab, R.M. and Namba, K. (2004) Structural and functional analysis of the C-terminal cytoplasmic domain of FlhA, an integral membrane component of the type III flagellar protein export apparatus in *Salmonella*. *J Mol Biol* **343**: 457–466.

Sankaranarayanan, S., De Angelis, D., Rothman, J.E. and Ryan, T.A. (2000) The use of pHluorins for optical measurements of presynaptic activity. *Biophys J* **79**: 2199–208

Sharp, L.L. Zhou, J. and Blair, D.F. (1995) Tryptophan-scanning mutagenesis of MotB, an integral membrane protein essential for flagellar rotation in *Escherichia coli*, *Biochemistry* **34**, 9166–9171.

Silverman, M. and Simon, M. (1974) Flagellar rotation and the mechanism of bacterial motility. *Nature* **249**: 73–74.

Slonczewski, J.L., Rosen, B.P., Alger, J.R. and Macnab, R.M. (1981) pH homeostasis in *Escherichia coli*: measurement by ^{31}P nuclear magnetic resonance of methylphosphonate and phosphate. *Proc Natl Acad Sci USA* **78**: 6271–6275.

Sourjik, V. (2004) Receptor clustering and signal processing in *E. coli* chemotaxis. *TRENDS in Microbiology* **12**: 569–576

Sowa, Y. and Berry, R.M. (2008) Bacterial flagellar motor. *Q Rev Biophys* **41**: 103–132.

Sowa, Y., Hotta, H., Homma, M. and A. Ishijima. (2003) Torque-speed relationship of the Na^+-driven flagellar motor of *Viblio alginolyticus*. *J Mol Biol* **327**: 1043–1051.

Sowa, Y., Rowe, A.D., Leake, M.C., Yakushi, T., Homma, M., Ishijima, A. and Berry, R.M. (2005) Direct observation of steps in rotation of the bacterial flagellar motor. *Nature* **437**: 916–919.

Stolz, B. and Berg, H.C. (1991) Evidence for interactions between MotA and MotB, torque-generating elements of the flagellar motor of *Escherichia coli*. *J Bacteriol* **173**: 7033–7037.

Subach, O.M., Gundorov, I.S., Yoshimura, M., Subach, F.V., Zhang, J., Grüenwald, D., Souslova, E.A., Chudakov, D.M. and Verkhusha, V.V. (2008) Conversion of red fluorescent protein into a bright blue probe. *Chem. Biol.* **15**: 1116–1124.

Suzuki, H., Yonekura, K. and Namba, K. (2004). Structure of the rotor of the bacterial flagellar motor revealed by electron cryomicroscopy and single-particle image analysis. *J Mol Biol* **337**: 105–113.

Tang, H., Braun T.F. and Blair D.F. (1996) Motility protein complexes in the bacterial flagellar motor. *J Mol Biol* **261**: 209–221

Terahara, N., Krulwich, T.A. and Ito, M. (2008) Mutations alter the sodium versus proton use of a Bacillus clausii flagellar motor and confer dual ion use on *Bacillus subtilis* motors. *Proc Natl Acad Sci USA* **105**: 14359–14364.

Terashima, H., Fukuoka, H., Yakushi, T., Kojima, S. and Homma, M. (2006) The *Vibrio* motor proteins, MotX and MotY, are associated with the basal body of Na^+-driven flagella and required for stator formation. *Mol Microbiol* **62**: 1170–1180.

Thomas, D., Morgan, D.G. and DeRosier, D.J. (2001) Structures of bacterial flagellar motors from two FliF-FliG gene fusion mutants. *J Bacteriol* **183**: 6404–6412.

Thomas, D.R., Francis, N.R., Chen, X. and DeRosier, D.J. (2006) The three-dimensional structure of the flagellar rotor from a clockwise-locked mutant of *Salmonella enterica* serovar Typhimurium. *J Bacteriol* **188**: 7039–7048.

Togashi, F., Yamaguchi, S., Kihara M., Aizawa, S.-I. and Macnab, R.M. (1997) An extreme clockwise switch bias mutation in *fliG* of *Salmonella typhimurium* and its suppression by slow-motile mutations in *motA* and *motB*. *J Bacteriol* **179:** 2994–3003.

Tsien R.Y. (1998) The green fluorescent protein. *Annu Rev Biochem* **67**: 509–544.

Turner, L., Ryu, W.S. and Berg, H.C. (2000) Real-time imaging of fluorescent flagellar filaments. *J Bacteriol* **182**: 2793–2801.

Ueno, T., Oosawa, K. and Aizawa, S. (1992) M ring, S ring and proximal rod of the flagellar basal body of Salmonella typhimurium are composed of subunits of a single protein, FliF. *J Mol Biol* **227:** 672–677.

Ueno, H., Nishikawa, S., Iino, R., Tabata, K.V., Sakakihara, S., Yanagida, T. and Noji, H. (2010) Simple Dark-Field Microscopy with Nanometer Spatial Precision and Microsecond Temporal Resolution. *Biophys J* **98**: 2014–2023.

Urano, Y., Asanuma, D., Hama, Y., Koyama, Y., Barrett, T., Kamiya, M., Nagano, T., Watanabe, T., Hasegawa, A., Choyke, P.L. and Kobayashi, H. (2009) Selective molecular imaging of viable cancer cells with pH-activatable fluorescence probes. *Nat Med* **15**: 104–109.

Wagenknecht, T., DeRosier, D.J., Shapiro, L. and Weissborn, A. (1981) Three-dimensional reconstruction of the flagellar hook from Caulobacter crescentus. *J Mol Biol* **151**: 439‒465

Washizu, M., Jones, T.B. and Kaler, K.V. (1993) Higher-order dielectrophoretic effects: levitation at a field null. *Biochim Biophys Acta* **1158**: 40–46.

Wilks, J.C. and Slonczewski, J.L. (2007) pH of the Cytoplasm and Periplasm of *Escherichia coli*: Rapid Measurement by Green Fluorescent Protein Fluorimetry. *J Bacteriol* **189**: 5601–5607.

Wilson, M.L. and Macnab, R.M. (1988) Overproduction of the MotA protein of *Escherichia coli* and estimation of its wild-type level. *J Bacteriol* **170:** 588–597.

Wilson, M.L. and Macnab, R.M. (1990) Co-overproduction and localization of the *Escherichia coli* motility proteins MotA and MotB. *J Bacteriol* **172**: 3932–3939.

Yamaguchi, S., Fujita, H., Sugata, K., Taira, T. and Iino, T. (1984) Genetic analysis of H2, the structural gene for phase-2 flagellin in *Salmonella*. *J Gen Microbiol* **130**: 255–265.

Yamaguchi, S., Aizawa, S-I., Kihara, M., Isomura, M., Jones, C.J. and Macnab, R.M. (1986) Genetic evidence for a switching and energy-transducing complex in the flagellar motor of *Salmonella typhimurium*. *J Bacteriol* **168**: 1172–1179.

Yoshioka, K., Aizawa, S.-I. and Yamaguchi, S. (1995) Flagellar filament structure and cell motility of Salmonella typhimurium mutants lacking part of the outer domain of flagellin. *J Bacteriol* **177**: 1090–1093.

Yuan, J., and Berg, H.C. (2008) Resurrection of the flagellar rotary motor near zero load. *Proc Natl Acad Sci USA* **105**: 1182–1185.

Zhou, J., Fazzio, R.T. and Blair, D.F. (1995) Membrane topology of the MotA protein of *Escherichia coli*. *J Mol Biol* **251**: 237–242.

Zhou, J. and Blair, D.F. (1997) Residues of the cytoplasmic domain of MotA essential for torque generation in the bacterial flagellar motor. *J Mol Biol* **273**: 428–439.

Zhou, J., Lloyd, S. A. and Blair, D.F. (1998a) Electrostatic interactions between rotor and stator in the bacterial flagellar motor. *Proc Natl Acad Sci USA* **95**: 6436–6441.

Zhou, J., Sharp, L.L., Tang, H.L., Lloyd, S.A. and Blair, D.F. (1998b) Function of protonatable residues in the flagellar motor of *Escherichia coli*: a critical role for Asp32 of MotB. *J Bacteriol* **180**: 2729–2735.

Zilberstein, D., Agmon, V., Schuldiner, S. and Padan, E. (1984) *Escherichia coli* intracellular pH, membrane potential, and cell growth. *J Bacteriol* **158**: 246–252.

Publications

Original Papers

1. Morimoto, Y.V.*, Nakamura, S.*, Kami-ike, N., Namba, K. and Minamino, T. (2010) Charged residues in the cytoplasmic loop of MotA are required for stator assembly into the bacterial flagellar motor. *Molecular Microbiology* **78**: 1117-1129

2. Morimoto, Y.V.*, Che, Y-S.*, Minamino, T.* and Namba, K. (2010) Proton-conductivity assay of plugged and unplugged MotA/B proton channel by cytoplasmic pHluorin expressed in *Salmonella*. *FEBS letters* **584**: 1268–1272.

3. Minamino, T., Yoshimura, S.D., Morimoto, Y.V., González-Pedrajo, B., Kami-Ike, N. and Namba, K. (2009) Roles of the extreme N-terminal region of FliH for efficient localization of the FliH-FliI complex to the bacterial flagellar type III export apparatus. *Molecular Microbiology* **74**: 1471–1483.

   My contribution; I observed the co-localization of FliI-YFP with flagellar filament.

4. Nakamura, S.*, Morimoto, Y.V.*, Kami-ike, N., Minamino, T. and Namba, K. (2009) Role of a Conserved Prolyl Residue (Pro173) of MotA in the Mechanochemical Reaction Cycle of the Proton-Driven Flagellar Motor of Salmonella. *Journal of Molecular Biology* **393**: 300–307.

5. Okada, J., Morimoto, Y. and Toh, Y. (2009) Antennal motor activity induced by pilocarpine in the American cockroach. *Journal of Comparative Physiology A* **195**: 351–363.

   My contribution; I observed the kinetics of antennae of intact cockroach and analyzed the experimental data.

6. Morimoto, Y.V., Kojima, S., Namba, K. and Minamino, T. M153R mutation in a pH-sensitive green fluorescent protein stabilizes its fusion proteins. (In preparation)

* these authors contributed equally

International Conferences

1. ○Morimoto, Y.V., Kami-ike, N., Minamino, T. and Namba, K. Development of a high-resolution pH imaging system to detect local pH near the bacterial flagellar motor in *Salmonella*. Sensory Transduction in Microorganisms Gordon Research Conference, Ventura, CA, USA, January 2010.

2. ○Morimoto, Y.V., Kami-ike, N., Minamino, T. and Namba, K. Simultaneous Measurement of Intracellular pH and Bacterial Flagellar Motor Rotation in *Salmonella* using a High-resolution pH Imaging System. Innovative Nanoscience of Supermolecular Motor Proteins, Kyoto, Japan, September 2009.

3. ○Morimoto, Y., Che, Y-S., Minamino, T., Kami-ike, N. and Namba, K. Intracellular pH measurement of *Salmonella* with a pH-sensitive GFP, pHluorin, and a newly developed pH imaging system. T3SS - UK meeting 2008, Bristol, UK, September 2008.

Domestic conferences

1. ○森本雄祐，上池伸徳，南野徹，難波啓一． pH 感受性蛍光蛋白質を用いた高分解能細胞内 pH イメージング， 第 2 回光塾， 2010 年 12 月.

2. ○森本雄祐，中村修一，難波啓一，南野徹. バクテリアべん毛モーター固定子構成蛋白質 MotA の細胞質領域に存在する荷電残基の役割，日本生体エネルギー研究会 第 36 回討論会, 2010 年 11 月.

3. ○森本雄祐，中村修一，上池伸徳，難波啓一，南野徹. バクテリアのプロトン駆動型べん毛モーター固定子複合体 MotA/B の局在化の分子機構，第 48 回日本生物物理学会年会, 2010 年 9 月.

4. ○今田勝巳，南野徹，木下実紀，中村修一，森本雄祐，難波啓一. 細菌べん毛モーター回転スイッチ機構の構造からの考察，第 48 回日本生物物理学会年会, 2010 年

9 月.

My contribution; I preliminally measured the switching frequency of the flagellar motor of the cell producing FliG(ΔPAA) mutant.

5. ○森本雄祐，中村修一，難波啓一，南野徹. バクテリアのプロトン駆動型べん毛モーター固定子複合体の局在化の分子機構, 第７回２１世紀大腸菌研究会, 2010 年 6 月.

6. ○森本雄祐，上池伸徳，南野徹，難波啓一. 高分解能 pH イメージングシステムを用いた細胞内 pH と細菌べん毛の回転の同時計測，日本生体エネルギー研究会 第 35 回討論会, 2009 年 12 月.

7. ○今田勝巳，南野徹，木下実紀，中村修一，森本雄祐，難波啓一. 一方向回転変異を持つ FliG の構造から推測されるべん毛の回転方向制御機構, 特定領域研究「生体超分子構造」第 6 回公開シンポジウム, 2009 年 12 月.

My contribution; I preliminally measured the switching frequency of the flagellar motor of the cell producing FliG(ΔPAA) mutant.

8. ○森本雄祐，上池伸徳，南野徹，難波啓一. pH イメージングシステムを用いた細胞内 pH とべん毛モーター回転の同時計測，第 47 回日本生物物理学会年会, 2009 年 10 月.

9. ○中村修一，森本雄祐，上池伸徳，南野徹，難波啓一. プロトン駆動型細菌べん毛モーターのトルク発生における固定子蛋白質 MotA Pro-173 の機能解析，第 47 回日本生物物理学会年会, 2009 年 10 月.

My contribution; I constructed the plasmid pKSS13(P173A), and measured intracellular pH and swarming motility of the cell harboring pKSS13(P173A).

10. ○森本雄祐. 緑色蛍光蛋白質を用いた細胞内 pH の高分解能計測, 2009 おおさか研究会,2009 年 9 月.

11. ○森本雄祐，上池伸徳，南野徹，難波啓一. 高分解能 pH イメージングによる細胞

内 pH と細菌べん毛の回転の同時計測, 特定領域研究膜超分子モーターの革新的ナノサイエンス第 4 回班会議, 2009 年 6 月.

12.○森本雄祐, 蔡栄淑, 南野徹, 上池伸徳, 難波啓一. 高感度 pH イメージングシステムを用いた細菌の細胞内局所 pH の測定, 第 46 回日本生物物理学会年会, 2008 年 12 月.

13.森本雄祐, ○上池伸徳, 南野徹, 難波啓一. 高速高感度で単一菌体内 pH 分布を計測する顕微システムの開発, 第 46 回日本生物物理学会年会, 2008 年 12 月.

14.○蔡栄淑、中村修一、森本雄祐、上池伸徳、難波啓一、南野徹. べん毛モーター固定子タンパク質MotB(D33E)変異体とそのサプレッサー変異体モーターのトルク発生機構の解析, 第46回日本生物物理学会年会, 2008年12月.

My contribution; I measured intracellular pH of *Salmonella* cells overproducing MotA and MotB(D33E) mutant.

15.○中村修一, ○森本雄祐. プロトン駆動型べん毛モーターの回転計測とプロトン流の計測, 第14回べん毛研究交流会, 2008年3月.

16.○森本雄祐, 蔡栄淑, 南野徹, 上池伸徳, 難波啓一. pH感受性蛍光蛋白質フルオリンを用いた細菌の細胞内pH測定, 第45回日本生物物理学会年会, 2007年12月.

17.○森本雄祐, 南野徹, 上池伸徳, 難波啓一. pH 感受性蛍光蛋白質フルオリンを用いた細菌の細胞内 pH 測定, 第 4 回 21 世紀大腸菌研究会, 2007 年 7 月.

Award

1. ライカ顕微鏡フォトコンテスト 2009 優秀賞,「灯」, 森本雄祐, 2009 年 12 月